CONTROL METHODS FOR SYSTEMS WITH NONLINEAR INSTRUMENTATION: ROOT LOCUS, PERFORMANCE RECOVERY, AND INSTRUMENTED LQG

by

ShiNung Ching

A dissertation submitted in partial fulfillment
of the requirements for the degree of
Doctor of Philosophy
(Electrical Engineering: Systems)
in The University of Michigan
2009

Doctoral Committee:

Professor Pierre T. Kabamba, Co-Chair
Professor Semyon M. Meerkov, Co-Chair
Professor Emeritus Elmer G. Gilbert
Professor Jessy W. Grizzle
Assistant Professor Domitilla Del Vecchio

To Mom and Dad.

ACKNOWLEDGEMENTS

First, I would like to thank my mentors, Professors Pierre T. Kabamba and Semyon M. Meerkov, for their tireless effort, guidance, wisdom and inspiration, in what has been an immensely fulfilling intellectual and personal journey.

I would also like to convey my gratitude to Professors Elmer Gilbert, Jessy Grizzle and Domitilla Del Vecchio for their interest in my research and for serving as members of my dissertation committee. Many heartfelt thanks also go to R.G., for her support and encouragement during this process.

Finally, this work would not be possible without the love and support of my parents, Dr. Chan Yu and Yushive Ching, and my sister, Carly. Their commitment, dedication and sacrifice have truly given me the wings and the freedom to fly.

TABLE OF CONTENTS

LIST OF FIGURES

Figure

LIST OF APPENDICES

Appendix

CHAPTER I

INTRODUCTION

1.1 Motivation

The linear SISO feedback system of Figure 1.1 is, perhaps, the most widely studied configuration in control theory. Here, $P(s)$ is an LTI model of some plant that is to be controlled, while $C(s)$ is a controller that leads to the desired closed loop behavior. The signals u_ℓ and y_ℓ are the control and output, respectively. The signal d is an exogenous disturbance to be rejected, while r is a reference to be tracked. In reality, the controller is implemented in the configuration shown in Figure 1.2, where $f(\cdot)$ and $g(\cdot)$ are static nonlinearities corresponding to the actuator and sensor, respectively, and u, y are the altered control and output. The signals v and y_m denote the actuator and sensor (i.e., measured) outputs, respectively. Here, the plant model remains linear, based on the assumption that the controller maintains the system state in the vicinity of some operating point. Achieving this objective, however, may require

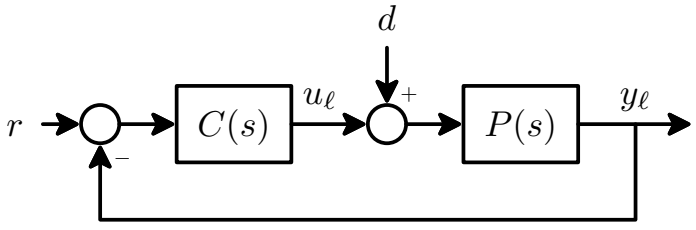

Figure 1.1: Basic linear SISO feedback system

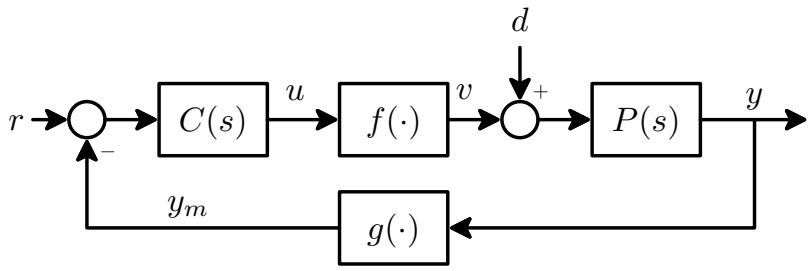

Figure 1.2: General linear plant/nonlinear instrumentation (LPNI) system

the application of large control signals or the precise measurement of small output signals. This, in turn, may be limited by nonlinearities in actuation and sensing, such as saturation, deadzone, quantization, etc. Hence, the configuration of Figure 1.2, referred to as a *Linear Plant/Nonlinear Instrumentation* (LPNI) system, is of significant interest.

The development of results for LPNI systems has been limited due to the analytical difficulties posed by the nonlinearities. Most work tends to focus on issues of stability for specific classes of $f(\cdot)$ and $g(\cdot)$, while issues pertaining to performance have largely remained unexplored. There is, however, one formulation of the LPNI system that has led to analytical tractability - when the exogenous inputs r and/or d are random. In this case, the method of stochastic linearization [1] can be applied, whereby the nonlinearities are replaced by equivalent gains N_a and N_s as shown in Figure 1.3. This is referred to as a closed-loop *quasilinear* system, where the signals $\hat{u}$, $\hat{v}$, $\hat{y}$ and $\hat{y}_m$ are intended to approximate u, v, y, and y_m, respectively. The gains N_a and N_s are expectations defined as

$$N_a = E\left[\frac{d}{d\hat{u}} f\left(\hat{u}\right)\right] \tag{1.1}$$

and

$$N_s = E\left[\frac{d}{d\hat{y}} g\left(\hat{y}\right)\right], \tag{1.2}$$

where $E[\,\cdot\,]$ is the expectation operator, and where the expectation is taken with

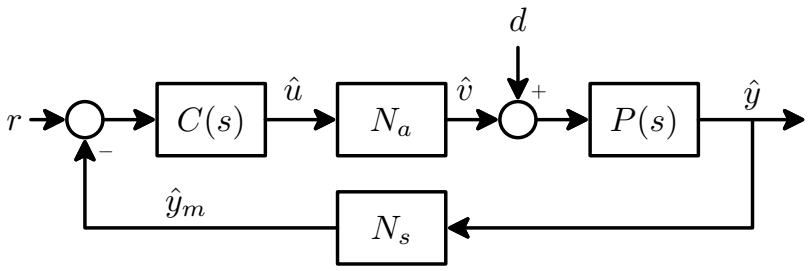

Figure 1.3: Quasilinear system

respect to the probability density functions of $\hat{u}$ and $\hat{y}$, respectively. This technique is analogous to the well-known method of describing functions for systems with sinusoidal inputs. In this manner, stochastic linearization offers a means to study disturbance rejection and tracking in LPNI systems. For tracking, the reference signal to be tracked is not a traditional step, but instead a random reference of specified bandwidth, which turns out to be useful in many real-world applications, for example, hard disk servos [2] and aerospace guidance [3].

In both disturbance rejection and tracking, stochastic linearization has been effectively used to approximate the behavior of the original LPNI system in terms of the steady-state variances σ_u^2, $\sigma_{\hat{u}}^2$ and σ_y^2, $\sigma_{\hat{y}}^2$. Thus, the following control problems can be addressed:

Problem 1: **Analysis:** Given $P(s)$, $C(s)$, $f(\cdot)$ and $g(\cdot)$ in Figure 1.2, characterize the performance of the LPNI system.

Problem 2: **Performance Recovery:** Let $P(s)$ and $C(s)$ achieve a satisfactory performance in the linear system of Figure 1.1. Given $f(\cdot)$ and $g(\cdot)$, redesign $C(s)$ so that the LPNI system of Figure 1.2 recovers this performance.

Problem 3: **Instrumentation Selection:** Let $P(s)$ and $C(s)$ achieve a satisfactory performance in the linear system of Figure 1.1. Select $f(\cdot)$ and $g(\cdot)$ so that the performance of the LPNI system of Figure 1.2 is within a

specified tolerance of that of the original linear design.

Problem 4: **Narrow-sense Design:** Given $P(s)$, $f(\cdot)$ and $g(\cdot)$ in Figure 1.2, design the controller $C(s)$ so that the LPNI system achieves the desired objective.

Problem 5: **Wide-sense Design:** Given $P(s)$ in Figure 1.2, design the controller $C(s)$ *and* select the instrumentation $f(\cdot)$ and $g(\cdot)$, so that the LPNI system achieves the desired objective.

Some of these problems have been partially addressed in existing control theory. For instance, for deterministic reference tracking, the method of anti-windup is a well-known performance recovery technique [4]. Similarly, for disturbance rejection, the SLQR/SLQG method solves the narrow-sense design problem [5]. A detailed survey of existing literature is provided in Section 1.3, below.

This dissertation is motivated by gaps in theory for addressing Problems 2, 3 and 5. Specifically,

i) the performance recovery problem for disturbance rejection;

ii) the narrow-sense design problem for reference tracking; and

iii) the wide-sense design problem for disturbance rejection,

have not been treated in the existing literature. This dissertation develops control methods for all three issues. It turns out that the results closely resemble well-known linear control theory. For example, Problem 4 is solved by a generalization of the well-known root locus technique, and the solution of Problem 5 is similar to the LQR/LQG synthesis technique. As such, it is anticipated that the results of this dissertation will be appealing to practicing control engineers. A more detailed formulation of the objectives of this dissertation is given below.

1.2 Objectives

This work develops the following three control design methods that address the above motivating problems.

1.2.1 Tracking random references: S-Root Locus

Consider the LPNI system subject to the random exogenous input r. This corresponds to a standard tracking control problem, where the reference is not a traditional step, but is a random signal. As mentioned, such references are common in a variety of physical systems. For the purposes of this work, r is generated by passing standard white noise w through a coloring filter of bandwidth Ω_r, as shown in Figure 1.4. We ask the following design question: How can the controller $C(s)$ be designed so that the reference is tracked well?

This question, which is in the category of narrow-sense design, i.e., Problem 4 above, is answered by generalizing the well-known Root Locus design technique. The Root Locus method is used for tracking controller design in the case of deterministic (e.g., step) references in linear systems. It uses admissible domains for closed loop poles in the complex plane, which guide adjustment of the controller structure and gain, leading to the desired system behavior. The S-Root Locus technique, developed herein, creates an equivalent methodology for the LPNI system with random reference. It focuses specifically on the case when $f(\cdot)$ is a saturation nonlinearity

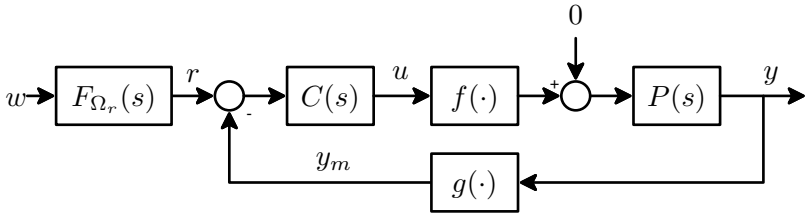

Figure 1.4: LPNI system subject to random reference (S-root locus problem)

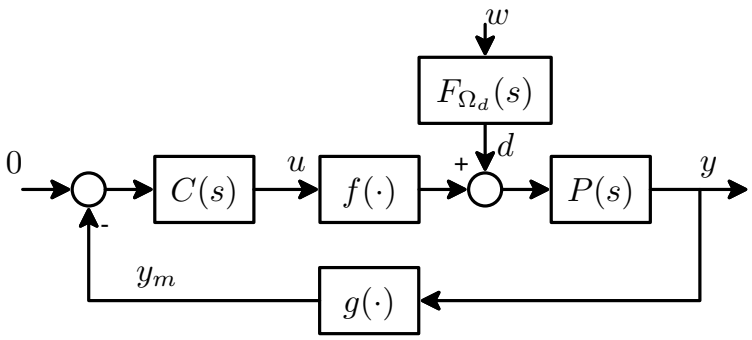

Figure 1.5: LPNI system subject to disturbance (boosting problem)

(S stands for saturation) and $g(\cdot)$ is linear, but can be generalized to other cases as well. The objectives are

i) Establish admissible domains in the s-plane that lead to a desired quality of random tracking in linear systems,

ii) Develop the notion of S-poles. These are poles of the quasilinear system, which predict the tracking quality of the LPNI system,

iii) Develop the S-Root Locus, which characterizes the behavior of the S-poles as a function of the controller gain.

To meet the control objective, $C(s)$ is chosen so that the S-root locus enters the admissible domain for random tracking, and the controller gain is selected so that the dominant S-poles lie in this domain. As such, the S-Root Locus provides a design tool for LPNI systems that is the analog of classical root locus.

1.2.2 Recovery of linear performance: Boosting

Consider the LPNI system shown in Figure 1.5, where d is a random disturbance of some bandwidth Ω_d generated by passing white noise through the filter $F_{\Omega_d}(s)$. This corresponds to a standard disturbance rejection problem, where the objective is to achieve a specification in terms of the output variance σ_y^2. Control engineers faced

with this problem often obtain $C(s)$ by completing a design for the system of Figure 1.1 (in terms of σ_{y_ℓ}), using linear techniques such as LQG. The assumption is that, when implemented in the LPNI configuration of Figure 1.2, the performance does not degrade 'too much'. However, in many cases, degradation may be appreciable, such that

$$\sigma_y^2 > \sigma_{y_\ell}^2. \tag{1.3}$$

The *boosting* technique, developed herein, studies how, and under what conditions, $C(s)$ can be modified so that the above degradation is eliminated. Hence, it addresses the performance recovery problem, i.e., Problem 2 above. The specific objective is to derive conditions under which $C(s)$ can be augmented by a scalar 'boosting' gain, such that the quasilinear system recovers the intended linear performance, i.e.,

$$\sigma_{\hat{y}}^2 = \sigma_{y_\ell}^2.$$

The boosting methodology allows the use of *any* linear design technique for LPNI systems with *arbitrary* $f(\cdot)$ and $g(\cdot)$.

1.2.3 Simultaneous design of controller and instrumentation: ILQR/ ILQG

Consider the LPNI system shown in Figure 1.6, where d is, again, a random disturbance of given bandwidth, and the control objective is disturbance rejection.

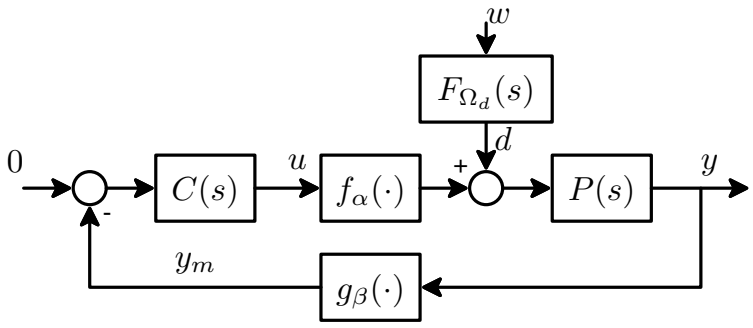

Figure 1.6: LPNI system subject to disturbance (ILQR/ILQG problem)

Here, the actuator and sensor nonlinearities are not a priori specified, but can be selected by the designer. Thus, they are denoted as $f_\alpha(\cdot)$ and $g_\beta(\cdot)$, where α and β are selectable parameters that define the instrumentation. For example, α may denote the authority of a saturation, while β may denote the width of a deadzone.

As described in the Instrumentation Selection problem, i.e., Problem 3 above, the selection of α and β is often influenced by a desire to 'minimally degrade' an existing linear design. As such, sensors and actuators might be chosen with performance that exceeds what is actually required to achieve the desired specification. Conversely, if the 'better' instrumentation is unavailable, then the designer may compensate by designing the controller in an unnecessarily aggressive manner. Both situations are inefficient. How, then, can one achieve the best balance between the controller and the instrumentation?

The method of *Instrumented LQR/LQG* (ILQR/ILQG) aims to resolve this question by providing a means of synthesizing both controller and instrumentation to minimize an augmented version of the conventional LQR/LQG performance index given by

$$J = \sigma_{\hat{y}}^2 + \rho\sigma_{\hat{u}}^2 + \mathcal{W}(\alpha, \beta), \tag{1.4}$$

where $\rho > 0$ and $\mathcal{W}$ models the 'cost' of the instrumentation as a function of α and β. In this manner, ILQR/ILQG is a method for simultaneous design of controller and instrumentation.

The main objectives are as follows:

i) Solve the ILQR problem: When all states are available, find a state-feedback $u = Kx$, and instrumentation parameters α and β that minimize (1.4),

ii) Solve the ILQG problem: When some states are unavailable, find $C(s)$, α and

β that minimize (1.4).

The solution of these problems provides a novel method that explicitly addresses the design of both controller and nonlinear sensors and actuators. By using the familiar LQR/LQG framework, it does so in a way that is consistent with well-established linear techniques.

1.3 Relevant Work

The following section provides a brief overview of relevant literature.

1.3.1 Stochastic linearization

The theory of stochastic linearization was first introduced in [6, 7], and is comprehensively described in the monographs [8] and [1]. In [8] it is referred to as the method of 'random input describing functions', while in [1] it is referred to as 'statistical linearization.' As suggested in [1], it has most frequently been used to study mechanical systems subject to random vibrations. Typically, the exogenous signal has been assumed Gaussian, although many recent works, such as [9,10], have examined other types of random excitation.

There have been various attempts to characterize the accuracy of stochastic linearization, which are extensively cataloged in [11, 12]. Most of these address the open loop environment, and are heavily based on numerical verification, though a limited number of analytical results have been established. More important for this dissertation is the accuracy in the closed loop environment, where no analytical characterization is available. Numerical studies, as found in [1,8], as well as [13,14], indicate that, in these situations, accuracy is high, generally within 10% in terms of the variances $\sigma_u^2, \sigma_{\hat{u}}^2$, $\sigma_y^2, \sigma_{\hat{y}}^2$ etc. More details on stochastic linearization and its accuracy are given in Chapter II.

1.3.2 Analysis of LPNI systems

Stability

Analysis of LPNI systems has generally centered on the issue of stability. Among the earliest work in this area is the theory of absolute stability, which ensures the asymptotic stability of the origin of the closed-loop LPNI system for nonlinearities in a given sector [15–17]. Later works have focused on stability for particular classes of nonlinearities, most commonly actuator saturation. In this case, it is established in [18, 19] that global stabilization cannot be achieved using linear feedback. This led to results on semi-global stabilization, such as [20, 21], which ensure a that a given domain of attraction is achieved. The work [22] gives a characterization of the this domain. These results are based primarily on the construction of appropriate Lyapunov functions. A comprehensive bibliography on control and stability in systems with saturating actuators is found in the volumes [23, 24], as well as the survey paper [25]. In addition to saturation, stability of LPNI systems has been examined for actuator deadzone [26, 27], backlash [28], and hysteresis [29]. More generally, for arbitrary actuator nonlinearities, suggested stabilization techniques are found in [30] and [31], which propose schemes based on inversion of the nonlinearity.

Stability analysis is also found in the case of nonlinear sensors. A discontinuous stabilizing control scheme was proposed in [32], and semi-global stabilization is examined in [33]. For sensor sector nonlinearities, [34] proposes an output feedback method for stabilization based on $\mathcal{H}_\infty$ controller design. The most common sensor nonlinearity found in the literature is quantization. Here, stability results are motivated by computer-based control, as well as applications related to communication over finite capacity links [35–37]. The system considered is typically formulated in discrete time, and stability assessed via construction of Lyapunov functions (see, for

instance, [38,39]). In this context, the problem of input to state stability is discussed in [40]. Only a few results are available for the case of a continuous time plant, notably [41] and [42], which propose a stabilizing $\mathcal{H}_\infty$ feedback scheme. These methods rely on an ability to 'tune' the quantization interval on-line.

Related to the above is the vast body of work on modern nonlinear control theory [43, 44], which study systems of the form

$$\dot{x} = f(x) + g(x)u. \tag{1.5}$$

Here, the dynamics of the actuator are modeled by $g(x)$, and techniques such as feedback linearization [45–47], are used for control. However, the LPNI systems of this dissertation cannot be easily studied in this form, since in (1.5), the control signal u enters in an affine manner. This allows for application of arbitrarily large control inputs, thus excluding static instrumentation nonlinearities such as saturation.

Performance

Although stability analysis has received significant treatment in the literature, analysis of the *performance* of LPNI systems is less common. In general, the performance of LPNI systems is ascertained via analysis of the system dynamics excited by the exogenous inputs. For the problem of rejecting random disturbances, this is done by means of the Fokker-Planck equation [48], which gives the stationary probability distributions of relevant signals. Analytical solution of this equation is generally impossible, except in certain low-order systems [49]. In higher order cases, stochastic linearization can be used, such as in [14], which characterizes the output variance of LPNI systems with saturating actuators.

For tracking, there is extensive literature on the phenomenon of controller windup, which describes the performance of integral control systems in the presence of sat-

urating actuators [4]. Related to this is the issue of tracking domains [50], which characterize the magnitude of the references that can be tracked in systems with saturating actuators. In a similar context, the notion of system type has been extended to LPNI systems in [51]. In the case of random references, [52] studies the tracking performance of a PD controller. In [53] and [54], stochastic linearization is used to develop tracking quality indicators that characterize the quality of random reference tracking, again, for systems with saturating actuators.

1.3.3 Instrumentation selection

There has been some effort at characterizing the performance of instrumentation in terms of its mechanical and electrical properties [55–58]. In particular, the monograph [59] describes, in considerable detail, the behavior of sensors and actuators in many real-world engineering problems. However, the approach is to focus on the linear dynamics of the instrumentation, with only a qualitative discussion of nonlinearities. More importantly, no systematic way of selecting the instrumentation is discussed. In [60], the selection of mechanical actuators is studied, though it is again based on purely physical considerations, such as force and displacement. There is no quantification of the performance degradation resulting from nonlinearities in instrumentation.

One work that does explicitly address the instrumentation selection problem posed in Section 1.1 is [61], where stochastic linearization is used to select the authority of a saturating actuator that ensures a certain level of performance degradation (in terms of disturbance rejection) from some original linear design.

Some research has been conducted on selecting the spatial *positioning* of instrumentation in mechanical structures, in particular [62–64]. In these publications, an iteration is used to optimize the position of sensors and actuators in a physical space.

In [62] an LQG framework is utilized, while convex optimization and LMIs are used in [64]. However, there is no specific treatment of instrumentation nonlinearities.

1.3.4 Performance recovery

Perhaps the best-known performance recovery technique for LPNI systems is the method of anti-windup, used in the problem of tracking deterministic references. This method is primarily used to mitigate the effects of actuator saturation on integral control schemes, and is described in detail in [4, 65, 66]. In the case of sensor saturation, anti-windup techniques have been proposed in [67, 68].

Performance recovery has also been examined in the context of sampled-data implementation of continuous linear controllers. These works, described in the monographs [69, 70], examine how the discrete implementation of linear controllers should be modified so that the intended performance is achieved. Similar approaches have been studied in the context of nonlinear plants [71]. Note that these publications focus on instrumentation sampling, and do not explicitly treat actuator and sensor nonlinearities.

1.3.5 Narrow-sense (controller only) design

The narrow-sense design problem has received some treatment in the existing literature, particularly in the context of saturating actuators. In particular, the disturbance rejection problem for LPNI systems with saturating actuators is treated in [72] for $\mathcal{L}_2$ disturbances using fixed-order compensators constructed from solution of a modified Ricatti equation. A similar technique is used in [73] in the discrete time setting. For arbitrary bounded disturbances, [74] provides a method that minimizes the $\mathcal{L}_1$ norm of an error through solution of a nonlinear program. Gain scheduling techniques are proposed in [75] and [76], using families of LQ and $\mathcal{H}_\infty$ compensators,

respectively. Related to these are linear parameter varying control approaches, such as [77]. In [78], an LMI approach is used for design, however the strategy is to ensure that the instrumentation operates in a linear regime. Model predictive control is also commonly used for design in the presence of constrained actuators (see, for instance, [79, 80]), since the constraints are easily incorporated into the on-line optimization. Here, the main issue is ensuring closed-loop stability with the resulting controllers [81].

A few works have used stochastic linearization for design, particularly in the context of linear quadratic optimization. In [82], the authors consider the problem of a nonlinear plant with linear actuator, which is the converse of the problem formulation studied here. In [13], a performance index is used that penalizes the output of the saturation, which is ineffective since this signal is inherently limited in magnitude. Most directly related to the results presented in this work are [5, 83], which provide a method to synthesize a controller that solves the classical LQR/LQG problem for the quasilinear system in the case of saturating actuators and sensors.

Work addressing performance issues for LPNI systems with nonlinear sensors is less prevalent, since, in many cases, there is a duality with the techniques used for nonlinear actuators. Most common are results for the case of quantization. In [84], the author proposes a scheme that minimizes the worst possible quantization error. Other approaches, such as [85–87], have been motivated by Kalman filtering, using the assumption that quantization effects can be modeled as a Gaussian random disturbance. In the area of hybrid systems, control techniques have been proposed that partition the state space of the plant according to the number of quantization intervals, and then apply switching control (for instance, [88–90]). For general sensor nonlinearities, [31] again provides schemes that use adaptive controllers. In [91,92], a

method is proposed that uses filtering to recover a signal corrupted by a non-invertible sensor nonlinearity, though it is only deployed in an open-loop environment. The same is true in [93, 94], which use artificial neural networks to manipulate the linear operating region of the sensor.

1.3.6 Wide-sense (controller and instrumentation) design

Very little research has been done on the wide-sense design problem. The closest related work is [95,96], which has examined the design of linear controllers along with the aforementioned optimal spatial positioning of instrumentation (see subsection 1.3.4 above). In this framework, [97] has recently examined the problem of designing both control and instrumentation, by using an LMI approach and constraining the instrumentation cost. Here, the 'cost' of instrumentation is defined as the inverse of the signal-to-noise ratio of each sensor or actuator, which enters as a parameter of the linear system. The results developed in this dissertation are different, since here actuators and sensors are treated explicitly as nonlinear functions in the feedback loop.

1.4 Dissertation Synopsis

1.4.1 Chapter guide

The outline of this dissertation is as follows. Chapter II presents an overview of the method of stochastic linearization and discusses its accuracy for the closed loop LPNI system. Chapter III begins by characterizing random reference tracking and proceeds to develop the S-root locus methodology. The boosting methodology is presented in Chapter IV. Chapter V formulates the ILQR and ILQG problems and presents solutions for each. Conclusions are formulated in Chapter VI, which also suggests a few possible extensions to the dissertation. All proofs are provided in the

Appendices.

1.4.2 Research approach

The research approach pursued in this dissertation consists of stochastically linearizing LPNI systems and developing a rigorous control theory for the resulting quasilinear systems. Many standard mathematical analysis techniques, such as the method of Lagrange multipliers, are used to obtain the results.

Since the objective is to develop design methodologies that are useful for practicing engineers, it is important to verify the theory on practical examples. For this purpose, a number of simulation studies are presented using the MATLAB and SIMULINK computational environments. In one case, experimental verification is carried out on a magnetic levitation device.

1.4.3 Original contributions

The original contributions in this dissertation are summarized below:

- Development of admissible domains in the complex plane for closed-loop poles, so that a linear system exhibits a high quality of random tracking (Chapter III).
- Development of the S-Root Locus, an extension of classical root locus, for tracking controller design in the presence of saturating actuators (Chapter III).
- Development of boosting, a method for recovering the disturbance rejection performance of a linear design, in the presence of nonlinear instrumentation (Chapter IV).
- Development of Instrumented LQR/LQG, a method for simultaneously synthesizing controller and instrumentation for the objective of disturbance rejection (Chapter V).

CHAPTER II

STOCHASTIC LINEARIZATION

2.1 Introduction

As it is well known, the output variance of a linear time-invariant system subject to Gaussian random excitation can be obtained via solution of a Lyapunov equation [98]. This is a well-established, analytically tractable computation. In the case of nonlinear systems, calculation of the output variance requires solution of the Fokker-Planck equation [48] to obtain the steady state probability density function of the signal of interest. It is a partial differential equation for which analytical solution is generally impossible [1]. Therefore, an alternative approach is required. In this dissertation, since the exogenous inputs are random, the method of stochastic linearization (SL) provides such an approach, thus facilitating study of LPNI systems which would otherwise be intractable.

As mentioned in Section 1.3.1, the SL method is described in detail in the monographs [8] and [1]. The remainder of this chapter reviews SL theory, and its application to LPNI systems.

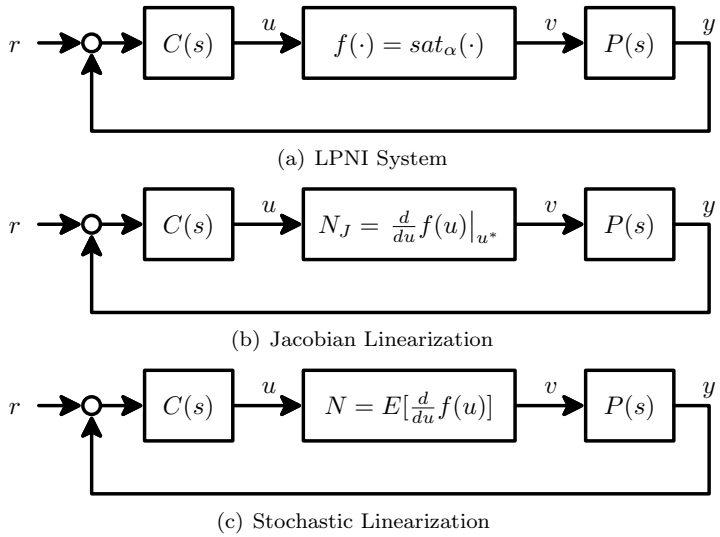

(a) LPNI System

(b) Jacobian Linearization

(c) Stochastic Linearization

Figure 2.1: Jacobian vs. stochastic linearization

2.2 The Idea: A Global Linearization

Traditionally, linearization is viewed as a local result, i.e., an approximate behavior of a nonlinear system in the vicinity of some operating point. The standard Jacobian linearization certainly has this property. Consider the basic LPNI system shown in Figure 2.1(a), where r is some exogenous random excitation. In Jacobian linearization, the nonlinearity is replaced by a linear gain N_J that is the derivative of $f(\cdot)$ evaluated at some operating point u^*, i.e.,

$$N_J = \frac{d}{du} f(u)\bigg|_{u^*},$$

resulting in Figure 2.1(b). Clearly, this linearization is accurate only if the exogenous signal r is sufficiently small. If, however, r is large, then the Jacobian linearization does not approximate the original LPNI system well. In this case, a so-called 'global' linearization must be sought.

Global linearization attempts to capture not only local properties, but behavior over a wide range of operating conditions. To accomplish this, the equivalent linear gain becomes a function not only of the nonlinearity, but the entire closed loop

system, including dynamic elements as well as exogenous inputs. A well-known example of this is the method of describing functions, or harmonic balance, which addresses the issue of oscillations in nonlinear systems subject to periodic excitation [44].

When the inputs are random, global linearization can be carried out with respect to the probability density function of the excitation. In control systems, random inputs are frequently considered in disturbance rejection problems. In tracking, although inputs are typically deterministic, many applications exist where the input can be viewed as a band limited random signal. In this spirit, this dissertation is based on the global linearization technique known as stochastic linearization. It converts the LPNI system of Figure 2.1(a) into the *quasilinear* system shown in Figure 2.1(c), where

$$N = E\left[\frac{d}{du}f(u)\right], \tag{2.1}$$

and the expectation is taken with respect to the probability density of u (recall that $E[\,\cdot\,]$ denotes the expectation operator). Thus, the right hand side of (2.1) is dependent on both $f(\cdot)$ *and* the distribution of u, which is, in turn, dependent on r and all other elements in the closed-loop system. Accordingly, the prefix *quasi* refers to the fact that the linearized gain N is a nonlinear function of all system parameters, including exogenous signals. The subsequent sections demonstrate how SL is carried out in LPNI systems.

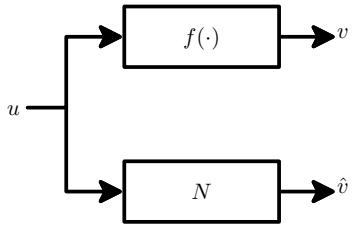

Figure 2.2: Stochastic linearization in the open-loop environment

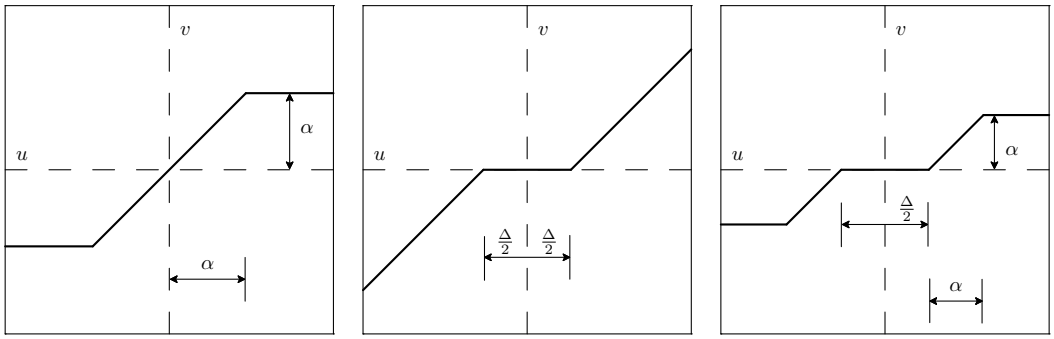

(a) Saturation (b) Deadzone (c) Saturation-deadzone

Figure 2.3: Common instrumentation nonlinearities

2.3 Open-loop Stochastic Linearization

Before examining stochastic linearization for the closed-loop LPNI system, it is useful to study the open loop case. Consider Figure 2.2, where $f(u)$ is a static nonlinearity with output v, and u is a zero-mean Gaussian process. According to stochastic linearization, the equivalent gain N is to be chosen to minimize the mean-square error, $E\left\{(v-\hat{v})^2\right\}$. The solution of this minimization problem can be obtained via a variational calculus argument [1], and the resulting linearized gain is given by the aforementioned expectation, i.e.,

$$N = E\left[\frac{d}{du}f(u)\right], \tag{2.2}$$

where it is assumed that the derivative exists except at a countable number of points. Below, (2.2) is evaluated for a few common instrumentation nonlinearities.

Saturation nonlinearity

Let $f(u)$ be the saturation function illustrated in Figure 2.3(a), described by

$$f(u) = sat_\alpha(u) = \begin{cases} \alpha, & u > +\alpha \\ u, & -\alpha \leq u \leq \alpha \\ -\alpha, & u < -\alpha. \end{cases} \tag{2.3}$$

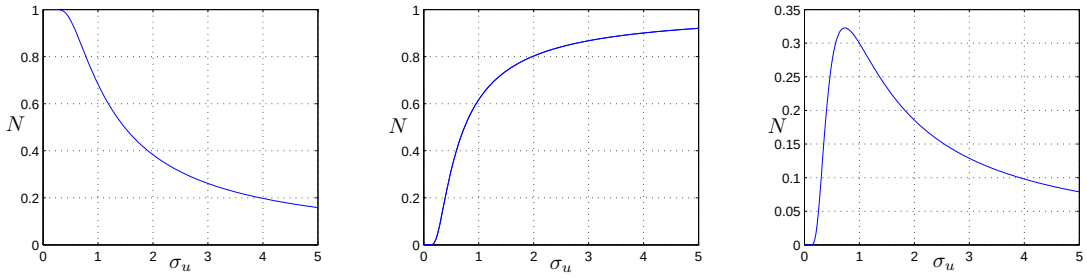

(a) Saturation (b) Deadzone (c) Saturation-deadzone

Figure 2.4: N as a function of σ_u for open-loop stochastic linearization

In this case, (2.2) becomes

$$\begin{aligned} N &= \int_{-\infty}^{\infty} \frac{d}{dx} sat_{\alpha}(x) \frac{1}{\sqrt{2\pi}\sigma_u} \exp\left(-\frac{x^2}{2\sigma_u^2}\right) dx \\ &= \int_{-\alpha}^{\alpha} \frac{1}{\sqrt{2\pi}\sigma_u} \exp\left(-\frac{x^2}{2\sigma_u^2}\right) dx \\ &= \operatorname{erf}\left(\frac{\alpha}{\sqrt{2}\sigma_u}\right), \end{aligned} \tag{2.4}$$

where

$$\operatorname{erf}(z) = \frac{2}{\pi} \int_0^z e^{-t^2} dt. \tag{2.5}$$

Thus, N is a function of the standard deviation σ_u of u, which is illustrated in Figure 2.4(a) for $\alpha = 1$. Note that, for this nonlinearity, N has an intuitive interpretation - it is the fraction of time that the signal u resides in the linear region of the saturation. Thus, as expected, N decreases monotonically as a function of σ_u.

Deadzone nonlinearity

Let $f(u)$ be the deadzone nonlinearity illustrated in Figure 2.3(b), described by

$$f(u) = dz_{\Delta}(u) = \begin{cases} u - \frac{\Delta}{2}, & u > +\frac{\Delta}{2} \\ 0, & -\frac{\Delta}{2} \leq u \leq \frac{\Delta}{2} \\ u + \frac{\Delta}{2}, & u < -\frac{\Delta}{2}. \end{cases} \tag{2.6}$$

Then,

$$\begin{aligned} N &= \int_{-\infty}^{\infty} \frac{d}{dx} dz_{\Delta}(x) \frac{1}{\sqrt{2\pi}\sigma_u} \exp\left(-\frac{x^2}{2\sigma_u^2}\right) dx \\ &= 1 - \int_{-\Delta/2}^{\Delta/2} \frac{1}{\sqrt{2\pi}\sigma_u} \exp\left(-\frac{x^2}{2\sigma_u^2}\right) dx \\ &= 1 - \operatorname{erf}\left(\frac{\Delta/2}{\sqrt{2}\sigma_u}\right), \end{aligned} \tag{2.7}$$

which is illustrated in Figure 2.4(b) for $\Delta = 1$. As expected, due to the deadzone, N increases as a function of σ_u.

Saturation-deadzone nonlinearity

Let $f(u)$ be the combination saturation-deadzone nonlinearity illustrated in Figure 2.3(c), described by

$$f(u) = satdz_{(\alpha,\Delta)}(u) = \begin{cases} \alpha, & u > +\alpha + \frac{\Delta}{2} \\ u - \frac{\Delta}{2}, & +\alpha + \frac{\Delta}{2} \geq u > +\frac{\Delta}{2} \\ 0, & -\frac{\Delta}{2} \leq u \leq \frac{\Delta}{2} \\ u + \frac{\Delta}{2}, & -\alpha - \frac{\Delta}{2} \leq u < -\frac{\Delta}{2} \\ \alpha, & u < -\alpha - \frac{\Delta}{2}. \end{cases} \tag{2.8}$$

Then,

$$\begin{aligned} N &= \int_{-\infty}^{\infty} \frac{d}{dx} satdz_{(\alpha,\Delta)}(x) \frac{1}{\sqrt{2\pi}\sigma_u} \exp\left(-\frac{x^2}{2\sigma_u^2}\right) dx \\ &= \int_{-\alpha-\frac{\Delta}{2}}^{\alpha+\frac{\Delta}{2}} \frac{1}{\sqrt{2\pi}\sigma_u} \exp\left(-\frac{x^2}{2\sigma_u^2}\right) dx - \int_{-\Delta/2}^{\Delta/2} \frac{1}{\sqrt{2\pi}\sigma_u} \exp\left(-\frac{x^2}{2\sigma_u^2}\right) dx \\ &= \operatorname{erf}\left(\frac{\alpha + \frac{\Delta}{2}}{\sqrt{2}\sigma_u}\right) - \operatorname{erf}\left(\frac{\Delta/2}{\sqrt{2}\sigma_u}\right), \end{aligned} \tag{2.9}$$

which is illustrated in Figure 2.4(c) for $\alpha = 1$, $\Delta = 1$. Due to the presence of both saturation and deadzone, the equivalent gain N is no longer monotonic in σ_u.

2.4 Closed-loop Stochastic Linearization

2.4.1 Basic assumptions

Figure 2.5 illustrates the general closed-loop LPNI configuration studied in this dissertation, and to which stochastic linearization is applied. It is interpreted as follows:

- $P(s)$ denotes an LTI model of the plant. Unless explicitly stated otherwise, this plant has all poles in the closed left half plane.
- $C(s)$ denotes an LTI controller. Unless explicitly stated otherwise, this controller has all poles in the closed left half plane.
- Unless explicitly stated otherwise, all roots of the characteristic function $1 + \gamma P(s)C(s)$ are in the open left half plane for $\gamma \in (0, 1]$.
- $f(\cdot)$ and $g(\cdot)$ denote static nonlinearities corresponding to actuator and sensor, respectively. For much of this dissertation, $f(\cdot)$ and $g(\cdot)$ are saturation nonlinearities of the form (2.3).
- $F_{\Omega_d}(s)$ and $F_{\Omega_r}(s)$ denote LTI coloring filters of $3dB$ bandwidth Ω_d and Ω_r, which generate Gaussian random processes d and r, respectively.
- w_r, w_d are independent, standard white noise excitations.

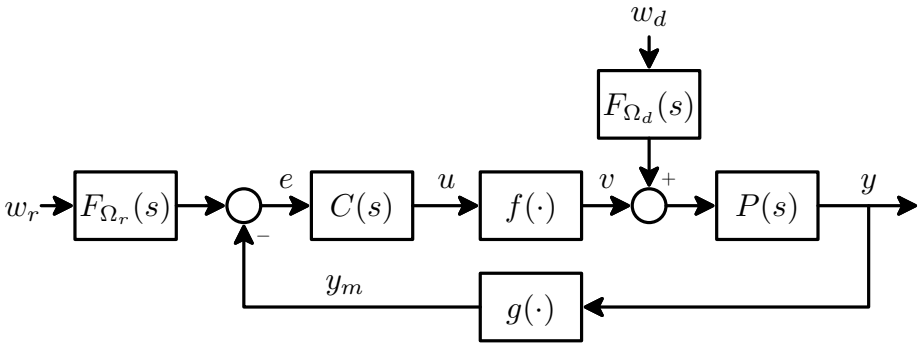

Figure 2.5: LPNI system subject to random excitations

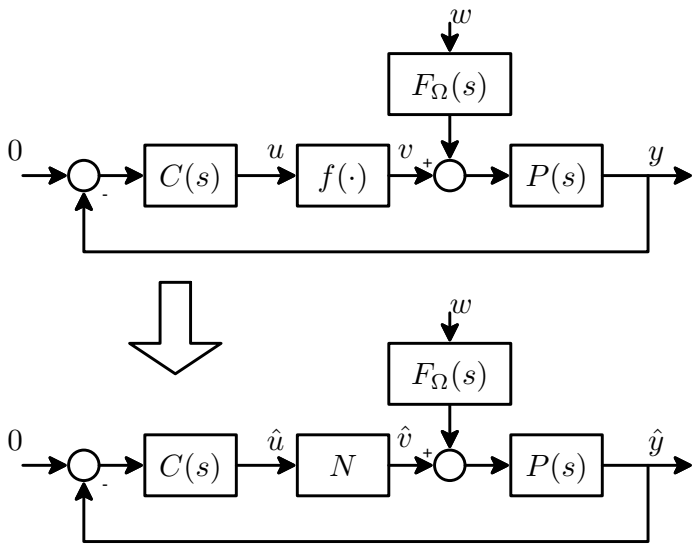

Figure 2.6: Closed-loop SL for LPNI system with nonlinear actuator only

- y, y_m, u, v, and e denote the plant output, sensor output, control signal, actuator output, and error signal, respectively.

2.4.2 Nonlinear actuator only

It is useful to begin by considering the LPNI system with nonlinear actuator and linear sensor, shown in Figure 2.6. Due to the closed loop nature, the distribution of u is difficult to obtain (it requires solution of the aforementioned Fokker-Planck equation), and hence, the expectation (2.2) cannot be evaluated. Thus, we make an approximation, and define the equivalent gain in terms of the quasilinear signal $\hat{u}$, i.e.,

$$N = E\left[\frac{d}{d\hat{u}} f(\hat{u})\right]. \tag{2.10}$$

The quasilinearization (2.10) is sub-optimal in the mean-square sense $E\left\{(v-\hat{v})^2\right\}$ for two reasons: (i) the distribution of u is non-Gaussian and (ii) consequently, the signals u and $\hat{u}$ are different. The first problem is mitigated by the fact that in most physical systems, the transfer function $P(s)$ provides low-pass filtering, i.e., the so-called *filter hypothesis*, which renders the signals u and y to be 'approximately'

Gaussian. This is elaborated upon in Section 2.5 below. Thus, we argue that u and $\hat{u}$ are 'close' in terms of their distributions, and the stochastically linearized system accurately predicts the behavior of the original LPNI system in terms of the variances of the signals $\hat{u}$, u, $\hat{y}$, y, etc.

In contrast to (2.2), the right hand side of (2.10) cannot be evaluated directly, since the distribution of $\hat{u}$ is itself a function of N. For example, in the system of Figure 2.6,

$$N = \int_{-\infty}^{\infty} \left[\frac{d}{dx} f(x)\right] \frac{1}{\sigma_{\hat{u}}\sqrt{2\pi}} \exp\left(-\frac{x}{2\sigma_{\hat{u}}^2}\right) dx, \tag{2.11}$$

where

$$\sigma_{\hat{u}} = \left\| \frac{F_\Omega(s)P(s)C(s)}{1 + P(s)NC(s)} \right\|_2, \tag{2.12}$$

and $\|\cdot\|_2$ denotes the 2-norm of a transfer function, understood as

$$\|H(s)\|_2 = \sqrt{\frac{1}{2\pi}\int_{-\infty}^{\infty} |H(j\omega)|^2 \, d\omega}. \tag{2.13}$$

Clearly, (2.11) can be rewritten as

$$N = \mathcal{F}\left(\left\| \frac{F_\Omega(s)P(s)C(s)}{1 + P(s)NC(s)} \right\|_2 \right), \tag{2.14}$$

where

$$\mathcal{F}(\sigma) = \int_{-\infty}^{\infty} \left[\frac{d}{dx} f(x)\right] \frac{1}{\sigma\sqrt{2\pi}} \exp\left(-\frac{x}{2\sigma}\right) dx. \tag{2.15}$$

Thus, N is a root of the equation

$$x - \mathcal{F}\left(\left\| \frac{F_\Omega(s)P(s)C(s)}{1 + xP(s)C(s)} \right\|_2 \right) = 0, \tag{2.16}$$

in the unknown x. Typically, this equation admits a unique solution, and thus, (2.10) defines N as an implicit function of $P(s)$, $C(s)$ and $F_\Omega(s)$. The case where the solution is not unique is discussed in Chapter III (Section 3.5).

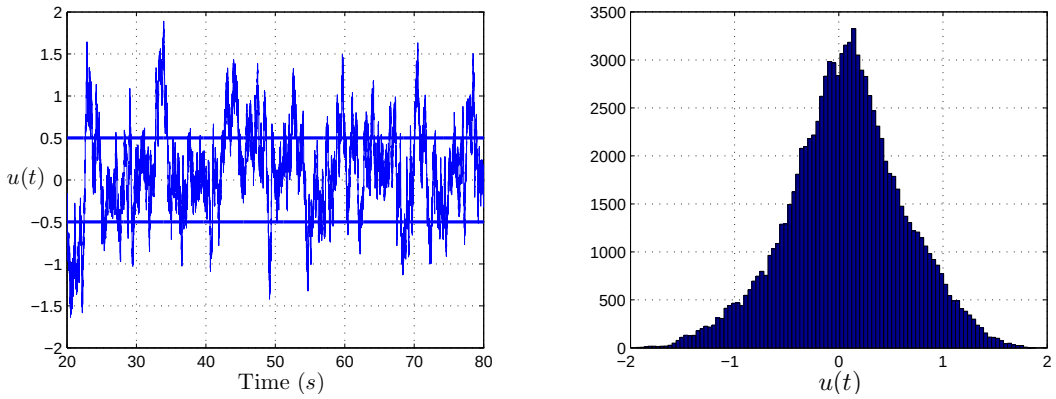

(a) Time trace of $u(t)$ (b) Histogram of $u(t)$

Figure 2.7: Time trace and histogram for Example 2.1

Closed-loop SL has particularly convenient properties when $f(\cdot)$ is the saturation nonlinearity (2.3). For this nonlinearity, $N \in [0, 1]$. Equation (2.16) becomes

$$x - \text{erf}\left(\frac{\alpha}{\sqrt{2}\left\|\frac{F_\Omega(s)P(s)C(s)}{1+xP(s)C(s)}\right\|_2}\right) = 0, \tag{2.17}$$

which, under the assumptions of Section 2.4.1, admits at least one solution in the interval $x \in [0, 1]$. This solution can be found to any accuracy using a standard bisection algorithm [99] (with initial conditions $x^- = 0$, $x^+ = 1$).

Example 2.1. Consider the system of Figure 2.6 where $P(s) = 1/(s+1)$, $F_\Omega(s) = 1$, $C(s) = 1$, and $f(\cdot) = sat_{0.5}(\cdot)$ from (2.3). For this system, (2.17) becomes

$$x - \text{erf}\left(\frac{0.5}{\sqrt{2}\left\|\frac{s+1}{s+1+x}\right\|_2}\right) = 0, \tag{2.18}$$

which has a unique solution $x = 0.6339$. Thus, the equivalent gain N that satisfies (2.10) is $N = 0.6339$, leading to $\sigma_{\hat{u}} = 0.5532$. Simulation of the LPNI system reveals that $\sigma_u = 0.5553$, which demonstrates the accuracy of stochastic linearization. Figure 2.7(a) illustrates a time trace of $u(t)$ in the LPNI system, noting that the saturation limits ± 0.5 are exceeded (i.e., the nonlinearity is activated) frequently. Despite this, as predicted, the histogram of $u(t)$, shown in Figure 2.7(b), is approximately Gaussian (a further discussion of this will follow in Section 2.5).

2.4.3 Nonlinear actuator and sensor

To illustrate SL in the case of both actuator and sensor nonlinearities, consider the SISO LPNI system of Figure 2.8. According to SL, the quasilinear gains are defined by

$$N_a = E\left[\frac{d}{d\hat{u}} f(\hat{u})\right], \tag{2.19}$$

$$N_s = E\left[\frac{d}{d\hat{y}} f(\hat{y})\right]. \tag{2.20}$$

Following the procedure of the previous section, we write

$$N_a = \mathcal{F}\left(\left\| \frac{F_\Omega(s)P(s)N_sC(s)}{1 + P(s)\,N_sC(s)\,N_a} \right\|_2\right), \tag{2.21}$$

$$N_s = \mathcal{G}\left(\left\| \frac{F_\Omega(s)P(s)}{1 + P(s)\,N_sC(s)\,N_a} \right\|_2\right), \tag{2.22}$$

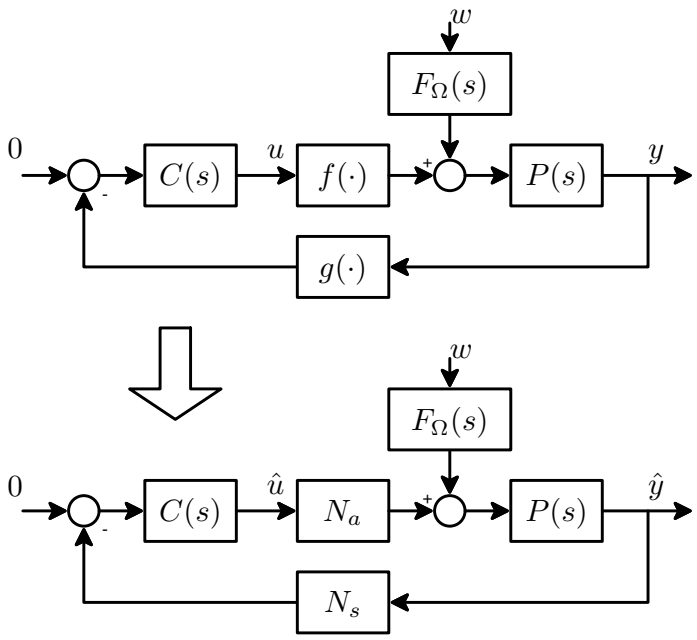

Figure 2.8: Closed-loop SL for LPNI system with nonlinear actuator and sensor

where

$$\mathcal{F}(\sigma) = \int_{-\infty}^{\infty} \left[\frac{d}{dx} f(x)\right] \frac{1}{\sigma\sqrt{2\pi}} \exp\left(-\frac{x}{2\sigma}\right) dx, \tag{2.23}$$

$$\mathcal{G}(\sigma) = \int_{-\infty}^{\infty} \left[\frac{d}{dx} g(x)\right] \frac{1}{\sigma\sqrt{2\pi}} \exp\left(-\frac{x}{2\sigma}\right) dx. \tag{2.24}$$

Accordingly, the task of finding the quasilinear gains N_a and N_s can be formulated as a 2-variable root-finding problem using the equations (2.21) and (2.22). Alternatively, since the system is SISO, an elimination procedure can be used to formulate an equivalent single-variable problem. Specifically, multiplying (2.21) and (2.22) results in

$$\hat{N} = \mathcal{F}\left(\left\| \frac{\mathcal{G}\left(\left\|\frac{F_\Omega(s)P(s)}{1+\hat{N}P(s)C(s)}\right\|_2\right) F_\Omega(s)P(s)C(s)}{1+\hat{N}P(s)C(s)} \right\|_2\right) \mathcal{G}\left(\left\| \frac{F_\Omega(s)P(s)}{1+\hat{N}P(s)C(s)} \right\|_2\right), \tag{2.25}$$

where $\hat{N} = N_a N_s$. Clearly, $\hat{N}$ is a root of the equation

$$x - \mathcal{F}\left(\left\| \frac{\mathcal{G}\left(\left\|\frac{F_\Omega(s)P(s)}{1+xP(s)C(s)}\right\|_2\right) F_\Omega(s)P(s)C(s)}{1+xP(s)C(s)} \right\|_2\right) \mathcal{G}\left(\left\| \frac{F_\Omega(s)P(s)}{1+xP(s)C(s)} \right\|_2\right) = 0, \tag{2.26}$$

in the unknown x. With $\hat{N}$ known, N_s is determined from (2.22). In turn, with $\hat{N}$ and N_s known, (2.21) determines N_a.

As described in the previous subsection, when $f(\cdot)$ and $g(\cdot)$ are saturation nonlinearities, $N_a \in [0,1]$ and $N_s \in [0,1]$, and thus, $\hat{N} \in [0,1]$. Moreover, under the assumptions of Section 2.4.1 the root-finding problem (2.26) has at least one solution in the interval $x \in [0,1]$. Thus, the equivalent gains can be found using a single-variable bisection on the left hand side of (2.26).

Example 2.2. Consider the LPNI system of Figure 2.8, with $P(s) = 1/(s+1)$, $F_\Omega(s) = 1$, $C(s) = 1$, $f(u) = sat_{0.5}(u)$, and $g(y) = sat_{0.5}(y)$.

For this system, (2.26) becomes

$$x - \operatorname{erf}\left(\frac{0.5}{\sqrt{2}\left\|\frac{\operatorname{erf}\left(\frac{0.5}{\sqrt{2}\left\|\frac{s+1}{s+1+x}\right\|_2}\right)}{s+1+x}\right\|_2}\right)\operatorname{erf}\left(\frac{0.5}{\sqrt{2}\left\|\frac{s+1}{s+1+x}\right\|_2}\right) = 0. \tag{2.27}$$

Using a bisection algorithm, it is possible to ascertain that $x = 0.5195$ is a solution of (2.27), and thus, the quasilinear gains satisfy $N_a N_s = 0.5195$. It follows immediately that $N_s = 0.6166$ and $N_a = 0.8428$.

2.4.4 Stochastic linearization in state-space representations

SL is readily applied when the system is formulated in state-space. For example, consider the SISO LPNI system of Figure 2.6 where the plant and actuator are given by

$$\begin{aligned} \dot{x} &= Ax + B_1 w + B_2 sat_\alpha(u) \\ y &= Cx, \end{aligned} \tag{2.28}$$

and the controller is the output-feedback

$$u = Ky.$$

Applying SL results in the quasilinear system

$$\begin{aligned} \dot{\hat{x}} &= (A + B_2 NKC)\hat{x} + B_1 w \\ \hat{u} &= K\hat{y} \\ \hat{y} &= C\hat{x}, \end{aligned} \tag{2.29}$$

where, as before,

$$N = \operatorname{erf}\left(\frac{\alpha}{\sqrt{2}\sigma_{\hat{u}}}\right). \tag{2.30}$$

It is well-known that, if $(A + B_2NKC)$ is Hurwitz,

$$\sigma_{\hat{u}}^2 = \text{tr}\left\{KCRC^TK^T\right\}, \tag{2.31}$$

where R is the unique positive semi-definite solution of the Lyapunov equation

$$(A + B_2NKC)R + R(A + B_2NKC)^T + B_1B_1^T = 0. \tag{2.32}$$

Thus, the quasilinear gain N is a root of the equation

$$x - \text{erf}\left(\frac{\alpha}{\sqrt{2}\sqrt{\text{tr}\left\{KCR(x)C^TK^T\right\}}}\right) = 0, \tag{2.33}$$

in the unknown x, where $R(x)$ satisfies

$$(A + xB_2KC)R(x) + R(x)(A + xB_2KC)^T + B_1B_1^T = 0. \tag{2.34}$$

Under the assumptions of Section 2.4.1, $R(x)$ is defined for every $x \in (0, 1]$, and can be obtained using well-known computational techniques. Indeed, in practice, this method is used the evaluate the 2-norms of the previous subsections. As before, bisection can be used to solve (2.33).

2.5 Accuracy of Stochastic Linearization

As mentioned in the Introduction, only a few studies have been completed on the accuracy of stochastic linearization in the closed loop environment. It was determined that, for many common systems, accuracy is very high [1, 8]. In this subsection, additional results are presented that reaffirm these findings.

2.5.1 Filter hypothesis

As described in Section 2.4.2, closed loop SL is justified by the filter hypothesis, i.e., that the lowpass filtering of $P(s)$ renders the signals u and y to be approximately

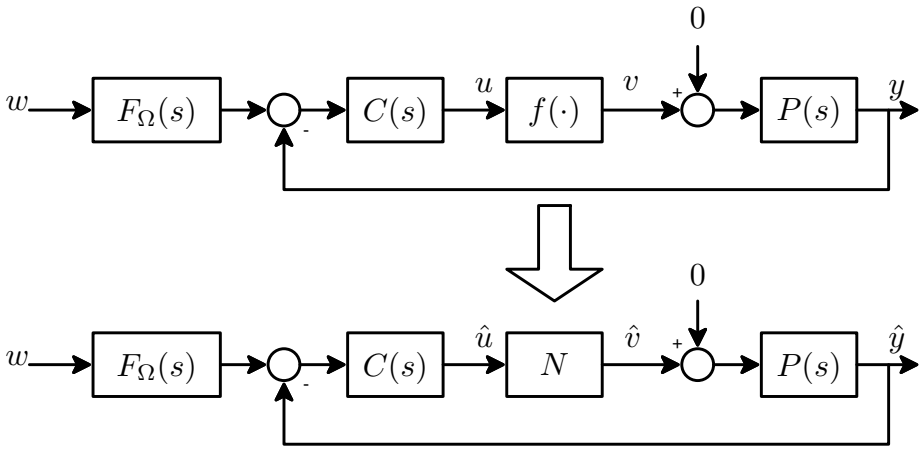

Figure 2.9: Closed-loop LPNI system to demonstrates the filter hypothesis

Gaussian. Consider the LPNI system illustrated in Figure 2.9, where

$$P(s) = \frac{1}{s+1}, F_\Omega(s) = 1, C(s) = 1, f(u) = sat_{10}(u).$$

For this system, stochastic linearization yields $N = 0.076$, which indicates that the actuator saturates almost always. The LPNI system is simulated for a sufficiently long duration and histograms are obtained of the signals v and y. These are illustrated in Figure 2.10, which also shows the probability density functions of $\hat{v}$ and $\hat{y}$ as obtained by stochastic linearization (recall that these are Gaussian). Clearly, the signal v is highly non-Gaussian, however, due to the filtering of $P(s)$, y becomes approximately Gaussian, coinciding well with the probability density function of $\hat{y}$.

This phenomenon is referred to as *Gaussianization*, and has been observed in numerous settings (see [100–102] and the references therein). Among the analytical characterizations are the following:

- In [100], the authors examine the output response of a first-order linear system excited by a random telegraph process (i.e., a binary process that takes the values ± 1, where the times between sign changes are independent and exponentially distributed). Gaussianization follows from showing that the moments of

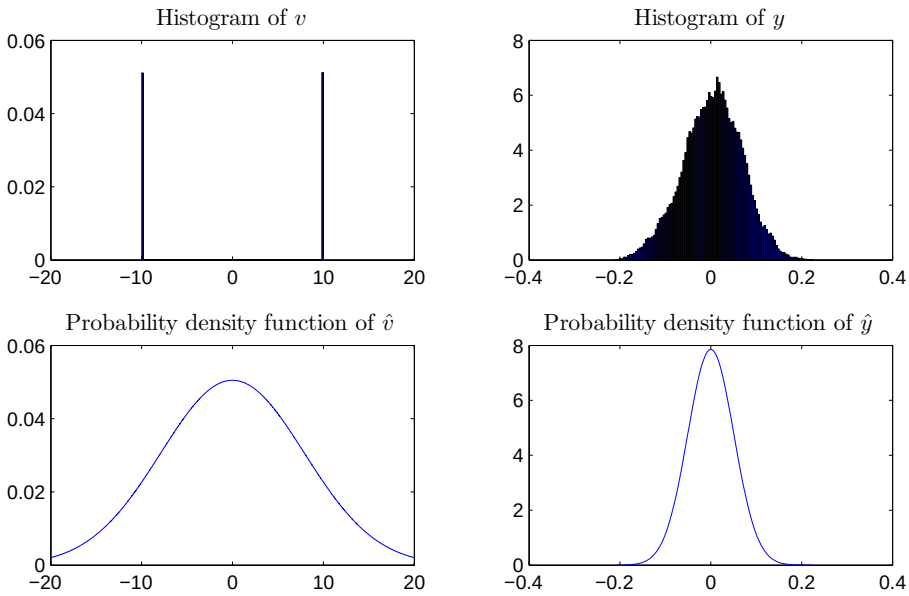

Figure 2.10: Histograms of v and y in comparison with the probability density functions of $\hat{v}$ and $\hat{y}$

the output tend to those of a Gaussian process.

- In [101], the authors explicitly solve the Fokker-Plank equation for a first-order linear system excited by a few specific classes of non-Gaussian excitation. Gaussianization is demonstrated by showing that the third and fourth central moments of the output tend to zero as the system bandwidth decreases.

- In [102], the author examines the output response of a linear system excited by a general stationary and/or delta correlated non-Gaussian random process. It is shown that, as the bandwidth of the linear system decreases, the high order *cumulants* [103] of the output tend to zero, which indicates that the output process becomes Gaussian.

Clearly, these examples of Gaussianization contribute to substantiating the filter hypothesis, which, as described above, supports the accuracy of stochastic linearization. This also suggests that SL may be inaccurate in those cases in which the plant

does not provide adequate low-pass filtering. However, since many controlled plants tend to be low-pass filtering, the SL method is justified as an accurate analysis tool for LPNI feedback control systems.

2.5.2 Numerical verification

To further illustrate the efficacy of stochastic linearization, the following Monte Carlo experiment is performed: Consider 3000 first and 2000 second order plants of the form:

$$P_1(s) = \frac{1}{Ts+1} \tag{2.35}$$

$$P_2(s) = \frac{\omega_n^2}{s^2 + 2\zeta\omega_n + \omega_n^2}. \tag{2.36}$$

The controller is $C(s) = K$, and the system parameters are randomly and equiprobably selected from the following

$$T \in [0.01, 10], \omega_n \in [0.01, 10], \zeta \in [0.05, 1], K \in [1, 20], \alpha \in (0.1, 1]. \tag{2.37}$$

Stochastic linearization is performed for each system, and the original nonlinear system is simulated to identify the approximation error, defined as:

$$e_{sl} = \frac{|\sigma_y - \sigma_{\hat{y}}|}{\sigma_{\hat{y}}}. \tag{2.38}$$

The histogram of e_{sl} is shown in Figure 2.11. Clearly, accuracy is very good - 71.4% of the systems yield $e_{sl} < 0.05$ and only 9.2% of systems yield $e_{sl} > 0.1$. Further analysis reveals that these latter cases occur when the signals u and y are highly non-Gaussian, and occur when either $T << 1$ or $\zeta << 1$ (i.e., when the plant is insufficiently low-pass).

2.6 Summary

The analysis of LPNI systems is complicated by the nonlinearities $f(\cdot)$ and $g(\cdot)$. The method of Jacobian linearization can be used to provide an approximation,

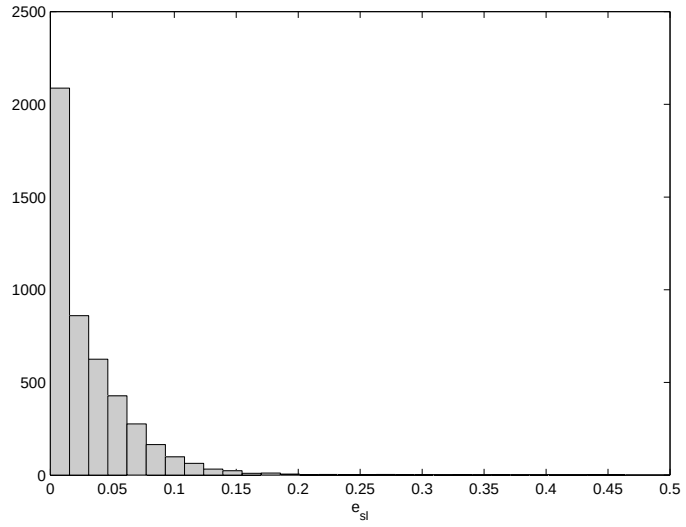

Figure 2.11: Histogram of e_{sl} for Monte Carlo accuracy experiment

however, it is only valid in some local operating region. In contrast, when the inputs are random, the method of stochastic linearization can be used to provide a global approximation of the LPNI system by replacing the nonlinearities with equivalent gains. These gains are defined as the expectations of the derivatives of $f(\cdot)$ and $g(\cdot)$, respectively, and hence, are functions of the system parameters and the exogenous input under consideration. The resulting system, referred to as quasilinear, can thus be used for analysis and design for the LPNI system. Under the filter hypothesis, i.e., the low-pass characteristic of the plant, stochastic linearization has been shown to be very high. This is corroborated by a Monte Carlo simulation involving a large number of randomly constructed closed-loop LPNI systems. Further examples on the accuracy of stochastic linearization will be presented in the subsequent chapters, which use SL to achieve the objectives formulated in Section 1.2.

CHAPTER III

TRACKING RANDOM REFERENCES: THE S-ROOT LOCUS

3.1 Introduction

Recall the following problem from the Introduction: How should a controller be designed so that the LPNI system, with a random reference signal, exhibits a high quality of tracking? In the case of deterministic (e.g., step) references, the root locus method is one of the best known tools for tracking controller design. However, for the problem posed above, it is insufficient for two reasons. First, it does not address tracking random references. This is important in certain applications, such as aerospace guidance [3], automotive navigation [104], and hard disk servo control [2]. Second, it fails to incorporate the effects of instrumentation, and in particular, the pervasive saturation nonlinearity. The present chapter in intended to overcome these limitations by extending, in a sense explained below, the root locus approach to LPNI systems with saturating actuators.

Consider the SISO tracking system of Figure 3.1. Here, $P(s)$ is the plant, $KC(s)$ is the controller, $K > 0$, and $F_\Omega(s)$ is a coloring filter with $3dB$ bandwidth Ω, which generates the reference r from standard white noise w_r; the signals y and u are,

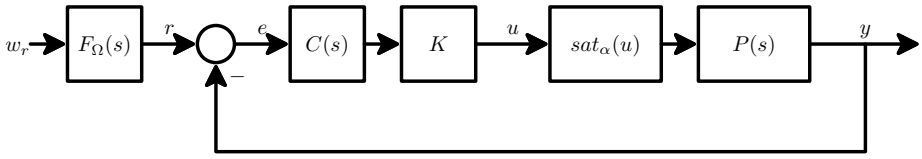

Figure 3.1: Closed loop system with saturating actuator

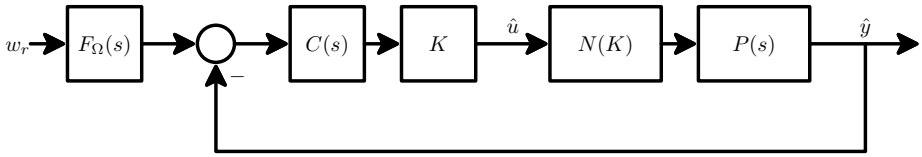

Figure 3.2: Equivalent quasilinear system

respectively, the system output and the input to the saturation element defined as

$$sat_\alpha(u) = \begin{cases} \alpha, & u > +\alpha \\ u, & -\alpha \leq u \leq \alpha \\ -\alpha, & u < -\alpha. \end{cases} \tag{3.1}$$

As described in Chapter II, stochastic linearization is used to study the system, whereby the saturation element is replaced by a gain, $N(K)$, defined as

$$N(K) = \operatorname{erf}\left(\frac{\alpha}{\sqrt{2}\left\|\frac{F_\Omega(s)KC(s)}{1+N(K)KC(s)P(s)}\right\|_2}\right). \tag{3.2}$$

Note that, in this case, the stochastically linearized gain is expressed as a function of the free parameter K. The value of $N(K)$ can be calculated from (3.2) using the standard bisection algorithm.

The locus traced by the closed loop poles of the quasilinear system of Figure 3.2 (referred to as *S-poles*) is called the *saturated root locus*, or S-root locus. It is the object of study in this chapter.

Denote the equivalent gain of the quasilinear system as

$$K_e(K) \triangleq KN(K). \tag{3.3}$$

Clearly, from (3.2), $K_e(K)$ can be obtained from the equation

$$K_e(K) = K\text{erf}\left(\frac{\alpha}{\sqrt{2}K\left\|\frac{F_\Omega(s)C(s)}{1+K_e(K)P(s)C(s)}\right\|_2}\right). \tag{3.4}$$

If $K_e(K) \to \infty$ as $K \to \infty$, the S-root locus may be the same as that of the feedback loop of Figure 3.1 in the absence of saturation (referred to as the *unsaturated* system). If, however, $K_e(K) < \infty$ as $K \to \infty$, the S-root locus terminates at points prior to the open loop zeros. It turns out that the latter may be the case, and in this chapter we show how these points, referred to as *S-termination points* can be calculated.

In addition, we investigate the relationship between the S-root locus and amplitude truncation of the reference signals. Clearly, this phenomenon does not arise in the unsaturated case. However, when the actuator is saturated, the trackable domain may be finite [54] and, as a result, sufficiently large reference signals might be truncated. To indicate when this phenomenon takes place, we equip the S-root locus with the so-called amplitude *S-truncation points*, and provide methods for their calculation. As it turns out, both the S-termination and S-truncation points depend on all transfer functions in Figure 3.1, as well as on the level of saturation α.

Although there are a large number of publications on saturating actuators (as mentioned in the Introduction, for instance, the recent monographs [23,105,106]), the root locus approach has not been investigated. Some intuitive recommendations for dealing with root locus under actuator saturation can be found in standard textbooks, for instance, in [107].

The outline of this chapter is as follows: Section 3.2 motivates the problem of tracking random references and establishes admissible domains in the s-plane where poles (and S-poles) should be placed to ensure a high quality of tracking. Section 3.3 introduces formal definitions of S-root locus, and classifies the scenarios considered.

Section 3.4 and 3.5 present methods of S-root locus construction when $K_e(K)$ is unique and non-unique, respectively, and an S-root locus design methodology is given. Section 3.6 discusses the issue of amplitude truncation, and Section 3.7 presents a method for calibrating the S-root locus. An application to a hard disk drive control problem is described in Section 3.8 and, finally, in Section 3.9, a summary is provided. All proofs are presented in Appendix A.

3.2 Tracking Random References

As with the classical root locus, it is first useful to identify admissible domains in the complex plane where closed loop poles should be placed to achieve a high quality of random tracking. Consider the prototype second order system described by

$$T(s) = \frac{\omega_n^2}{s^2 + 2\zeta\omega_n s + \omega_n^2}, \tag{3.5}$$

where ω_n and ζ are the natural frequency and damping ratio, respectively. Classical control theory defines admissible pole locations of (3.5) for tracking step references [108,109]. In some cases, however, random signals, rather than steps, must be tracked [2, 3, 104]. In these cases, using the step-based admissible pole domains may lead to overdesign. Therefore, for the purspose of design, it is necessary to quantify the admissible pole domains for random reference tracking with specified quality. To this end, using the so-called tracking quality indicators introduced in [53], this section characterizes where the closed loop poles should be located in the s-plane so that the tracking quality indicators are sufficiently small and, therefore, random reference tracking is of a high quality. It turns out that the resulting admissible domains are less restrictive than those for tracking steps, and, therefore, warrant consideration in control system design.

The development of the admissible domains is organized as follows: Section 3.2.1

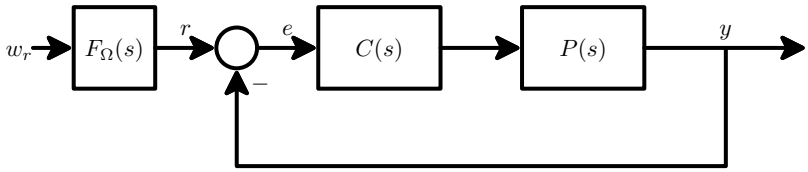

Figure 3.3: Tracking control system with a random reference

reviews the tracking quality indicators, Section 3.2.2 uses their level curves to construct admissible pole domains for the prototype second order system, and Section 3.2.3 extends the results to higher order systems. An application to a hard disk drive control problem is described in Section 3.2.4.

3.2.1 Random references and tracking quality indicators

System and references considered: Consider the closed loop SISO linear system shown in Figure 3.3, where

$$C(s)P(s) = \frac{\omega_n^2}{s\left(s + 2\zeta\omega_n\right)}, \tag{3.6}$$

and thus the closed loop transfer function from reference r to output y is (3.5).

For the purposes of this work, we assume that $F_\Omega(s)$ is a 3^{rd} order Butterworth filter with $3db$ bandwidth Ω, i.e.,

$$F_\Omega(s) = \sqrt{\frac{3}{\Omega}}\left(\frac{\Omega^3}{s^3 + 2\Omega s^2 + 2\Omega^2 s + \Omega^3}\right), \tag{3.7}$$

where the gain $\sqrt{3/\Omega}$ is introduced to ensure that $\sigma_r^2 = 1$, where σ_r^2 denotes the variance of r.

Remark 3.1. The approach developed here is applicable to any rational $F_\Omega(s)$. Moreover, if one uses higher order Butterworth filters, the results remain practically unchanged. Thus, for simplicity, we use $F_\Omega(s)$ defined by (3.33).

Random Sensitivity Function: The analysis that follows is based on the Random

Sensitivity Function introduced in [53], which is defined as

$$RS\left(\Omega,\omega_n,\zeta\right)=\sqrt{\frac{1}{2\pi}\int_{-\infty}^{\infty}\left|F_\Omega(j\omega)S(j\omega)\right|^2 d\omega}, \tag{3.8}$$

where $S(s)$ is the standard sensitivity function for the linear system in Figure 3.3, i.e.,

$$S\left(s\right)=\frac{s^2+2\zeta\omega_n s}{s^2+2\zeta\omega_n s+\omega_n^2}. \tag{3.9}$$

Note that $RS(\Omega,\omega_n,\zeta)$ is simply the standard deviation, σ_e, of the error signal e.

It is easy to see that RS depends not on Ω and ω_n separately, but on their ratio, i.e.,

$$RS\left(\Omega,\omega_n,\zeta\right)=RS\left(\frac{\Omega}{\omega_n},\zeta\right). \tag{3.10}$$

Indeed, using the substitution

$$\omega=\Omega\hat{\omega}, \tag{3.11}$$

expression (3.8) can be rewritten as

$$RS\left(\Omega/\omega_n\right)=\sqrt{\int_{-\infty}^{\infty}\frac{3}{2\pi}\left|\frac{\Psi\left(j\hat{\omega}\right)}{j\hat{\omega}^3+2j\hat{\omega}^2+2j\hat{\omega}+1}\right|^2 d\hat{\omega}}, \tag{3.12}$$

where

$$\Psi\left(j\hat{\omega}\right)=\frac{\rho^2 j\hat{\omega}^2+2\zeta\rho j\hat{\omega}}{\rho^2 j\hat{\omega}^2+2\zeta\rho j\hat{\omega}+1} \tag{3.13}$$

and

$$\rho=\frac{\Omega}{\omega_n}. \tag{3.14}$$

The quantity Ω/ω_n is referred to as the *dimensionless bandwidth*. Below, we denote the Random Sensitivity function either as $RS(\Omega)$ or as $RS(\Omega/\omega_n)$, depending on the issue at hand.

Tracking quality indicators - definitions: It is shown in [53] that the quality of random reference tracking is good if each of the following tracking quality indicators,

defined by $RS(\Omega)$, is sufficiently small:

$$I_1 = \lim_{\Omega \to 0} RS\left(\Omega\right), \tag{3.15}$$

$$I_2 = \frac{\Omega}{R\Omega_{BW}}, \tag{3.16}$$

$$I_3 = RM_r - 1, \tag{3.17}$$

where

$$R\Omega_{BW} = \min\left\{\Omega : RS\left(\Omega\right) = \frac{1}{\sqrt{2}}\right\}, \tag{3.18}$$

$$RM_r = \max_{\Omega} RS\left(\Omega\right). \tag{3.19}$$

The indicator I_1 describes the static unresponsiveness of the system. The indicator I_2 describes dynamics of the response; in particular, if it is large, it signifies the presence of lagging or oscillatory behavior. The indicator I_3 serves to discriminate between these two behaviors, and, in particular, characterizes the oscillatory features of the system output. Since the system under consideration is of Type 1, indicator $I_1 = 0$, which ensures that no degradation occurs due to static unresponsiveness. Therefore, we concentrate below on I_2 and I_3 only.

Tracking quality indicators - computation: Consider minimal state space realizations of $S(s)$ and $F_\Omega(s)$, given by

$$\mathcal{S} = \left[\begin{array}{c|c} A_{\mathcal{S}} & B_{\mathcal{S}} \\ \hline C_{\mathcal{S}} & D_{\mathcal{S}} \end{array}\right]$$

and

$$\mathcal{F}_\Omega = \left[\begin{array}{c|c} A_{\mathcal{F}}\left(\Omega\right) & B_{\mathcal{F}}\left(\Omega\right) \\ \hline C_{\mathcal{F}} & 0 \end{array}\right],$$

where the representation of $F_\Omega(s)$ is in observable canonical form, so that $C_\mathcal{F}$ is independent of Ω. Clearly,

$$\mathcal{SF}_\Omega = \left[\begin{array}{c|c} A^* & B^* \\ \hline C^* & D^* \end{array}\right],$$

where

$$A^* = \left[\begin{array}{c|c} A_\mathcal{F} & 0 \\ \hline B_\mathcal{S}C_\mathcal{F} & A_\mathcal{S} \end{array}\right], B^* = \left[\begin{array}{c} B_\mathcal{F} \\ \hline 0 \end{array}\right],$$
$$C^* = \left[\begin{array}{c|c} D_\mathcal{S}C_\mathcal{F} & C_\mathcal{S} \end{array}\right], D^* = 0.$$

Then, the Random Sensitivity Function can be computed as

$$\|F_\Omega S\|_2^2 = tr\left(C^* W C^{*T}\right), \tag{3.20}$$

where W is the solution of the Lyapunov equation

$$A^* W + W A^{*T} + B^* B^{*T} = 0. \tag{3.21}$$

Solving (3.21) analytically can be accomplished using standard symbolic manipulation software. This provides a means to analytically evaluate the indicators for various closed loop pole locations.

3.2.2 Admissible domains for random reference tracking by prototype second order system

As it follows from the above, the admissible pole domain for tracking random references is the intersection of two sets in the s-plane defined by the inequalities

$$I_2 \leq \gamma, \tag{3.22}$$

$$I_3 \leq \eta, \tag{3.23}$$

where γ and η are sufficiently small positive constants. Clearly, the boundaries of these sets are level curves of I_2 and I_3. Below, these level curves are constructed.

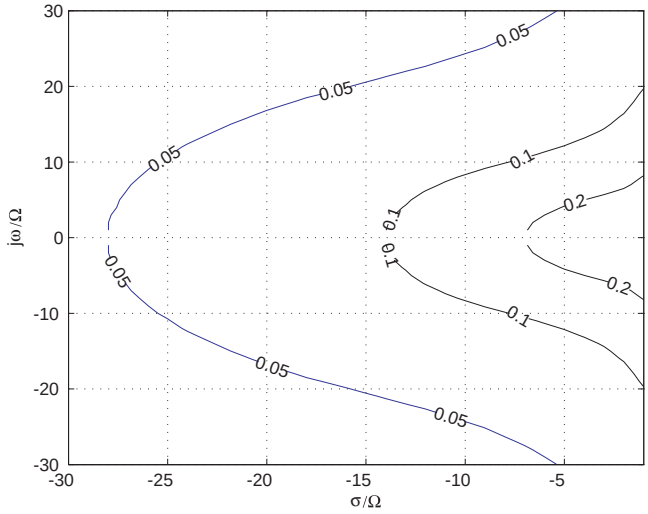

Figure 3.4: Level curves of I_2

Admissible domains from the point of view of I_2:

Assume that the closed loop transfer function (3.5) has poles $s_1, s_2 = \sigma \pm j\omega$, $\sigma < 0$. We are interested in studying the behavior of I_2 as σ and ω vary.

In order to make the level curves of I_2 independent of Ω, using the normalization introduced in Section 3.2.1, we view I_2 as a function of 'dimensionless' pole locations $(\sigma/\Omega) \pm j(\omega/\Omega)$. Figure 3.4 depicts these level curves, calculated using the method described in Section 3.2.1.

Thus, all poles located to the left of the curve $I_2 = \gamma$ result in acceptable tracking quality. It has been shown in [4] that $\gamma \leq 0.4$ generally leads to good behavior. Clearly, the smaller γ, the better the quality of tracking. Nevertheless, some amount of quality degradation always occurs and, as mentioned in subsection 3.2.1, can be due to either dynamic lagging or excessive oscillations. To prevent the latter, it is necessary to amend the admissible domain with a specification on I_3.

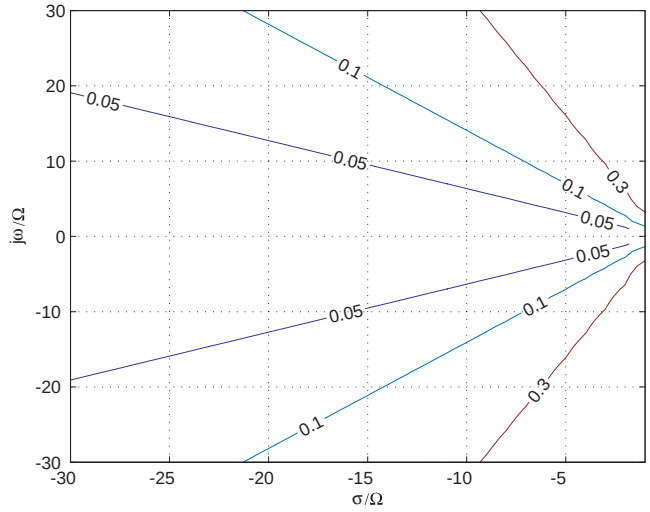

Figure 3.5: Level curves of I_3

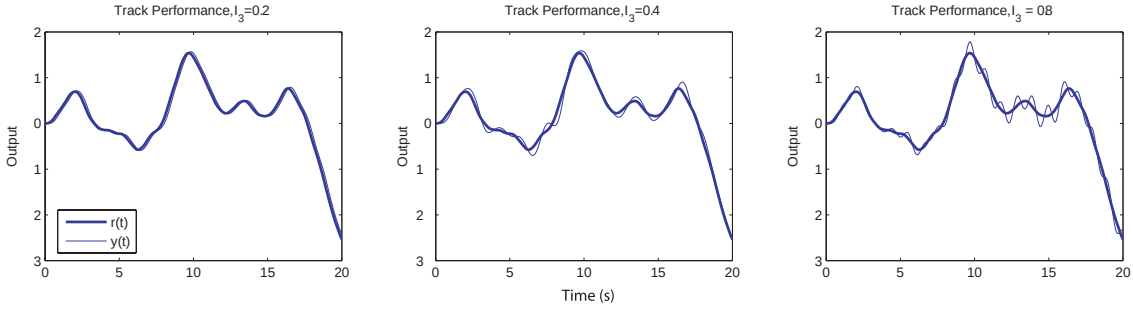

Figure 3.6: Tracking quality for various values of I_3, with $\sigma_e = 0.1$.

Admissible domains from the point of view of I_3:

Figure 3.5 presents the level curves of I_3 in the above normalized coordinates. Since these level curves are almost radial straight lines, it follows that, as the damping ratio ζ of the closed loop poles decreases, the value of I_3 increases. Such an increase implies the appearance of oscillations in the output response (see, for instance, Figure 3.6, which shows the tracking quality for various I_3 with the same error standard deviation $\sigma_e = 0.1$). Therefore, it is of importance to determine the values of η in (3.23), which lead to acceptable oscillatory properties of tracking. This can be accomplished by ensuring that the sensitivity function $S(s)$ does not amplify spectral

components beyond the input bandwidth Ω. For that purpose, a design rule can be inferred from the magnitude characteristic of $S(s)$ for the prototype second order system. We restrict $S(s)$ to a peak of no more than $5dB$, which corresponds to a value of $\zeta = 0.3$. This, in turn, corresponds to a value of $I_3 = 0.3$.

Complete admissible domain:

The complete admissible domain now becomes the intersection of the regions defined by

$$I_2 \leq \gamma, I_3 \leq \eta, \tag{3.24}$$

where $\gamma \leq 0.4$ and $\eta \leq 0.3$. For the reference signal with $\Omega = 1$ and for $\gamma = 0.1$ and $\eta = 0.3$, the complete admissible domain is illustrated in Figure 3.8. Of immediate note are the similarities between Figure 3.8 and the classical desired region for the tracking of step references [108, 109]. Indeed, the requirement on I_2 is analogous to the classical requirement on rise time, while that on I_3 can be correlated with percent overshoot. Nevertheless, quantitatively the two domains are different.

Remark 3.2. The above admissible domain has been obtained under the assumption that $\sigma_r = 1$, where σ_r is the standard deviation of the reference signal (see subsection 3.2.1). In general, however, σ_r may take arbitrary values. Clearly, due to linearity, the quality of tracking does not change relative to the magnitude of σ_r. Hence, the admissible domains constructed above remain valid for any σ_r.

Remark 3.3. Figure 3.7 illustrates the relationship between I_2 and σ_e when $\sigma_r = 1$ and $\zeta = 1$. Clearly, for $I_2 < 0.25$ this relationship is approximately linear. Repeating this numerical analysis for various ζ, it is possible to ascertain that, for $\sigma_e < 0.25$, if $I_2 = \gamma$, then the following takes place:

$$\sigma_e \leq \gamma \sigma_r. \tag{3.25}$$

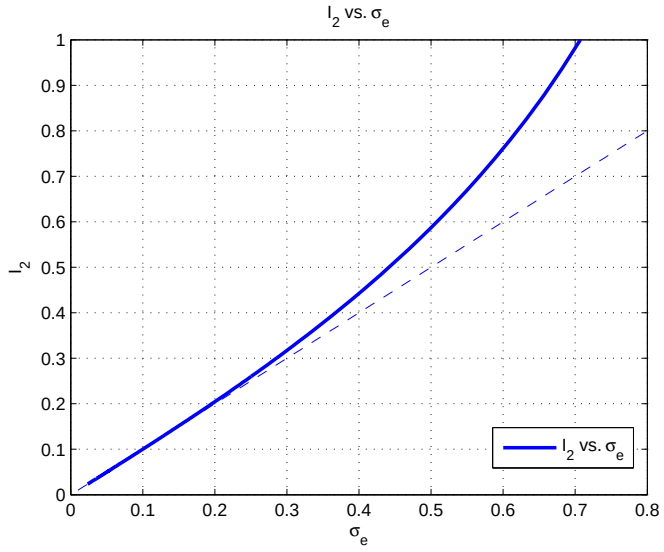

Figure 3.7: σ_e and corresponding I_2 values, $\sigma_r = 1$, $\zeta = 1$

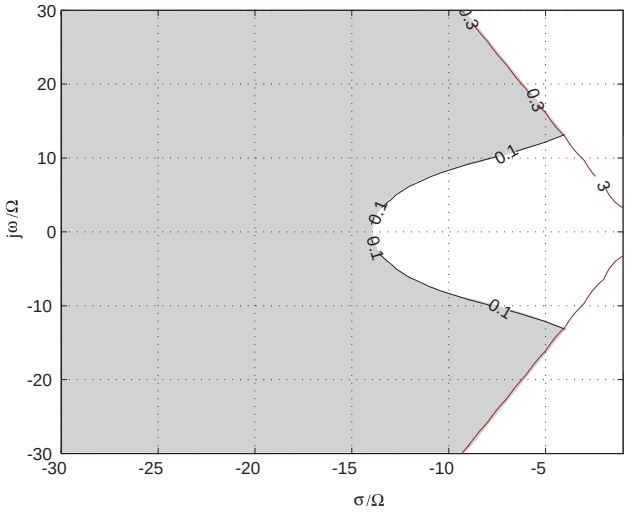

Figure 3.8: Admissible domain for $I_2 < 0.1$, $I_3 < 0.3$, $\Omega = 1$

Hence, $I_2 \leq \gamma$ implies that the standard deviation of the tracking error is at most $\gamma\sigma_r$.

3.2.3 Higher order systems

In classical controller design, it is often sufficient to consider a small number of dominant poles (and zeros) as a low order approximation to the full system dynamics.

Moreover, in many of these cases, it is sufficient to consider a single pair of dominant poles, yielding an approximation that is the prototype second order system. Generally, a valid low order approximation is constructed by attempting to satisfy the following condition as closely as possible [108]:

$$\frac{|S_H(j\omega)|^2}{|S_L(j\omega)|^2} \cong 1, \forall \omega > 0. \tag{3.26}$$

Here, $S_H(s)$ denotes the actual high order sensitivity function, while $S_L(s)$ is the low order approximation.

Under the assumption that (3.26) holds, it follows directly from (3.8) that

$$\frac{RS_H(\Omega)}{RS_L(\Omega)} \cong 1, \forall \Omega, \tag{3.27}$$

where $RS_H(\Omega)$ and $RS_L(\Omega)$ are the high and low order random sensitivity functions obtained from $S_H(s)$ and $S_L(s)$, respectively. Consequently, the indicators I_2 and I_3 are roughly equal for the high and low order models, and we conclude that the high order system exhibits a quality of random tracking that is similar to that of its low order approximation.

3.2.4 Example: Hard disk drive

One of the notable applications for random tracking is hard disk servo control [2]. Here, the control objective is to maintain the disk head above a circular track. Due to various sources of irregularity, these tracks tend to deviate from a perfect circle, and the deviations may be modelled as bandlimited Gaussian processes. The resulting problem is one of tracking a random reference, and we may use the admissible domains derived above to design an appropriate controller.

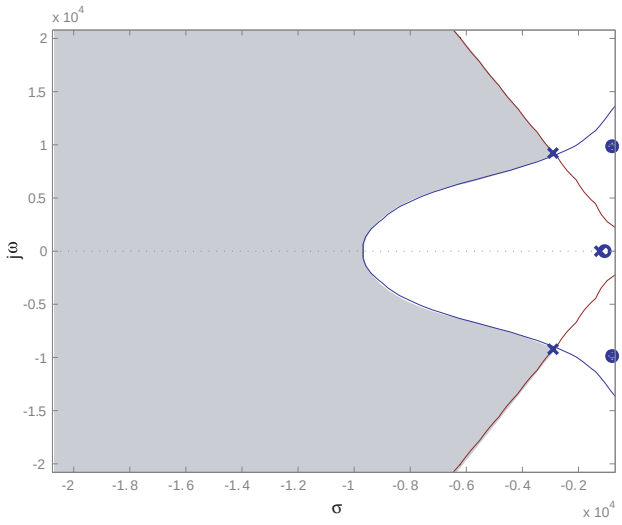

Figure 3.9: Admissible domain for the hard disk drive and pole-zero map of the closed loop system

The following performance specification was introduced in [53]:

$$\sigma_e \leq 0.06\sigma_r, \forall \Omega \leq 692 rad/s. \tag{3.28}$$

Thus, $\gamma = 0.06$, and from (3.25), we determine that to meet the specification we require $I_2 \leq 0.06$. Imposing the additional requirement that $I_3 \leq 0.3$, we obtain the admissible domain shown in Figure 3.9. Note that we have simply taken the normalized admissible domain from Figure 3.4 and scaled the coordinates by $\Omega = 692$. Based on this domain, we design a controller such that a pair of dominant poles is placed at:

$$s_1, s_2 = (-2.83 \pm j9.06) \times 10^3,$$

which lie approximately at the intersection of the $I_2 = 0.06$ and $I_3 = 0.3$ level curves.

In [53], a model was given for a disk servo as:

$$P_D(s) = \frac{4.382 \times 10^{10} s + 4.382 \times 10^{15}}{s^2 \left(s^2 + 1.596 \times 10^3 s + 9.763 \times 10^7\right)}. \tag{3.29}$$

By employing a standard root-locus based control design, using the above admissible domain, the following controller is obtained:

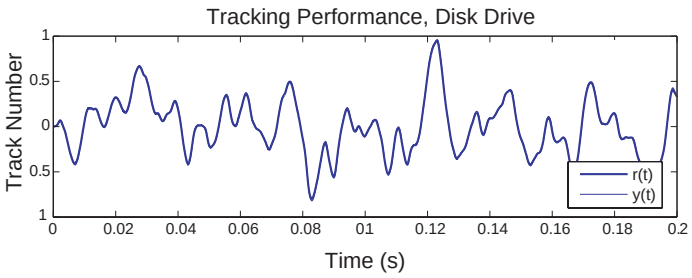

Figure 3.10: Tracking performance of the hard disk drive system

$$C(s) = \frac{K(s+1058)(s^2+1596s+9.763\times10^7)}{(s^2+3.719\times10^4 s+5.804\times10^8)^2}, \tag{3.30}$$

where

$$K = 5.7214\times10^5. \tag{3.31}$$

Applying this controller to $P_D(s)$, results in the closed loop pole-zero configuration shown in Figure 3.9. Note that this controller leads to a number of approximate stable pole-zero cancellations and, consequently, yields a pair of dominant poles at the desired locations. The resulting tracking error is $\sigma_e = 0.0425\sigma_r$, which satisfies the design specifications given in (3.28). Figure 3.10 illustrates the quality of tracking in the time domain, where the output completely overlays the reference signal.

It is interesting to compare $C(s)$ to the controller presented in [53]. In particular, in [53], a $5th$ order controller was designed using an $\mathcal{H}_\infty$ method, achieving an error variance of $\sigma_e = 0.056\sigma_r$. Clearly, we are able to exceed this performance with a $4th$ order controller using simple pole placement in an appropriately calculated admissible domain.

3.2.5 Using the admissible domains in LPNI systems

This section quantifies the admissible pole domains for tracking band-limited signals in linear systems. In particular, it is shown that level curves of the tracking quality indicators can be viewed as boundaries of admissible domains in the same

manner as rise time and overshoot are utilized for tracking steps. Based on the technique developed, it is possible to design controllers using classical techniques with demonstrably good performance. Most importantly, these domains will facilitate the design of similar controllers for the quasilinear system, thus achieving the main objective of this Chapter: random tracking in LPNI systems.

3.3 S-Root Locus: Definitions and Cases Considered

3.3.1 Definitions

Definition 3.4 (Saturated Closed Loop Poles)**.** The saturated closed loop poles (*S-poles*) of the nonlinear system of Figure 3.1 are the poles of the quasilinear system of Figure 3.2, i.e., the poles of the transfer function from r to $\hat{y}$:

$$T(s) = \frac{K_e(K)C(s)P(s)}{1 + K_e(K)C(s)P(s)}. \tag{3.32}$$

Typical of the method of stochastic linearization, the standard deviation of the tracking error, $\sigma_{\hat{e}}$, in the quasilinear system is close (generally within 10%) to the standard deviation, σ_e, of the original system with a saturating actuator [14]. For example, if

$$\begin{aligned} &P(s) = \tfrac{1}{s(s+1)}, C(s) = 1, \Omega = 1rad/s, \alpha = 0.05, \\ &K = 5, F_\Omega(s) = \sqrt{\tfrac{3}{\Omega}} \left(\tfrac{\Omega^3}{s^3+2\Omega s^2+2\Omega^2 s+\Omega^3} \right), \end{aligned} \tag{3.33}$$

it follows from (3.4) that $K_e(K) = 0.0399$ and $\sigma_{\hat{e}} = 0.999$, while simulation of the corresponding nonlinear system yields $\sigma_e = 0.986$ (i.e., an error of 2%). Additional examples can be found in [54]. Since $\sigma_{\hat{e}}$ is defined by the poles of $T(s)$, we conclude that these saturated closed loop poles characterize the tracking performance of the original system.

Definition 3.5 (S-Root Locus)**.** The S-root locus is the path traced by the saturated closed loop poles when $K \in [0, \infty)$.

Since $K_e(K)$ enters (3.32) as a usual gain, and

$$0 \leq K_e(K) \leq K,$$

the S-root locus is a proper or improper subset of the unsaturated root locus.

3.3.2 Cases of S-root loci considered

Define the auxilliary transfer function, $T_\gamma(s)$, as

$$T_\gamma(s) = \frac{F_\Omega(s)\, C(s)}{1 + \gamma P(s)\, C(s)}. \tag{3.34}$$

It turns out that the properties of the S-root locus depend on the properties of $T_\gamma(s)$ and the solutions of (3.4). Specifically, we consider two cases: (i) when (3.34) is stable for all $\gamma > 0$, and (ii) when (3.34) is stable only on a finite interval $\gamma \in [0, \Gamma)$, $\Gamma < \infty$, and

$$\lim_{\gamma \to \Gamma} \|T_\gamma(s)\|_2 = \infty. \tag{3.35}$$

Additionally, we consider cases where (3.4) has either a unique or multiple solutions. Accordingly, this work addresses four cases of S-root loci. These cases are indicated in Table 3.1, which also specifies the sections where they are addressed.

Table 3.1: Cases of S-root locus considered

	$T_\gamma(s)$ stable $\forall \gamma > 0$	$T_\gamma(s)$ stable only for $\gamma \in [0, \Gamma)$, $\Gamma < \infty$
$K_e(K)$ unique	Case 1, Section 3.4	Case 2, Section 3.4
$K_e(K)$ non-unique	Case 3, Section 3.5	Case 4, Section 3.5

3.4 S-Root Locus when $K_e(K)$ is Unique

As in the unsaturated case, we are interested in the points of origin and termination of the S-root locus. The points of origin clearly remain the same as in the unsaturated case. The points of termination, however, may not be the same because,

as it turns out, $K_e(K)$ may not tend to infinity as K increases. To discriminate between these two cases, we need the following equation

$$\beta - \left\| \frac{F_\Omega(s)\, C(s)}{1 + \left(\frac{\alpha\sqrt{2/\pi}}{\beta}\right) P(s)\, C(s)} \right\|_2 = 0, \tag{3.36}$$

in the unknown β. Note that, while (3.36) is always satisfied by $\beta = 0$, it may admit nonzero solutions as well. However, the uniqueness of $K_e(K)$ implies the uniqueness of solution of (3.36). Indeed, we have the following.

Lemma 3.6. *If $K_e(K)$ is unique for all K, then*

i) $K_e(K)$ is continuous and strictly monotonically increasing.

ii) Equation (3.36) admits at most one positive solution $\beta = \beta^* > 0$.

Theorem 3.7. *Assume that $T_\gamma(s)$ is stable for all $\gamma > 0$ and (3.4) admits a unique solution for all $K > 0$, i.e., Case 1. Then,*

$$\text{(i)} \lim_{K\to\infty} K_e(K) = \frac{\alpha\sqrt{2/\pi}}{\beta^*} < \infty \tag{3.37}$$

if and only if (3.36) admits a unique solution $\beta = \beta^* > 0$;

$$\text{(ii)} \lim_{K\to\infty} K_e(K) = \infty \tag{3.38}$$

if and only if $\beta = 0$ is the only real solution of (3.36).

Theorem 3.8. *Assume that $T_\gamma(s)$ is stable only for $\gamma \in [0, \Gamma)$, $\Gamma < \infty$, (3.35) holds, and (3.4) admits a unique solution for all $K > 0$, i.e., Case 2. Then,*

$$\lim_{K\to\infty} K_e(K) = \frac{\alpha\sqrt{2/\pi}}{\beta^*} < \Gamma, \tag{3.39}$$

where $\beta = \beta^* > 0$ is the unique positive solution of (3.36).

Note that (3.39) implies that, under the conditions of Theorem 3.8, the S-root locus can never enter the right half plane.

As it follows from Theorems 3.7 and 3.8, in the limit of $K \to \infty$, the quasilinear system of Figure 3.2 has a closed loop transfer function given by

$$T_{terminal}(s) = \frac{\kappa C(s) P(s)}{1 + \kappa C(s) P(s)}, \tag{3.40}$$

where

$$\kappa = \lim_{K \to \infty} K_e(K). \tag{3.41}$$

Definition 3.9 (S-Termination Points)**.** The S-termination points of the S-root locus are the poles of $T_{terminal}(s)$.

Thus, as $K \to \infty$, the S-poles travel monotically along the S-root locus from the open loop poles to the S-termination points. If $\kappa = \infty$, then the S-termination points coincide with the open loop zeros; otherwise, the S-root locus terminates prematurely.

Example 3.10. Consider the system of Figure 3.2 with

$$P(s) = \frac{s + 15}{s(s + 2.5)}, \alpha = 0.1, \tag{3.42}$$

and $C(s), \Omega$, and $F_\Omega(s)$ as defined in (3.33). It is straightforward to verify that, for this system, $T_\gamma(s)$ is stable for all $\gamma > 0$ and (3.4) admits a unique solution for $K > 0$, i.e., the conditions of Theorem 3.7 are satisfied. Since (3.36) admits a positive solution $\beta = 0.709$, (3.37) and (3.41) result in $\kappa = 0.1125$. Figure 3.11 shows $K_e(K)$ as a function of K. When K is small, we see that $K_e(K) \approx K$, since the actuator does not saturate. Clearly, as K increases, $K_e(K)$ indeed tends to the limit κ.

Figure 3.12 shows both the unsaturated and S-root locus for Example 3.10. Here, and in all subsequent figures, the S-termination points are indicated by small squares.

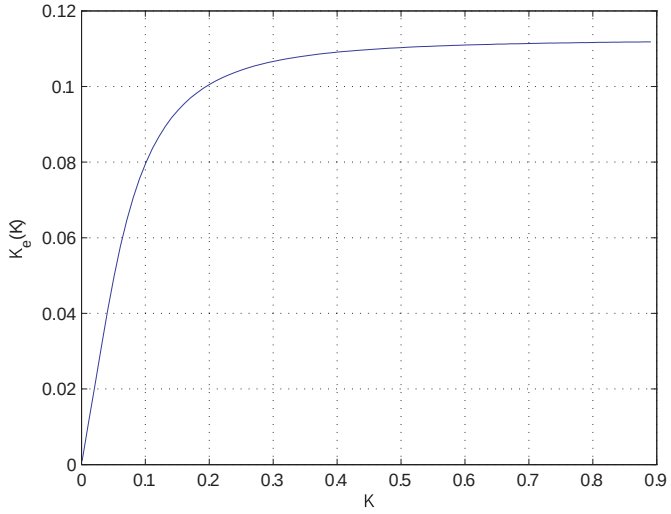

Figure 3.11: $K_e(K)$ as K tends to ∞ for Example 3.10 with $\alpha = 0.1$

The shaded area of Figure 3.12 represents the admissible domain for a high quality of tracking derived in [110]. Clearly, the S-root locus never enters the admissible domain, and the achievable tracking quality is limited by the S-termination points. Figure 3.13 shows the output of the nonlinear and quasilinear systems when $K = 150$ (i.e., when the saturated closed loop poles are located close to the S-termination points). Clearly, the tracking quality of the stochastically linearized system is poor due to dynamic lag. As predicted, the same is true for the original nonlinear system.

To improve the tracking performance, we increase α to 0.2. As illustrated in Figure 3.14, this causes the S-root locus to enter the admissible domain, and hence, choosing K large enough results in a high quality of tracking. This is verified in Figure 3.15, where we see that the quality of tracking is good for both the stochastically linearized and original nonlinear systems.

Example 3.11. Consider the system of Figure 3.2 with

$$P(s) = \frac{1}{s(s+1)(s+2)}, \alpha = 1, \tag{3.43}$$

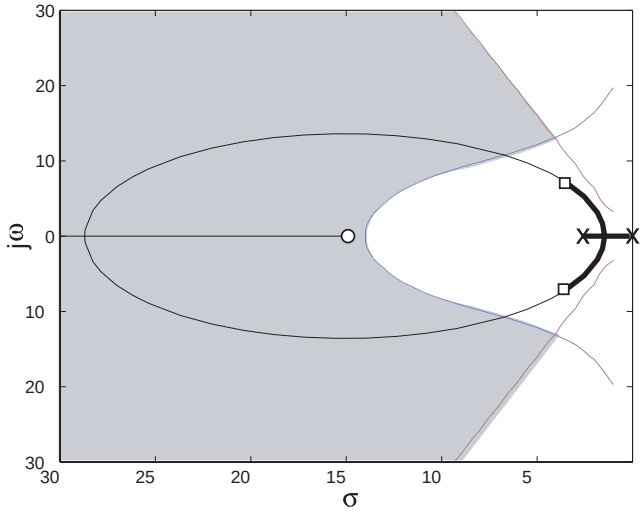

Figure 3.12: Unsaturated (thin line) and S-root locus (thick line) for Example 3.10 with $\alpha = 0.1$

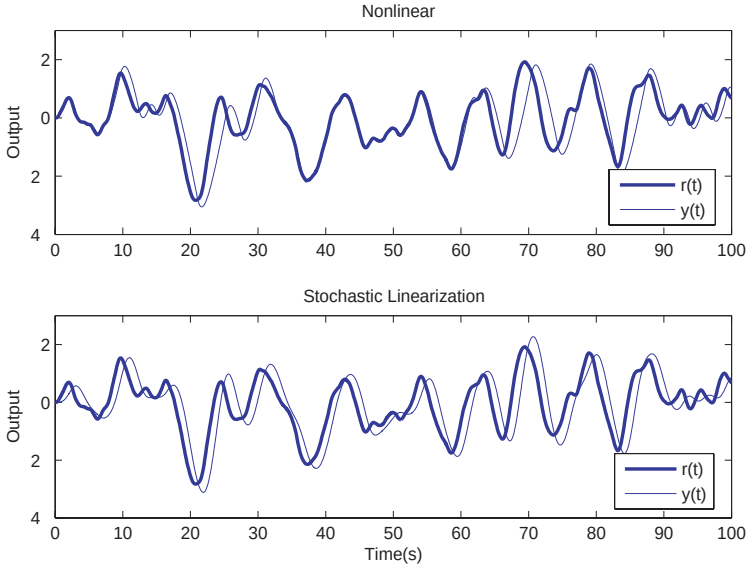

Figure 3.13: Tracking quality with S-poles located near the S-termination points ($K = 150$) for Example 3.10 with $\alpha = 0.1$

and $C(s), \Omega$, and $F_\Omega(s)$ as defined in (3.33). It is easily verified that $T_\gamma(s)$ is stable only for $\gamma \in [0, 5.96)$ and (3.4) has a unique solution for $K > 0$, i.e., the conditions of Theorem 3.8 are satisfied. Noting that $\beta = 1.1$ is the solution to (3.36), it follows from (3.39) and (3.41) that $\kappa = 0.722$. The resulting S-root locus, illustrated in Figure 3.16, never enters the right half plane.

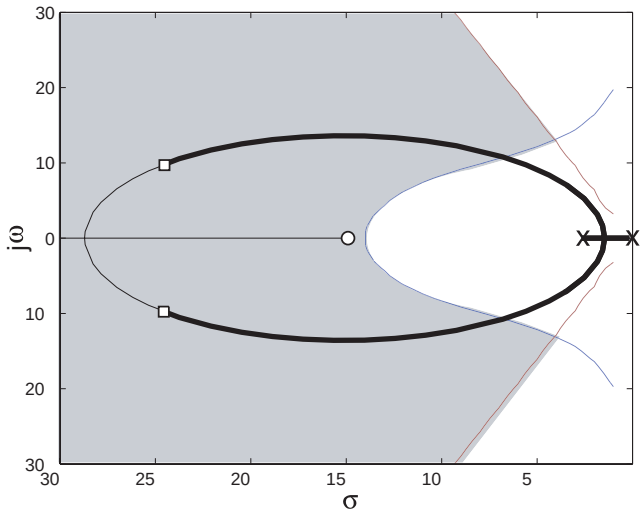

Figure 3.14: Unsaturated and S-root locus for Example 3.10 with $\alpha = 0.2$

3.5 S-Root Locus when $K_e(K)$ is Non-Unique

In some cases, (3.4) admits multiple solutions. To illustrate the complexities that arise in this situation, consider the following motivating example.

3.5.1 Example

Consider the system of Figure 3.1 defined by

$$P(s) = \frac{s^2 + 10s + 27.25}{s^2(s+5)}, \alpha = 0.4, \Omega = 1.1 rad/s, K = 5, \tag{3.44}$$

with $C(s)$ and $F_\Omega(s)$ as in (3.33). Figure 3.17 illustrates the left and right hand sides of (3.4) for this system, where it is clear that three solutions exist:

$$K_e^{(1)} = 0.1283, K_e^{(2)} = 1.0153, K_e^{(3)} = 4.35. \tag{3.45}$$

We are interested in the behavior of these solutions not only for $K = 5$, but for all $K > 0$. Accordingly, Figure 3.18 shows $K_e(K)$ as a function of K for the above example, from which a number of important observations can be made:

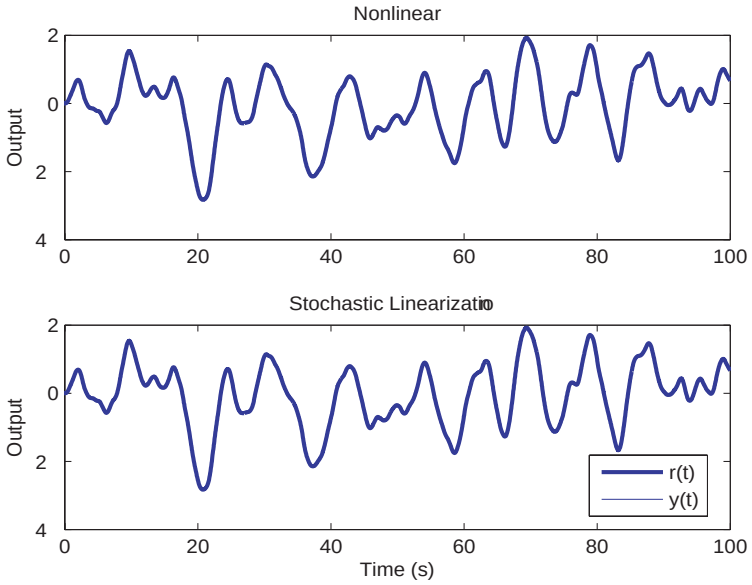

Figure 3.15: Tracking quality with poles located near the S-termination points ($K = 150$) for Example 3.10 with $\alpha = 0.2$

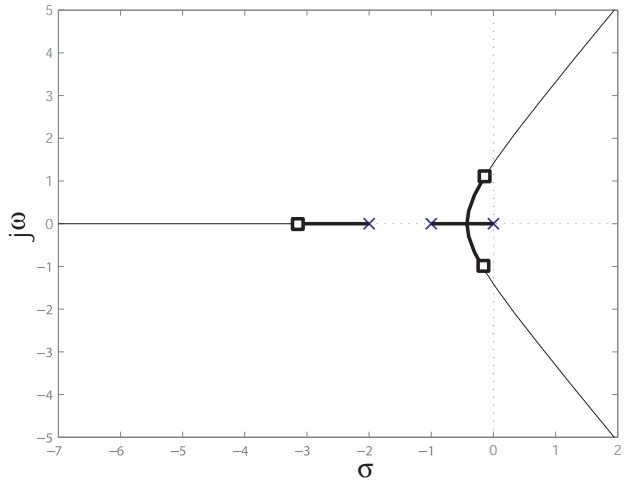

Figure 3.16: Unsaturated and S-root locus for Example 3.11

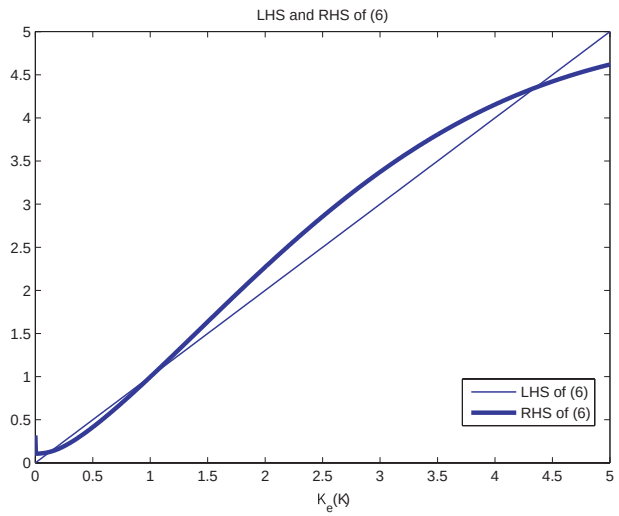

Figure 3.17: Left and right hand sides of (3.4) for the system defined in (3.44)

- For $K < 2.55$, the solution of (3.4) is unique; multiple solutions exist for all $K \geq 2.55$.

- As $K \to \infty$, three possible limiting values of $K_e(K)$ occur:

$$\kappa_1 = 0.1285, \kappa_2 = 1.0154, \kappa_3 = \infty. \tag{3.46}$$

  Thus, the S-root locus has three different S-termination points.

- At $K = 2.55$, the S-root locus has an *S-origination point*, corresponding to the appearance of two additional solutions.

- The range of $K_e(K)$ excludes the open interval between κ_1 and κ_2, that is, $(0.1285, 1.0154)$.

The branches of Figure 3.18 imply the following phenomenology of S-poles behavior for the system of Figure 3.1. For $K < 2.55$, there exists a unique set of three S-poles, and the closed loop behaves accordingly. For $K > 2.55$, there are three sets of S-poles, and due to the stochastic nature, the system behavior can be characterized as jumping from one of these sets to another. It could be argued that the set of

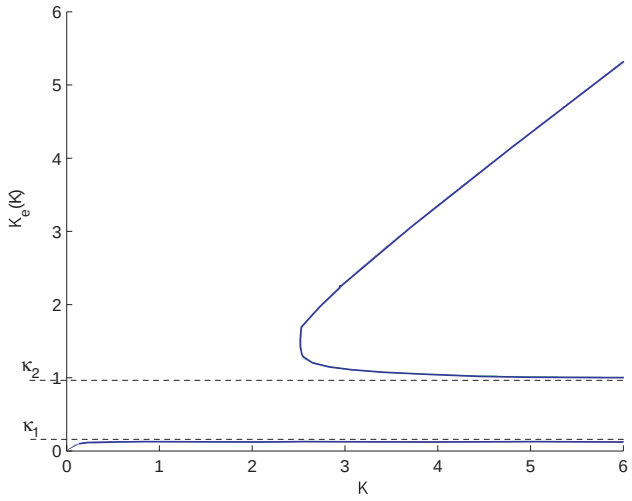

Figure 3.18: $K_e(K)$ as a function of K for the system defined in (3.44)

S-poles defined by the negative slope branch of Figure 3.18 does not correspond to a sustainable steady state, and therefore, the jumping phenomenon occurs between the poles defined by the positive slope branches of Figure 3.18.

To substantiate this phenomenology, consider the system of Figure 1 defined by (3.44). As mentioned before, this system leads to three values of $K_e(K)$ (defined in (3.45)) and, therefore, to three corresponding values of the steady state standard deviation of error:

$$\sigma_{\hat{e}}^{(1)} = 2.49, \sigma_{\hat{e}}^{(2)} = 0.31, \sigma_{\hat{e}}^{(3)} = 0.053. \tag{3.47}$$

Since the value of $\sigma_{\hat{e}}^{(2)}$ corresponds to $K_e(K)$ on the negative slope branch of Figure 3.18, it is expected that the closed loop system exhibits jumping between $\sigma_{\hat{e}}^{(1)}$ and $\sigma_{\hat{e}}^{(3)}$. To illustrate this behavior we simulate the system at hand for $10,000$ seconds and examine the standard deviation over a 100 second moving window. The results are shown in Figure 3.19. As one can see, the 'simulated standard deviation', $\tilde{\sigma}_{\hat{e}}$, jumps roughly between the values of 0.05 and 2.5. This corroborates the described phenomenology.

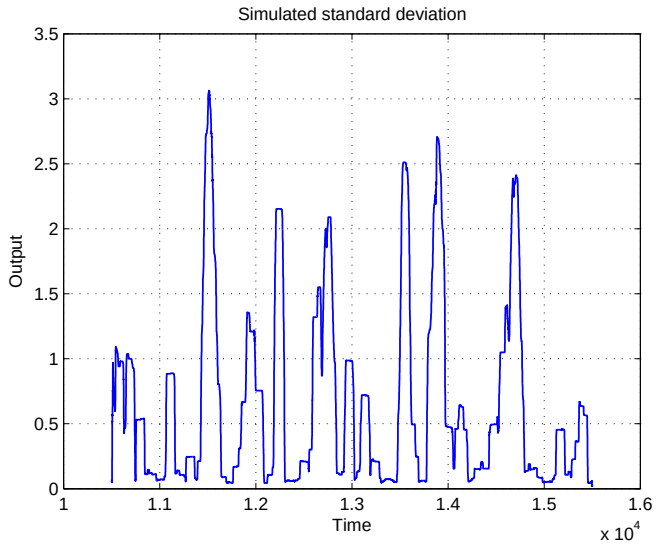

Figure 3.19: Simulated standard deviation, $\tilde{\sigma}_{\hat{e}}$, for the system defined in (3.44)

These features give rise to the S-root locus illustrated in Figure 3.20, where the arrows indicate the movement of the S-poles as K increases. The S-termination points are denoted, as before, by the squares, while the S-origination points are indicated by strikes orthogonal to the root locus. The parts of the S-root locus corresponding to the jumping phenomenon are indicated by broken lines. The insets of Figure 3.20 are intended to clarify the S-root locus in the vicinity of the S-termination points. Note that the S-root locus does not contain the parts of the unsaturated root locus corresponding to $K_e(K) \in (0.1283, 1.0153)$. Thus, the S-root locus for this system differs from the unsaturated case in the following:

- It contains areas of uncertain behavior due to the jumping phenomenon.
- It is only a proper subset of the unsaturated root locus, missing an intermediate portion.

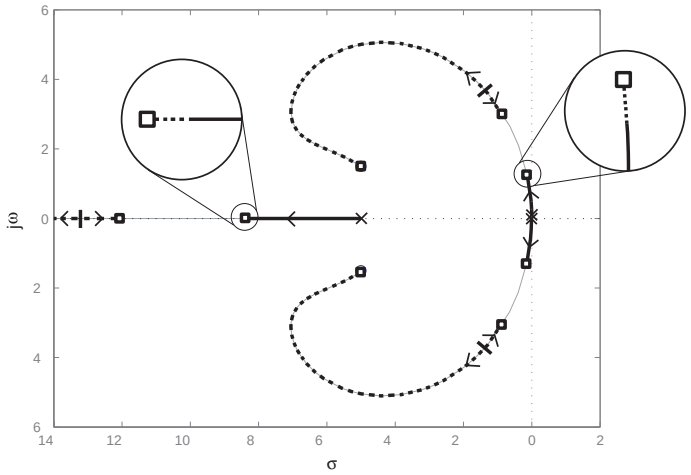

Figure 3.20: S-root locus for the system defined in (3.44)

3.5.2 General analysis of systems with non-unique $K_e(K)$

It is, of course, desirable to formulate general results pertaining to the multiple solutions case. Although the complexities outlined above lead to analytical difficulties, some useful deductions can be made.

Theorem 3.12. *Assume that* (3.4) *has multiple solutions, and the only solution of* (3.36) *is* $\beta = 0$. *Then:*

i) The S-root locus coincides with the unsaturated root locus, parameterized by $K_e(K)$ *rather than* K.

ii) There exists an S-origination point, implying that there is a range of K *for which the jumping phenomenon takes place.*

As an illustration of Theorem 3.12, consider the system of (3.44), with $\alpha = 0.53$. In this case, (3.36) admits a unique solution $\beta = 0$, but $K_e(K)$ is non-unique for some K (see Figure 3.21). The resulting S-root locus is shown in Figure 3.22.

Theorem 3.13. *Assume that* (3.4) *has multiple solutions, and, along with* $\beta_0 = 0$,

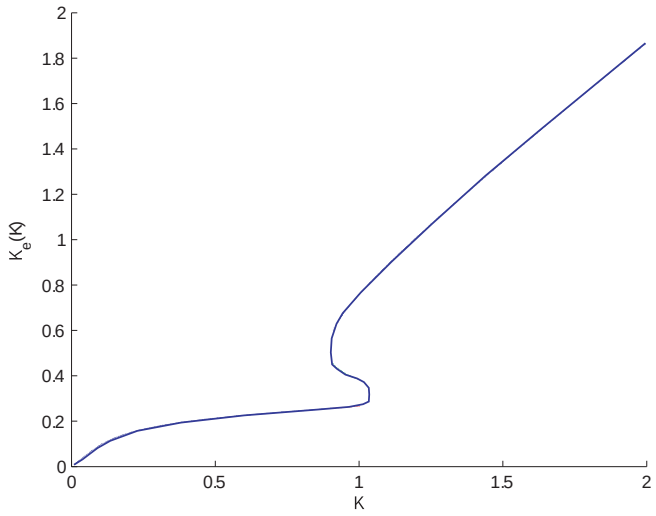

Figure 3.21: $K_e(K)$ as K tends to infinity for the system defined in (3.44) with $\alpha = 0.53$

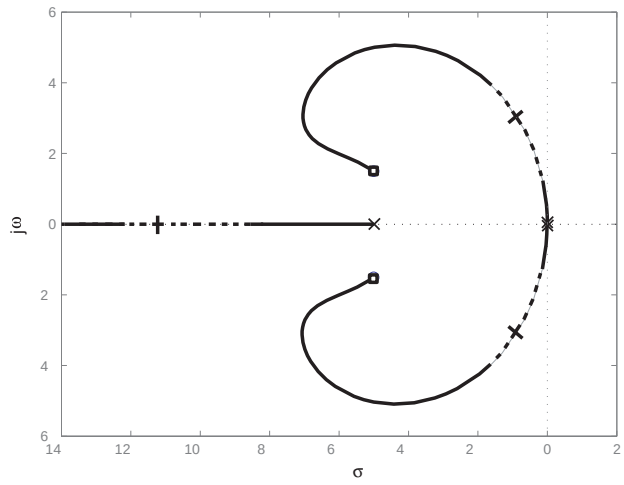

Figure 3.22: S-root locus for the system defined in (3.44) with $\alpha = 0.53$

(3.36) *admits solutions* $\beta = \beta_i > 0$, $i = 1, 2, ..., n$. *Then:*

i) Each β_i *corresponds to an S-termination point defined by*

$$\kappa_i = \frac{\alpha\sqrt{2/\pi}}{\beta_i}, \tag{3.48}$$

and (3.40).

ii) If n *is even, then the solution* $\beta_0 = 0$ *also gives a termination point, defined by* $\kappa_0 = \infty$.

iii) Assume that (3.36) *admits at least one simple positive solution. Then the S-root locus is a proper subset of the unsaturated root locus.*

The motivating example (3.44) can be viewed as an illustration of Theorem 3.13.

3.5.3 Approach to controller design for non-unique $K_e(K)$

As discussed above, a closed loop system with a controller $C(s)$, which leads to multiple solutions of (3.4), exhibits quite a complex behavior. Indeed, the random 'jumping' from one set of closed loop S-poles to another, results in different tracking errors on different time intervals. Although it is possible to evaluate the residence time [111] in each set of closed loop S-poles and then estimate the 'average' value of the tracking error, this value, even when small, would not necessarily guarantee good system performance for all time intervals.

Therefore, we propose a design methodology intended to avoid multiple solutions of (3.4). To accomplish this, we propose to select, if possible, a controller $C(s)$, which results in a unique $K_e(K)$ for all $K > 0$, and then select K so that the closed loop S-poles are at the desired locations. A question arises as to when such a $C(s)$ does exist. The answer is as follows:

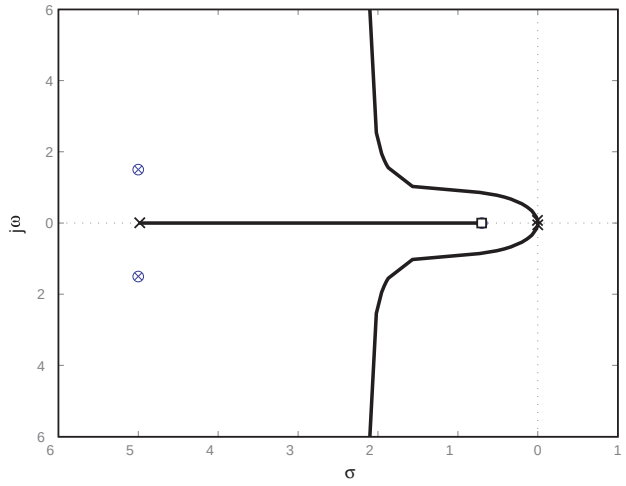

Figure 3.23: S-root locus for the system defined in (3.44) with $C(s)$ as in (3.49)

Theorem 3.14. *If $P(s)$ is stable and minimum phase, and $F_\Omega(s)/P(s)$ is strictly proper, there exists $C(s)$ such that the solution of (3.4) is unique for all $K > 0$.*

For the example system (3.44), selecting

$$C(s) = \frac{s + 0.7}{s^2 + 10s + 27.25}, \tag{3.49}$$

results in a unique $K_e(K)$ (with $\kappa = \infty$, as per Theorem 3.7). The resulting S-root locus is illustrated in Figure 3.23.

In the remainder of the chapter, we will assume that $K_e(K)$ is unique for all K.

3.6 S-Root Locus and Amplitude Truncation

In the previous sections we have used the S-root locus to characterize the dynamics of systems with saturating actuators. However, the performance may be poor not only due to the location of S-poles, but also due to output truncation by the saturation. Accordingly, in this section we introduce and compute S-truncation points, which characterize the region of the S-root locus where truncation does not occur. To accomplish this we use the notion of trackable domain introduced in [54].

The trackable domain, TD, is defined by the magnitude of the largest step input that can be tracked in the presence of saturation. For the system of Figure 3.1, it is defined as [54]:

$$TD = \left| \frac{1}{KC\left(0\right)} + P\left(0\right) \right| \alpha, \tag{3.50}$$

where $C(0)$ and $P(0)$ are the DC gains of the controller and plant respectively. Clearly, the trackable domain is infinite when $P(s)$ has at least one pole at the origin; otherwise, it is finite, assuming that $C(0) \neq 0$. Although (3.50) is based on step signals, it has been shown in [54] that TD can also be used to characterize the tracking quality of random signals. In particular, in [54], a tracking quality indicator was introduced to account for the finite trackable domain vis-à-vis the size of the signal to be tracked. This indicator was defined as

$$I_0 = \frac{\sigma_r}{TD}, \tag{3.51}$$

where σ_r is the standard deviation of the reference signal. Specifically, when $I_0 < 0.4$, tracking practically without output truncation is possible, whereas for $I_0 > 0.4$ it is not. To formalize this threshold, and keeping in mind that TD is monotonically decreasing in K (and therefore, I_0 is monotically increasing), we introduce the following definition.

Definition 3.15 (S-truncation point)**.** The S-truncation points are defined as the poles of

$$T_{tr}\left(s\right) = \frac{K_{tr}C(s)P(s)}{1 + K_{tr}C\left(s\right)P\left(s\right)}, \tag{3.52}$$

where

$$K_{tr} = K_e\left(K_{I_0}\right) \tag{3.53}$$

and

$$K_{I_0} = \min\left\{K > 0 : I_0 > 0.4\right\}. \tag{3.54}$$

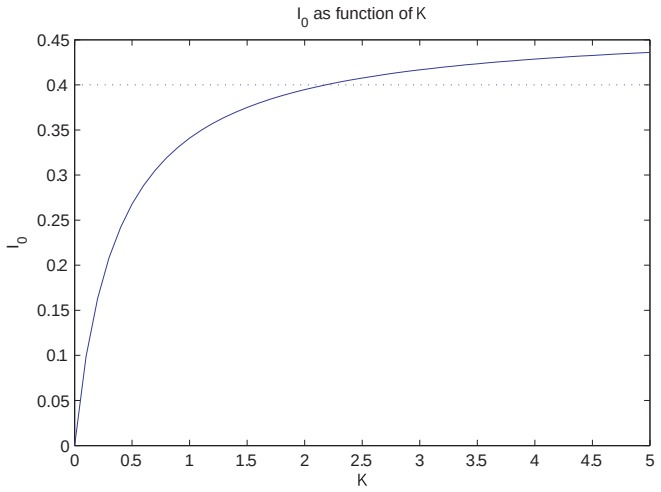

Figure 3.24: I_0 as a function of K for Example 3.16

Note that when $P(s)$ has a pole at the origin, $I_0 = 0$, and the S-root locus has no S-truncation points. To illustrate the utility of S-truncation points, consider the following example.

Example 3.16. Consider the system of Figure 3.1 defined by

$$P(s) = \frac{s+20}{(s+15)(s+0.5)}, C(s) = 1, \alpha = 0.8, \Omega = 1,$$

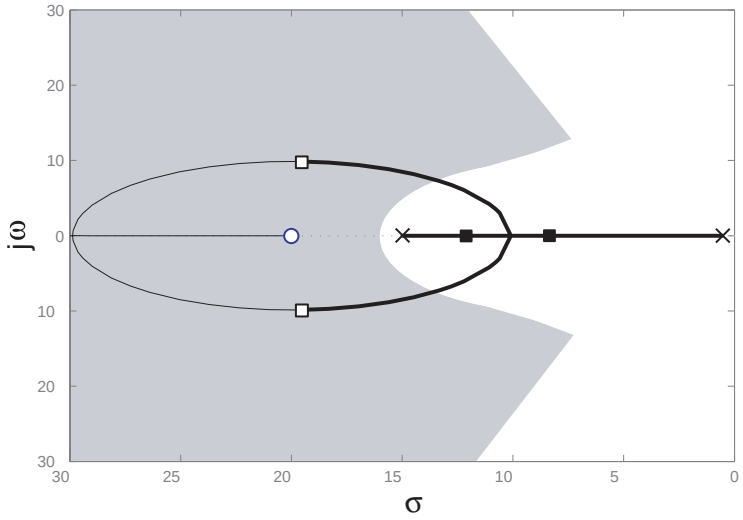

Figure 3.25: S-root locus for Example 3.16 with $\alpha = 0.8$

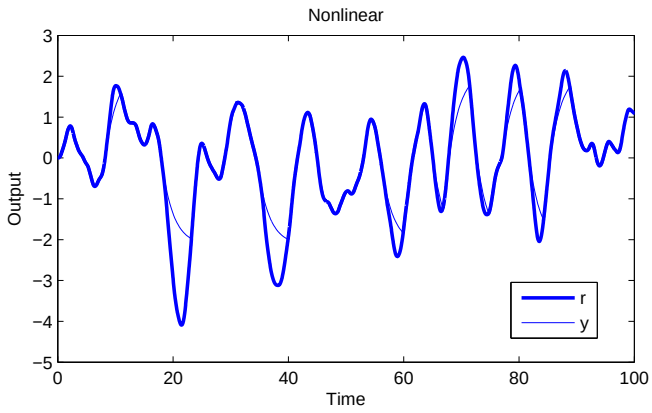

Figure 3.26: Tracking quality when $K = 20$ for Example 3.16 with $\alpha = 0.8$

and $F_\Omega(s)$ as in (3.33). As obtained from Theorem 3.7, the limiting gain of this system is $\kappa = 20.015$ (the S-termination points are obtained through (3.40)). Figure 3.24 shows I_0 for this system as a function of K, from which we determine that $K_{I_0} = 2.2$. The truncation gain can then be evaluated as $K_{tr} = K_e(2.2) = 2.15$. The resulting S-root locus is given in Figure 3.25, where the S-termination and S-truncation points are denoted by the usual and solid squares, respectively. Although the S-root locus enters the shaded region for high quality dynamic tracking, the position of the truncation points limit the achievable performance. Figure 3.26 illustrates the output response of the system when the control gain is $K = 20 > K_{I_0}$. The saturated closed loop poles are located at $-16 \pm j9.5$ (i.e., in the admissible domain), but beyond the truncation points. This leads to good dynamic tracking, but with a clipped response. Clearly, this can be remedied by increasing α, as illustrated in Figure 3.27, which shows the S-root locus when $\alpha = 1.5$. Figure 3.28 shows the corresponding plot for the same location of S-poles as before. Clearly the clipping practically does not occur (the output overlays the reference).

In conclusion, note that if S-truncation points exist, then they occur prior to the S-termination points (since the latter correspond to $K = \infty$).

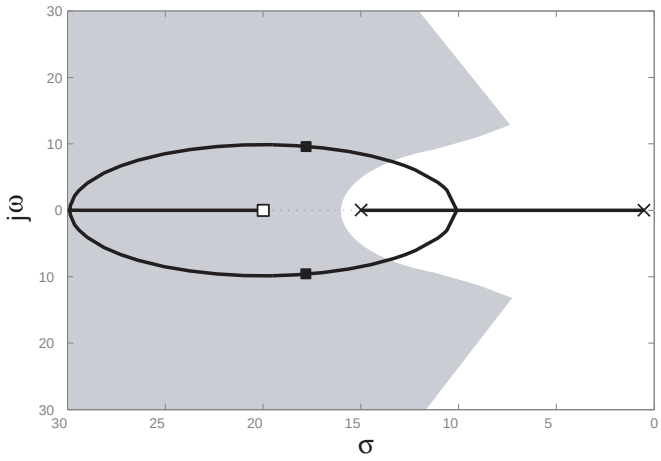

Figure 3.27: S-root locus for Example 3.16 with $\alpha = 1.5$

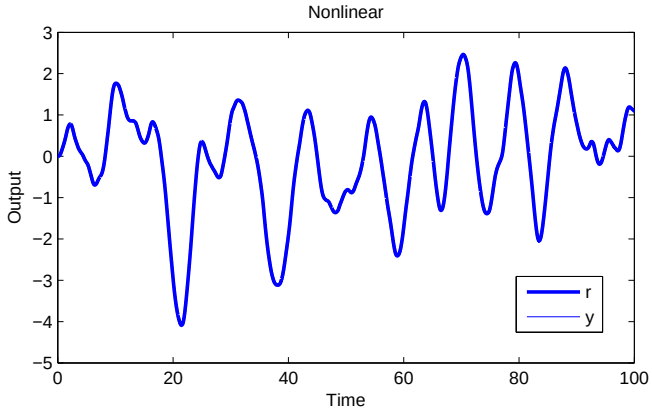

Figure 3.28: Tracking quality for Example 3.16 with $\alpha = 1.5$

3.7 Calibration of the S-Root Locus

Let s^* be an arbitrary point on the S-root locus, i.e.,

$$1 + K_e(K)\, C(s^*)\, P(s^*) = 0, \tag{3.55}$$

where

$$0 \leq K_e(K) < \kappa. \tag{3.56}$$

To calibrate the S-Root Locus implies to find the particular K such that (3.55) is satisfied (i.e., the S-poles are located at s^*). This is accomplished by the following Corollary of Theorem 3.12.

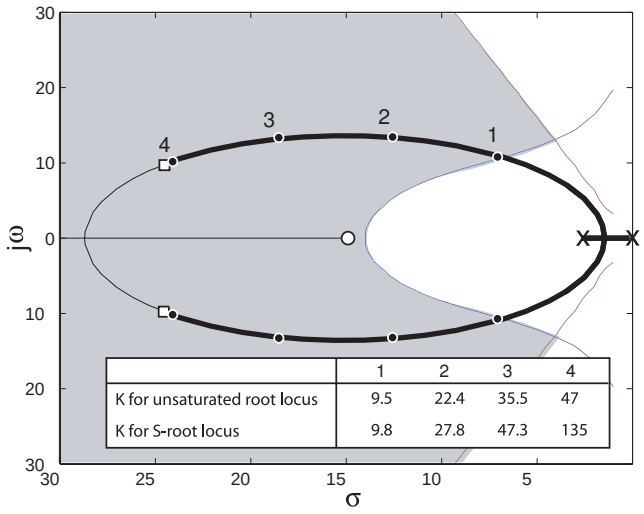

Figure 3.29: Difference in calibration between unsaturated and S-root locus

Corollary 3.17. *For arbitrary s^* on the S-Root Locus, there exists a unique $K^* > 0$ such that $K = K^*$ satisfies (3.55). Moreover, K^* is the unique solution of*

$$K_e = K^* erf\left(\frac{\alpha}{\sqrt{2}K^*\left\|\frac{F_\Omega(s)C(s)}{1+K_eP(s)C(s)}\right\|_2}\right), \tag{3.57}$$

where

$$K_e = \frac{1}{|C(s^*)P(s^*)|}. \tag{3.58}$$

Note that (3.57) can be solved by a standard bisection algorithm. Figure 3.29 illustrates the differences in calibration gains between an unsaturated and S-root locus (using the system of Example 3.10).

3.8 Application: Hard Disk Drive

We consider the hard disk drive servo problem of Section 3.2.4, where the control objective is to maintain the disk head above a circular track that exhibits random irregularities which can be modelled as a bandlimited noise. The model for the plant

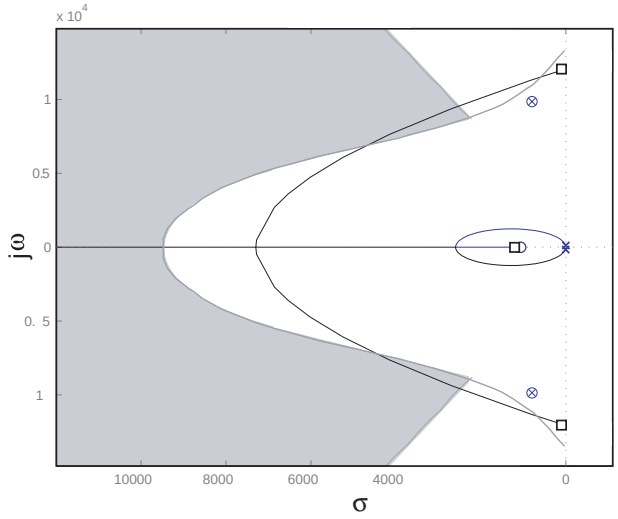

Figure 3.30: S-Root Locus for hard disk drive example

was given as

$$P_D(s) = \frac{4.382 \times 10^{10} s + 4.382 \times 10^{15}}{s^2 \left(s^2 + 1.596 \times 10^3 s + 9.763 \times 10^7\right)}, \tag{3.59}$$

while the controller was selected as

$$C(s) = \frac{K(s + 1058)\left(s^2 + 1596s + 9.763 \times 10^7\right)}{\left(s^2 + 3.719 \times 10^4 s + 5.804 \times 10^8\right)^2}. \tag{3.60}$$

From [2], we impose the additional assumption that the input to the plant is constrained by a saturation with $\alpha = 0.006$. The bandwidth of the reference is $692 rad/s$, and $F_\Omega(s)$ is as defined in (3.33). For this system, the conditions of Theorem 3.8 hold, and it results in

$$\kappa = 1.0509 \times 10^6.$$

The corresponding S-root locus is shown in Figure 3.30, where the admissible domain is indicated by the shaded region. Note that since $P_D(s)$ contains poles at the origin, the S-root locus does not have S-truncation points. To meet the performance specification, we select K so that

$$K_e(K) = 5.7214 \times 10^5, \tag{3.61}$$

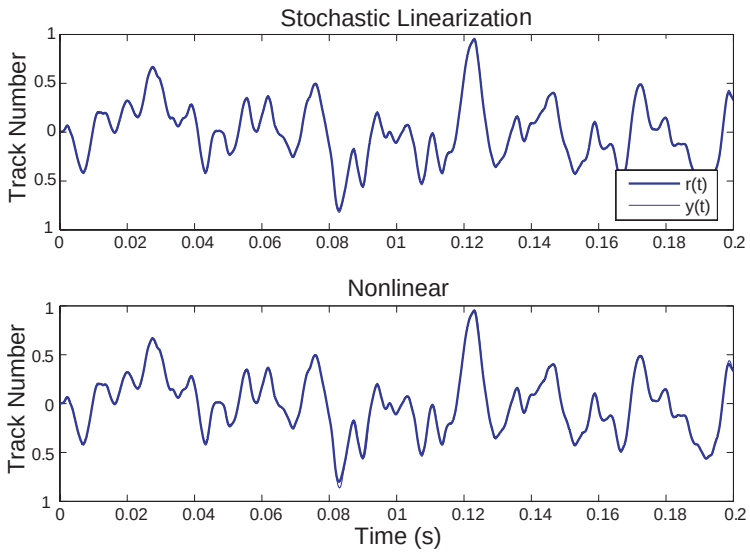

Figure 3.31: Tracking performance, hard disk drive example

which results in a pair of dominant S-poles located at $(-2.83 \pm j9.06) \times 10^3$, i.e., in the admissible domain. Using Corollary 3.17 with (3.61) yields:

$$K = 6.208 \times 10^5.$$

Figure 3.31 illustrates the tracking quality for both the stochastically linearized and original nonlinear systems. As predicted, the nonlinear system exhibits a tracking quality similar to that of the stochastically linearized system, and achieves a standard deviation $\sigma_e = 0.047\sigma_r$. It is noteworthy that this performance matches that obtained in [54], where a nonlinear antiwindup controller was utilized.

3.9 Summary

This chapter has presented a new methodology - the *S-root locus* - to design controllers for tracking random reference signals in the presence of saturation. The technical approach utilizes stochastic linearization, whereby the saturation nonlinearity is replaced by a static gain that depends on the variance of the signal at its input. The poles of the resulting quasilinear system are the so-called S-poles and can

be used to predict the quality of tracking. Specifically, good tracking requires that the S-poles be located in desirable regions of the complex plane. The path traced by the S-poles as the controller gain changes is the so-called S-root locus and is always a subset of the unsaturated root locus, i.e., the root locus obtained by removing the saturation. Hence, the S-root locus methodology introduced in this paper is similar to the classical root locus methodology in that both require certain poles to be located in desirable regions of the complex plane.

There are, however, significant differences between the S-root locus and the classical root-locus methodologies. Specifically:

a) *S-termination:* As the control gain tends to infinity, the equivalent gain may tend to a finite value (see Theorem 1). This phenomenon is referred to as S-termination, and results in the S-root locus terminating at points prior to the open loop zeros.

b) *S-truncation:* The phenomenon of S-truncation refers to quality degradation due to output truncation. This occurs when the magnitude of the signal to be tracked lies outside of the feasible domain specified by the level of saturation.

c) *S-origination:* For small control gain, stochastic linearization is guaranteed to yield a unique gain as a surrogate of the saturation. As the control gain increases, however, stochastic linearization may yield multiple gains, leading to the phenomenon of S-origination.

d) *Jumping:* When stochastic linearization yields multiple gains, they correspond to several combinations of S-pole locations. In that case, the system behavior jumps (transitions) between the options defined by the various combinations of S-pole locations.

The formulation of the S-root locus design methodology and the analytic de-

scription of the above phenomena constitute the main original contributions of this chapter.

CHAPTER IV

RECOVERING LINEAR PERFORMANCE: BOOSTING

4.1 Introduction

Consider the linear feedback system shown in Figure 4.1, where $C(s)$ is the controller and $P(s)$ is the plant. The signals u_ℓ, y_ℓ and w denote the controller output, plant output, and standard white input disturbance, respectively. Assume that the controller is designed to achieve a certain level of disturbance rejection, specified in terms of the output variance $\sigma^2_{y_\ell}$. As discussed in Chapter I, in reality, the controller is implemented in the LPNI configuration shown in Figure 4.2, where $f(\cdot)$ and $g(\cdot)$

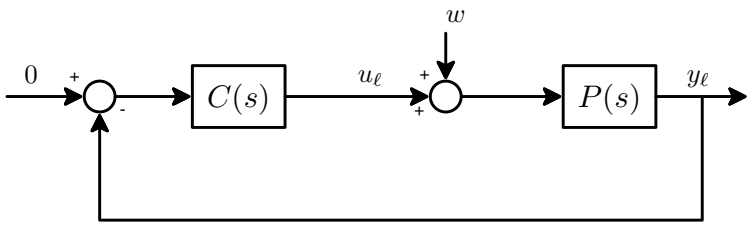

Figure 4.1: Basic linear feedback system

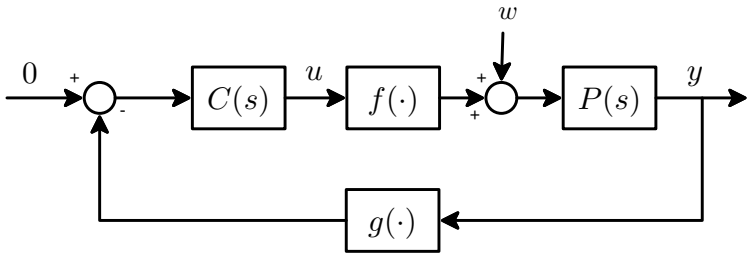

Figure 4.2: Feedback system with nonlinear instrumentation

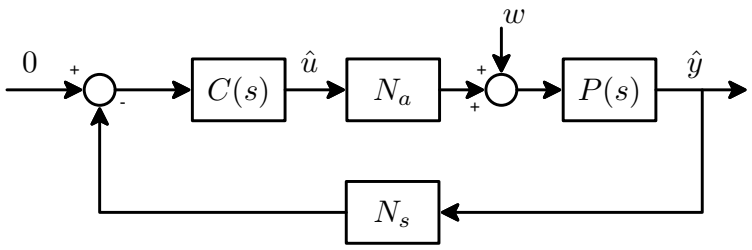

Figure 4.3: Quasilinear feedback system for boosting

represent static nonlinearities in the actuator and sensor, respectively.

The performance of the LPNI system typically degrades in comparison with that of the original linear system in the sense that

$$\sigma_y^2 > \sigma_{y\ell}^2. \tag{4.1}$$

This chapter presents a technique, referred to as *boosting*, that describes how, under certain conditions, the gain of $C(s)$ can be increased to eliminate this degradation. Thus, the main contribution is a method to recover the performance of a linear design in the presence of nonlinear instrumentation.

As described in Chapter II, quantifying (4.1) is difficult since analytical evaluation of σ_y^2 requires solution of the Fokker-Planck equation, which is possible in only a few special cases [49]. Thus, stochastic linearization is used to study the LPNI system. Recall from Chapter II that in SL, the LPNI system is replaced by the *quasilinear* system shown in Figure 4.3, where the quasilinear gains are defined as

$$N_a := E\left[\frac{d}{d\hat{u}} f\left(\hat{u}\right)\right], \tag{4.2}$$

and

$$N_s := E\left[\frac{d}{d\hat{y}} g\left(\hat{y}\right)\right]. \tag{4.3}$$

The boosting method amounts to a modification of the controller $C(s)$ so that the quasilinear system completely recovers the performance of the original *linear* system,

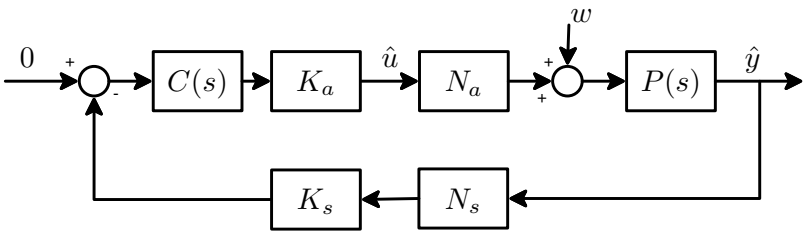

Figure 4.4: Boosted quasilinear system

i.e.,

$$\sigma_{\hat{y}} = \sigma_{y_\ell}. \tag{4.4}$$

This is achieved by introducing scalar gains K_a and K_s, as shown in Figure 4.4. The idea is to compensate for the effects of $f(u)$ and $g(y)$ by selecting K_a and K_s to offset N_a and N_s respectively, so that

$$K_a N_a = K_s N_s = 1, \tag{4.5}$$

where we assume that N_a and N_s are nonzero. Note that, in the quasilinear system, N_a and N_s are functions of K_a and K_s, which makes the boosting problem nontrivial. Since K_s, K_a and $C(s)$ commute, boosting can be implemented by placing a single gain at the output of $C(s)$ as shown in Figure 4.5, where

$$K_{boost} := K_a K_s. \tag{4.6}$$

In addition, we establish a separation principle, which enables K_a and K_s to be evaluated from two simpler sub-problems:

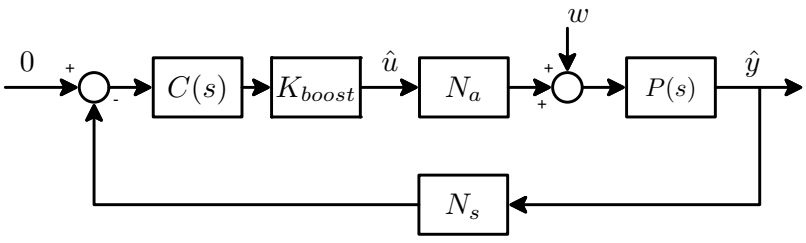

Figure 4.5: Equivalent boosted quasilinear system

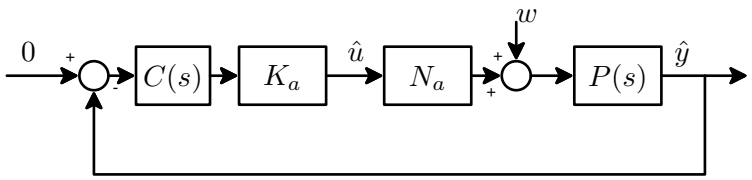

Figure 4.6: a-Boosted quasilinear system

(1) a-boosting, i.e., boosting to account for *only* a nonlinear actuator (i.e., under the assumption that $g(y) = y$), and

(2) s-boosting, i.e., boosting to account for *only* a nonlinear sensor (i.e., under the assumption that $f(u) = u$).

The chapter is organized as follows: Section 4.2 provides a detailed problem formulation. Sections 4.3 and 4.4 present solutions for the a- and s-boosting problems respectively. These results are combined in Section 4.5, which explains the case when $f(u)$ and $g(y)$ are simultaneously present. In Section 4.7, the accuracy of the results is validated both statistically and experimentally. A summary is formulated in Section 4.9, and proofs are provided in Appendix B.

4.2 Problem Formulation

As it was stated above, recovering the performance of the linear feedback loop of Figure 4.1 in the presence of the nonlinearities of Figure 5.1 can be accomplished by boosting. This method is separable into two parts: boosting to compensate for actuator nonlinearity, and boosting to compensator for sensor nonlinearity. Hence, the following two problems are formally posed.

4.2.1 a-Boosting

Consider the LPNI system with $g(y) = y$. Hence, the only nonlinearity is the actuator $f(u)$ and Figure 4.4 reduces to Figure 4.6. Here, since w is standard white

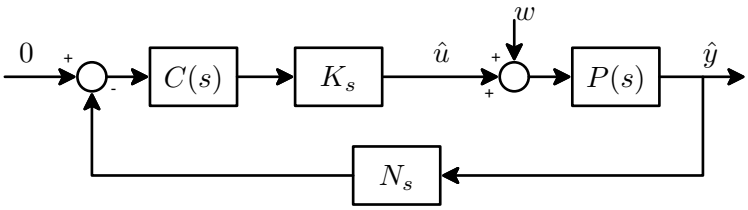

Figure 4.7: s-Boosted quasilinear system

noise, (4.2) becomes

$$N_a = \int_{-\infty}^{\infty} f'(x) \frac{1}{\sigma_{\hat{u}}\sqrt{2\pi}} \exp\left(-\frac{x}{2\sigma_{\hat{u}}^2}\right) dx. \tag{4.7}$$

Define the real analytic function

$$\mathcal{F}(\sigma) := \int_{-\infty}^{\infty} f'(x) \frac{1}{\sigma\sqrt{2\pi}} \exp\left(-\frac{x}{2\sigma^2}\right) dx. \tag{4.8}$$

Since

$$\sigma_{\hat{u}} = \left\| \frac{P(s)\, C(s) K_a}{1 + P(s)\, N_a K_a C(s)} \right\|_2, \tag{4.9}$$

where

$$\|H\|_2 = \sqrt{\frac{1}{2\pi} \int_{-\infty}^{\infty} |H(j\omega)|^2 \, d\omega}, \tag{4.10}$$

(4.7) can be rewritten as

$$N_a = \mathcal{F}\left(\left\| \frac{P(s)\, C(s) K_a}{1 + P(s)\, N_a K_a C(s)} \right\|_2 \right). \tag{4.11}$$

The problem of a-boosting is to find K_a, if possible, such that

$$K_a N_a = 1, \tag{4.12}$$

where N_a itself depends on K_a through (4.11).

4.2.2 s-Boosting

Consider the LPNI system with $f(u) = u$. Hence, Figure 4.4 reduces to Figure 4.7, where

$$N_s = \int_{-\infty}^{\infty} g'(x) \frac{1}{\sigma_{\hat{y}}\sqrt{2\pi}} \exp\left(-\frac{x}{2\sigma_{\hat{y}}^2}\right) dx. \tag{4.13}$$

Define the function

$$\mathcal{G}(\sigma) := \int_{-\infty}^{\infty} g'(x) \frac{1}{\sigma\sqrt{2\pi}} \exp\left(-\frac{x}{2\sigma^2}\right) dx. \tag{4.14}$$

Since

$$\sigma_{\hat{y}} = \left\| \frac{P(s)}{1 + P(s) N_s K_s C(s)} \right\|_2, \tag{4.15}$$

(4.13) can be rewritten as

$$N_s = \mathcal{G}\left(\left\| \frac{P(s)}{1 + P(s) N_s K_s C(s)} \right\|_2 \right). \tag{4.16}$$

The problem of s-boosting is to find K_s, if possible, such that

$$K_s N_s = 1, \tag{4.17}$$

where, again, N_s is a function of K_s through (4.16).

Remark 4.1. The structure of the LPNI system of Figure 5.1 implies that the problems of a- and s-boosting are not dual. Indeed, observe that for a-boosting, the gain K_a appears in the forward path between w and the input of the actuator nonlinearity, $\hat{u}$. For s-boosting, K_s does *not* appear in the path from w to the input of the sensor $\hat{y}$. Consequently, the numerator of the transfer function in (4.11) contains a boosting gain, whereas that in (4.16) does not. Thus, the two problems are different, and must be addressed separately.

4.3 a-Boosting

As implied by (4.11) and (4.12), the problem of a-boosting is equivalent to finding K_a that satisfies

$$K_a \mathcal{F}\left(\left\| \frac{P(s) C(s) K_a}{1 + P(s) N_a K_a C(s)} \right\|_2 \right) = 1. \tag{4.18}$$

Theorem 4.2. *a-Boosting is possible if and only if*

$$x\mathcal{F}\left(x\left\|\frac{P\left(s\right)C(s)}{1+P\left(s\right)C\left(s\right)}\right\|_2\right)=1 \tag{4.19}$$

has a positive solution in x. Any positive solution of (4.19) *yields a boosting gain*

$$K_a=x. \tag{4.20}$$

The existence and uniqueness of K_a depend on the specific form of $\mathcal{F}(\cdot)$. This is analyzed below for the common saturation nonlinearity. Other nonlinearities can be treated analogously.

4.3.1 Actuator saturation

Consider the a-boosted system of Figure 4.6 and let $f(\cdot)$ be the static saturation of authority α, i.e.,

$$f(u)=sat_\alpha(u)=\begin{cases}\alpha, & u>+\alpha\\ u, & -\alpha\le u\le\alpha\\ -\alpha, & u<-\alpha.\end{cases} \tag{4.21}$$

In this case, it was shown in Chapter II that

$$\mathcal{F}(\sigma)=\text{erf}\left(\frac{\alpha}{\sqrt{2}\sigma}\right). \tag{4.22}$$

Hence,

$$N_a=\text{erf}\left(\frac{\alpha}{\sqrt{2}\left\|\frac{P(s)C(s)K_a}{1+P(s)N_aK_aC(s)}\right\|}\right). \tag{4.23}$$

It follows from Theorem 4.2 and (4.22) that a-boosting for the saturation nonlinearity (3.1) is possible if and only if the equation

$$x\text{erf}\left(\frac{c}{x}\right)=1 \tag{4.24}$$

has a positive solution in x, where

$$c = \frac{\alpha}{\sqrt{2}\left\|\frac{P(s)C(s)}{1+P(s)C(s)}\right\|_2}. \tag{4.25}$$

Theorem 4.3. *Equation* (4.24) *admits a unique positive solution if and only if*

$$\alpha > \sqrt{\frac{\pi}{2}}\left\|\frac{P(s)C(s)}{1+P(s)C(s)}\right\|_2. \tag{4.26}$$

Note that since

$$\sigma_{u_\ell} = \left\|\frac{P(s)C(s)}{1+P(s)C(s)}\right\|_2 \tag{4.27}$$

and

$$\sqrt{\frac{\pi}{2}} \approx 1.25, \tag{4.28}$$

the following can be stated:

Rule-of-thumb 1. *a*-Boosting for a saturating actuator is possible if

$$\alpha > 1.25\sigma_{u_\ell}. \tag{4.29}$$

Remark 4.4. As it has been shown in [61],

$$\alpha > 2\sigma_{u_\ell}, \tag{4.30}$$

without boosting, leads to no more than 10% performance degradation of the linear design. In comparison, the above rule-of-thumb achieves complete performance recovery, with actuators that have less authority than recommended in [61].

4.3.2 Performance recovery by redesigning $C(s)$

If (4.19) does not have a solution, i.e., *a*-boosting is impossible, a question arises: Can $C(s)$ be redesigned in some other way to achieve $\sigma_{\hat{y}} = \sigma_{y_\ell}$? The answer depends on the ability to find a controller that simultaneously achieves the performance specification *and* yields a solution to (4.19). Such a controller is said to be *boostable*.

In the case of actuator saturation, the boosting condition (4.26) implies that finding a boostable controller is a linear minimum-effort control problem, i.e., the problem of finding a controller that minimizes σ_{u_ℓ} for a specified performance level σ_{y_ℓ}. One method for accomplishing this is given in [112], where a controller $C_{opt}(s)$ is synthesized that yields the desired output σ_y with minimum control effort. If (4.26) is not satisfied by this $C_{opt}(s)$, then no linear boostable controller exists.

4.4 s-Boosting

As implied by (4.16) and (4.17), the problem of s-boosting is equivalent to finding K_s that satisfies

$$K_s \mathcal{G}\left(\left\| \frac{P(s)}{1 + P(s) N_s K_s C(s)} \right\|_2\right) = 1. \tag{4.31}$$

Since, unlike a-boosting, K_s enters the argument of $\mathcal{G}$ only as a factor of N_s, and for s-boosting $N_s K_s = 1$, the solution of (4.31) is always possible and is given by

$$K_s = \frac{1}{\mathcal{G}\left(\left\| \frac{P(s)}{1+P(s)C(s)} \right\|_2\right)}. \tag{4.32}$$

This result warrants further investigation since it suggests that linear performance may be recovered in the presence of *any* sensor nonlinearity. It turns out that, although an s-boosting gain can always be found, in some cases the accuracy of stochastic linearization may be poor. Thus, certain conditions should be satisfied before using s-boosting. These are developed in Section 4.7.

Below, explicit expressions are given for the function $\mathcal{G}$ in (4.32) for various types of sensor nonlinearities.

4.4.1 Sensor saturation

In the case where $g(y)$ is a symmetric saturation of range α, the right hand side of (4.16) becomes

$$\mathcal{G}(\sigma) = erf\left(\frac{\alpha}{\sqrt{2}\sigma}\right). \tag{4.33}$$

4.4.2 Sensor deadzone

Let $g(y)$ be a symmetric deadzone of the form

$$g(y) = \begin{cases} y - \frac{\Delta}{2}, & y > +\frac{\Delta}{2} \\ 0, & -\frac{\Delta}{2} \leq y \leq \frac{\Delta}{2} \\ y + \frac{\Delta}{2}, & y < -\frac{\Delta}{2}. \end{cases} \tag{4.34}$$

In this case, the right hand side of (4.16) becomes

$$\mathcal{G}(\sigma) = 1 - erf\left(\frac{\Delta/2}{\sqrt{2}\sigma}\right). \tag{4.35}$$

4.4.3 Sensor quantization

Let $g(y)$ be a mid-tread quantizer of the form

$$\begin{aligned} g(y) = \frac{\Delta}{2} \sum_{k=1}^{m} &\left[\operatorname{sgn}\left(2y + \Delta\left(2k-1\right)\right) \times \right. \\ &\left. \operatorname{sgn}\left(2y - \Delta\left(2k-1\right)\right)\right]. \end{aligned} \tag{4.36}$$

Then,

$$\mathcal{G}(\sigma) = Q_m\left(\frac{\Delta}{\sqrt{2}\sigma}\right), \tag{4.37}$$

where

$$Q_m(z) := \frac{2z}{\sqrt{\pi}}\left[\sum_{k=1}^{m} e^{-\frac{1}{4}(2k-1)^2(z)^2}\right]. \tag{4.38}$$

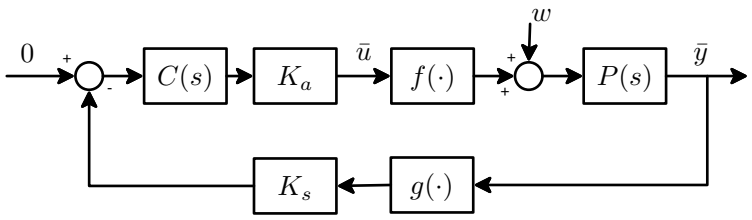

Figure 4.8: LPNI system with boosted controller for stability verification

4.5 Simultaneous a- and s-Boosting

The following separation principle ensures that the results of Sections 4.3 and 4.4 remain applicable when actuator and sensor nonlinearities are simultaneously present.

Theorem 4.5. *Simultaneous a- and s-boosting is possible if and only if each is possible independently. Moreover, the boosting gains K_a and K_s are the same as the individual a- and s-boosting gains, respectively.*

4.6 Stability Verification in the Problem of Boosting

It is important to verify the stability of the original LPNI system with the boosted controller. This amounts to performing stability analysis for the nonlinear system shown in Figure 4.8.

The stability properties of the LPNI system can be ascertained using the theory of absolute stability. Here, the global asymptotic stability of the origin can be verified by using tools such as the circle or Popov criterion [15, 44], which require that the nonlinearities be contained in a certain sector. Although these are strong results, the conditions are only sufficient and not necessary.

In general, for the LPNI system of Figure 4.8, the local stability of any equilibrium can be ascertained via Lyapunov's indirect method [44]. For example, in the case where $f(\cdot)$ and $g(\cdot)$ are saturation functions of the form (4.21), the origin is

asymptotically stable if the numerator of the equation

$$1 + K_a K_s C(s) P(s) = 0$$

has all roots in the open left half plane. In this case, the region of attraction can be estimated by using well-known Lyapunov function-based techniques [23, 105].

In addition to these, as reviewed in Section 1.3.2, many other methods are available for stability analysis in LPNI systems.

4.7 Accuracy of Stochastic Linearization in the Problem of Boosting

It is assumed that the boosted quasilinear system accurately predicts the behavior of the corresponding nonlinear system. In this section, validation of the accuracy of stochastic linearization when boosting is performed. Design guidelines are formulated to avoid cases when accuracy is poor.

4.7.1 Accuracy in the problem of a-boosting

To validate the accuracy of stochastic linearization in the context of boosting, the following statistical study, similar to that considered in Section 2.5.2, is performed: We consider 2500 first-order and 2500 second-order plants of the form:

$$P_1(s) = \frac{1}{Ts + 1}, \tag{4.39}$$

$$P_2(s) = \frac{\omega_n^2}{s^2 + 2\zeta\omega_n + \omega_n^2}. \tag{4.40}$$

The controller is $C(s) = K$ and the actuator is a saturation of the form (3.1). The system parameters are randomly and equiprobably selected from the following sets:

$T \in [0.01, 10]$,

$\omega_n \in [0.01, 10], \zeta \in [0.05, 1]$,

$K \in [1, 20]$

$\alpha \in (\alpha_{min}, 2\alpha_{min}]$,

where α_{min} is the right hand side of (4.26). Boosting is performed for each system, and the LPNI system is simulated to identify the error of stochastic linearization, defined as

$$e_{SL} = \frac{|\sigma_y - \sigma_{\hat{y}}|}{\sigma_{\hat{y}}}. \tag{4.41}$$

Accuracy is very good: 73.6% of the systems yield $e_{SL} < 0.05$ and only 8.7% of systems yield $e_{SL} > 0.1$. Further analysis reveals that these latter cases occur when the signals u and y are highly non-Gaussian. This is consistent with the assumption of stochastic linearization, namely that those signals should be approximately Gaussian.

Remark 4.6. In general, stochastic linearization is accurate when the closed loop linear system provides a sufficient amount of low-pass filtering [1]. A similar situation holds for the method of describing functions.

4.7.2 Accuracy of s-boosting

A similar statistical study is performed to validate the accuracy of stochastic linearization in the context of s-boosting. Here, the sensor is assumed to be a mid-tread quantizer of the form (5.71), and $C(s) = K$. We consider 1000 first- and 1000 second-order plants of the form (4.39) and (4.40), with system parameters chosen equiprobably from the sets:

$T \in [0.01, 10]$,

$\omega_n \in [0.01, 10], \zeta \in [0.05, 1]$,

$K \in [1, 20]$,

$m \in [1, 10]$, $\Delta \in (0, 4\sigma_y]$,

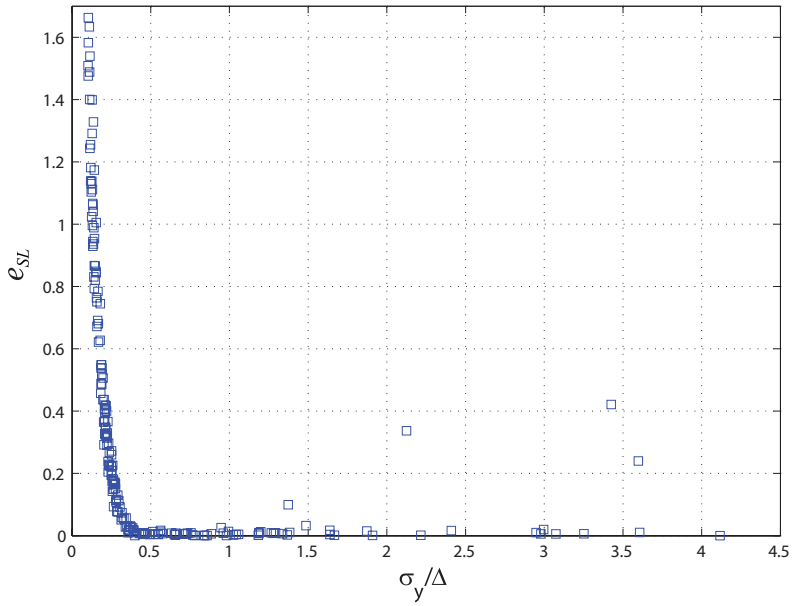

Figure 4.9: e_{SL} as function of σ_y/Δ

where σ_y is the nominal linear performance to be recovered. As illustrated in Figure 4.9, simulation reveals that accuracy degrades significantly as the ratio σ_y/Δ decreases. This is expected, since when σ_y/Δ is small, most of the output signal lies in the quantizer deadzone. Hence, the nonlinear system operates in an effectively open loop regime. Our experience indicates that to avoid this situation, the following should be observed:

$$\frac{\sigma_y}{\Delta} > 0.33. \tag{4.42}$$

This leads to:

Rule-of-thumb 2. s-Boosting for a quantized sensor is possible if

$$\Delta < 3\sigma_y. \tag{4.43}$$

Remark 4.7. Recall that Δ is the *total* deadzone width, and hence (4.43) stipulates that the deadzone 'amplitude', i.e., $\Delta/2$, should be no greater than 1.5 standard deviations. This rule-of-thumb may seem generous, since intuition would suggest

that $\Delta/2$ should be, at most, one standard deviation. The extra deadzone width allowance comes from boosting, which increases the loop gain.

When (4.42) is satisfied, the accuracy of s-boosting is similar to that of a-boosting. Again, accuracy is generally very good, and fails in those scenarios where the plant has insufficient filtering characteristics.

Remark 4.8. Similar results hold when $g(y)$ is the symmetric deadzone (4.34). In general, Rule-of-thumb 2 should be observed for any sensor nonlinearities that exhibit small gain near the origin.

4.8 Experimental Validation of Boosting: MagLev

To illustrate the efficacy of boosting on a physical system, consider the problem of controlling the vertical displacement of a magnetically suspended ball (Maglev), illustrated in Figure 4.10. The input of the system is the current $i(t)$, while the output is the vertical displacement of the ball $y(t)$.

To coincide with a commercial Maglev experimental apparatus (Feedback Inc. Magnetic Levitation System), the following linearized model and the disturbance intensity, provided by the manufacturer, are used:

$$P(s) = \frac{Y(s)}{I(s)} = \frac{-37.20}{s^2 - 2180}, \tag{4.44}$$

$$\sigma_w^2 = 1.2 \times 10^{-5}. \tag{4.45}$$

Consider the PID controller

$$C(s) = 200 + 5s + \frac{200}{s}, \tag{4.46}$$

which stabilizes the linear system. The resulting output standard deviation is

$$\sigma_{y_\ell} = 0.029cm. \tag{4.47}$$

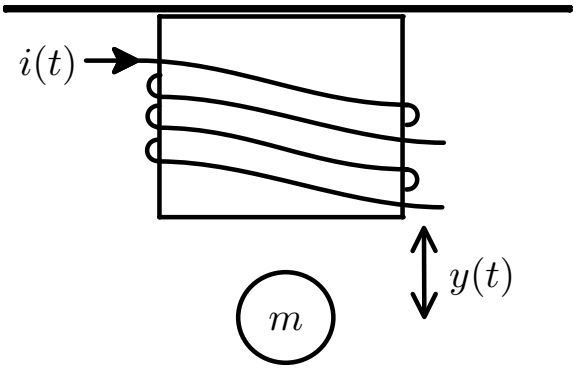

Figure 4.10: Magnetically suspended ball

The experimental apparatus is configured so that the current to the plant is constrained by a saturation with authority $\alpha = \pm 0.3A$. The measured output is quantized by $\Delta = 0.005cm$. Simulation of the system with this nonlinear instrumentation results in

$$\sigma_y = 0.049cm, \tag{4.48}$$

a degradation of 83%.

It is easily verified that $\sigma_{u_\ell} = 0.1069$, and hence (4.26) is satisfied. Thus, the conditions of Theorem 4.5 are met and boosting can be used to recover the original linear performance. Solving (4.24) and (4.32) results in

$$K_{boost} = 2.8. \tag{4.49}$$

Using this boosting gain in a MATLAB simulation yields the desired result:

$$\sigma_y = 0.0271cm. \tag{4.50}$$

This result is verified experimentally. The boosted controller $\bar{C}(s) = K_{boost}C(s)$ is applied to the MagLev through standard AD/DA hardware, and a pseudo-white noise excitation is applied at the input of the plant. The resulting experimentally measured output standard deviation is

$$\sigma_{\tilde{y}} = 0.0252cm, \tag{4.51}$$

where $\tilde{y}$ denotes the output signal. Thus, a successful recovery of the designed performance is demonstrated.

4.9 Summary

A typical approach to disturbance rejection in LPNI systems involves designing in a purely linear setting, using techniques such as conventional LQR/LQG. In this situation, the designer may find that the anticipated performance degrades when their controller is applied in the actual LPNI configuration. The main contribution of this chapter is the method of boosting, whereby a scalar gain is applied to the existing controller, such that linear performance is recovered in a quasilinear system that faithfully represents the original LPNI system. The conditions for boosting are easily checked, and the technique is demonstrated to be effective for a large number of systems. It allows designers to use familiar tools in a linear setting, and then recover the intended performance in the presence of nonlinear instrumentation.

CHAPTER V

SIMULTANEOUS DESIGN OF CONTROLLER AND INSTRUMENTATION: ILQR/ILQG

5.1 Introduction

Consider the LPNI system shown in Figure 5.1, where the actuator and sensor nonlinearities $f_\alpha(\cdot)$ and $g_\beta(\cdot)$ are parameterized by α and β, respectively. The control objective is disturbance rejection, specified in terms of the variance, σ_z^2, of the performance output, z. As demonstrated in the previous chapter, the conventional LQR/LQG method, in combination with boosting, can be used to achieve this objective (i.e., execute a purely linear design, then recover performance in the LPNI system via boosting). As an alternative to boosting, a modified LQR/LQG technique, referred to as SLQR/SLQG (where S stands for saturation), has been developed in [5, 83]. Using this technique, and given the nonlinearities $f_\alpha(\cdot)$ and $g_\beta(\cdot)$, the designer can synthesize $C(s)$ directly, so that σ_z^2 satisfies the specification. But when the instrumentation is not *a priori* specified, how can one synthesize the controller *and* the instrumentation, *simultaneously*, so that the desired performance is achieved? This is the question addressed in this chapter.

Specifically, we develop the ILQR/ILQG methodology (where I stands for instrumented), which finds the controller $C(s)$ and the instrumentation $f_\alpha(\cdot)$ and $g_\beta(\cdot)$ that minimize an augmented version of the traditional quadratic performance index

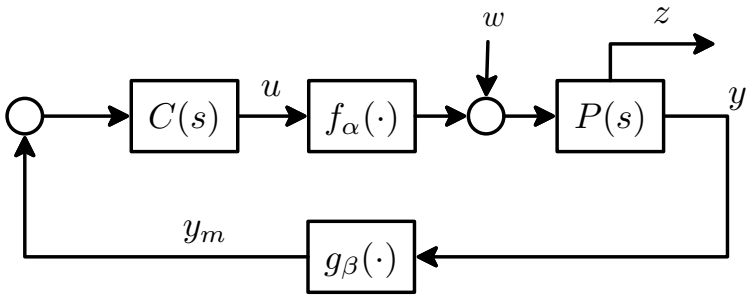

Figure 5.1: LPNI system for ILQR/ILQG

given by

$$J = \sigma_z^2 + \mathcal{W}(\alpha, \beta). \tag{5.1}$$

Here, $\mathcal{W}(\alpha, \beta)$ describes the 'cost' of the instrumentation as a function of the parameters of the nonlinearities. Thus, ILQR/ILQG results in simultaneous controller and instrumentation design.

As in the previous chapters, the technical approach is based on the method of stochastic linearization, which leads to an analytically tractable problem.

The remainder of this chapter is organized as follows. Section 5.2 provides the problem formulation. Sections 5.3 and 5.4 present solutions for the ILQR and ILQG problems, respectively. Generalizations of these problems are discussed in Section 5.5 and a detailed example is presented in Section 5.6. A summary is provided in Section 5.7. All proofs are given in Appendix C.

5.2 Problem Formulation

To make the problem formulation concrete, we assume that the actuator and sensor nonlinearities are saturation functions of the form (3.1) with parameters α and β, respectively. In Section 5.5, a generalization to other nonlinearities is presented. With this in mind, consider the LPNI system shown in Figure 5.2, where $P(s)$ is the plant, $C(s)$ is the controller, $F_1(s)$, $F_2(s)$ are coloring filters, and $H_1(s)$, $H_2(s)$ are

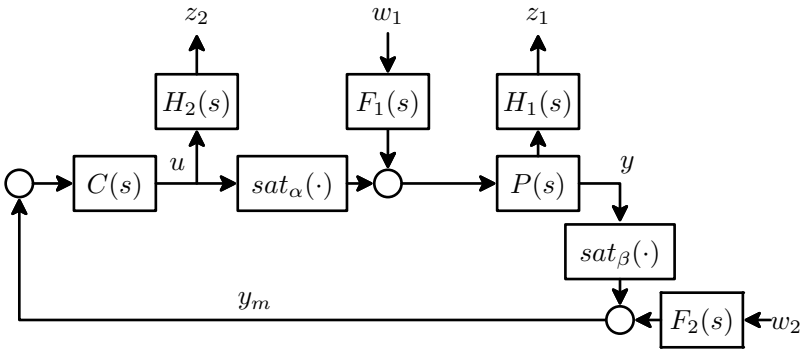

Figure 5.2: LPNI system configuration for ILQR/ILQG problem formulation

weighting filters. The signals $u, y, y_m \in \mathbf{R}$ are, respectively, the control, plant output, and measured output, while w_1, $w_2 \in \mathbf{R}$ are independent white noise processes. The controlled (performance) outputs are $z_1, z_2 \in \mathbf{R}$.

Remark 5.1. The assumption that signals are scalar is made to simplify the technical presentation. This is not restrictive, and generalization to multivariable systems is discussed in Section 5.5.

Assume that the system has a state-space representation

$$\begin{aligned} \dot{x}_G &= Ax_G + B_1 w + B_2 sat_\alpha(u) \\ z &= C_1 x_G + D_{12} u \\ y &= C_2 x_G \\ y_m &= sat_\beta(y) + D_{21} w, \end{aligned} \tag{5.2}$$

where x_G is the state vector of the LPNI system, $w = [w_1 \ w_2]^T$ and $z = [z_1 \ z_2]^T$. Assume, also, that the instrumentation cost $\mathcal{W}(\alpha, \beta)$ is given by

$$\mathcal{W}(\alpha, \beta) = \eta_a \alpha^2 + \eta_s \beta^2, \tag{5.3}$$

where $\eta_a, \eta_s > 0$.

Based on this formalization, three problems can be posed:

E1. *Exact analysis problem*: Given α and β, determine σ_z^2.

E2. *Exact controller design problem*: Given α and β, design a controller that minimizes

$$J = \sigma_z^2.$$

E3. *Exact simultaneous instrumentation and controller design problem*: Design a controller and select α and β in order to minimize

$$J = \sigma_z^2 + \eta_a \alpha^2 + \eta_s \beta^2.$$

As discussed in Section 5.1, solution of these problems is all but impossible since σ_z^2 cannot be analytically evaluated. However, using SL, (5.2) can be approximated by the quasilinear system

$$\begin{aligned} \dot{\hat{x}}_G &= A\hat{x}_G + B_1 w + B_2 N_a \hat{u} \\ \hat{z} &= C_1 \hat{x}_G + D_{12}\hat{u} \\ \hat{y}_m &= N_s C_2 \hat{x}_G + D_{21} w, \\ N_a &= \text{erf}\left(\frac{\alpha}{\sqrt{2}\sigma_{\hat{u}}}\right) \\ N_s &= \text{erf}\left(\frac{\beta}{\sqrt{2}\sigma_{\hat{y}}}\right). \end{aligned} \tag{5.4}$$

Accordingly, one can consider the following *quasilinear* problems:

Q1. *Quasilinear analysis problem*: Given α and β, determine $\sigma_{\hat{z}}^2$.

Q2. *Quasilinear controller design problem*: Given α and β, design a controller that minimizes

$$J = \sigma_{\hat{z}}^2.$$

Q3. *Quasilinear simultaneous instrumentation and controller design problem*: Design a controller, and select α and β in order to minimize

$$J = \sigma_{\hat{z}}^2 + \eta_a \alpha^2 + \eta_s \beta^2.$$

The problems Q1 and Q2 have been addressed in [14] and [5], respectively. The problem Q3 is the subject of this paper. It is referred to as:

- *ILQR*, when the only nonlinearity is in the actuator and the controller is a linear state feedback of the form

$$\hat{u} = K\hat{x}_G; \tag{5.5}$$

- *ILQG*, when both actuator and sensor are nonlinear, and the controller is an output feedback of the form

$$\begin{aligned} \dot{\hat{x}}_C &= M\hat{x}_C - L\hat{y}_m \\ \hat{u} &= K\hat{x}_C. \end{aligned} \tag{5.6}$$

Since the controllers (5.5) and (5.6), along with instrumentation $f_\alpha(\cdot)$ and $g_\beta(\cdot)$, are intended to be used in the LPNI system of Figure 5.2, the following problem must also be considered:

V1. *Verification problem*: With the ILQR/ILQG controller

$$u = Kx_G \tag{5.7}$$

or

$$\begin{aligned} \dot{x}_C &= Mx_C - Ly_m \\ u &= Kx_C, \end{aligned} \tag{5.8}$$

and instrumentation $f_\alpha(\cdot)$ and $g_\beta(\cdot)$, determinine the stability and domain of attraction of the resulting closed-loop LPNI system.

The ILQR and ILQG problems, along with their associated verification problems, are considered in Sections 5.3 and 5.4, respectively.

5.3 ILQR Theory

5.3.1 ILQR synthesis

Consider the open-loop LPNI system

$$\begin{aligned} \dot{x}_G &= Ax_G + B_1 w + B_2 sat_\alpha(u) \\ z &= C_1 x_G + D_{12} u, \end{aligned} \tag{5.9}$$

with linear state feedback

$$u = Kx_G, \tag{5.10}$$

and assume the following:

Assumption 1. (a) (A, B_2) is stabilizable; (b) (C_1, A) is detectable; (c) $D_{12} = [0\ \sqrt{\rho}]^T$, $\rho > 0$; (d) $D_{12}^T C_1 = 0$; (e) A has no eigenvalues in the open right-half plane.

Remark 5.2. Assumptions (a)-(d) are standard in conventional LQR theory. Assumption (e) is used to ensure stability of the closed-loop LPNI system.

From (5.9) and (5.10), the closed-loop system is described by

$$\begin{aligned} \dot{x}_G &= Ax_G + B_2 sat_\alpha(Kx_G) + B_1 w \\ z &= (C_1 x_G + D_{12} K) x_G. \end{aligned} \tag{5.11}$$

Applying stochasic linearization to (5.11) results in

$$\begin{aligned} \dot{\hat{x}}_G &= (A + B_2 NK)\hat{x}_G + B_1 w \\ \hat{z} &= (C_1 x_G + D_{12} K)\hat{x}_G \\ \hat{u} &= K\hat{x}_G \\ N &= \operatorname{erf}\left(\tfrac{\alpha}{\sqrt{2}\sigma_{\hat{u}}}\right). \end{aligned} \tag{5.12}$$

The *ILQR Problem* is stated as follows: Find the value of the gain K and parameter α of the actuator, which ensure

$$\min_{K,\alpha} \left\{\sigma_{\hat{z}}^2 + \eta\alpha^2\right\}, \eta > 0, \tag{5.13}$$

where the minimization is over all pairs (K, α) such that $A + B_2NK$ is Hurwitz.

This is a constrained optimization problem, since (5.13) can be rewritten [14] as

$$\min_{K,\alpha} \left\{ \text{tr} \left\{ C_1 R C_1^T \right\} + \rho K R K^T + \eta \alpha^2 \right\}, \tag{5.14}$$

where R satisfies

$$(A + B_2NK)\, R + R\, (A + B_2NK)^T + B_1 B_1^T = 0, \tag{5.15}$$

with N defined by

$$K R K^T - \frac{\alpha^2}{2} \left[\text{erf}^{-1}(N) \right]^{-2} = 0. \tag{5.16}$$

In this paper, the Lagrange multiplier method is used to find the minimum.

Theorem 5.3. *Under Assumption 1, the ILQR problem is solved by*

$$K = -\frac{N}{\lambda + \rho} B_2^T Q, \tag{5.17}$$

$$\alpha = \text{erf}^{-1}(N) \sqrt{2} \sqrt{K R K^T}, \tag{5.18}$$

where (Q, R, N, λ) *is the unique solution of*

$$A^T Q + Q A - \frac{N^2}{\rho + \lambda} Q B_2 B_2^T Q + C_1^T C_1 = 0, \tag{5.19}$$

$$\begin{aligned} &\left(A - \tfrac{N^2}{\rho+\lambda} B_2 B_2^T Q \right) R + R \left(A - \tfrac{N^2}{\rho+\lambda} B_2 B_2^T Q \right)^T \\ &+ B_1 B_1^T = 0, \end{aligned} \tag{5.20}$$

$$\lambda - \frac{\rho}{\frac{N\sqrt{\pi}}{2\text{erf}^{-1}(\text{N})} \exp\left(\text{erf}^{-1}(N)^2 \right) - 1} = 0, \tag{5.21}$$

$$\eta - \frac{\lambda}{2 \left(\text{erf}^{-1}(N) \right)^2} = 0, \tag{5.22}$$

while the optimal ILQR cost is

$$\begin{aligned} \min_{K,\alpha} \left\{ \sigma_{\hat{z}}^2 + \eta \alpha^2 \right\} &= \text{tr} \left\{ C_1 R C_1^T \right\} + \rho \frac{N^2}{(\rho + \lambda)^2} B_2^T Q R Q B_2 \\ &+ 2\eta K R K^T \text{erf}^{-1}(N)^2 . \end{aligned} \tag{5.23}$$

Proof. See Appendix. □

To find the solution to (5.19)-(5.22), a standard bisection algorithm [99] can be used. Specifically, using (5.21) to substitute for λ in (5.22) yields

$$h\left(N\right)-\frac{\rho}{\eta}=0, \tag{5.24}$$

where

$$h\left(N\right)=N\sqrt{\pi}\mathrm{erf}^{-1}(N)\exp\left(\mathrm{erf}^{-1}\left(N\right)^{2}\right)-2\mathrm{erf}^{-1}(N)^{2}. \tag{5.25}$$

It is shown in the proof of Theorem 5.3 that $h(N)$ is continuous and monotonically increasing for $N\in[0,1)$. This leads to the following ILQR solution methodology:

For a given $\epsilon>0$,

(a) Find an ϵ-precise solution N of (5.24) using bisection (with initial conditions $N^{-}=0,N^{+}=1$);

(b) Find λ from (5.21) or (5.22);

(c) Find Q from (5.19);

(d) Find R from (5.20);

(e) Compute K and α from (5.17) and (5.18).

Remark 5.4. Note that ILQR is a proper generalization of conventional LQR. Indeed, observe from (5.24) that as η approaches 0, N tends to 1 and, from (5.22), λ tends to 0. Hence, α tends to ∞ (i.e., the actuator becomes linear) and (5.17), (5.19) and (5.20) reduce to the standard LQR equations.

Remark 5.5. ILQR can also be viewed as a generalization of SLQR theory [5]. Indeed, if α is fixed, (5.22) becomes superfluous and (5.18) becomes a constraint, so that the minimization (5.14) amounts to solution of the SLQR problem.

5.3.2 ILQR performance limitations

Assume that ρ and η are design parameters, and denote the first term in right hand side of (5.23) as $\gamma^2(\rho,\eta)$, i.e.,

$$\gamma^2(\rho,\eta) := \mathrm{tr}\left\{C_1 R(\rho,\eta) C_1^T\right\}, \tag{5.26}$$

where, from (5.20), $R(\rho,\eta) \geq 0$. Note that $\gamma^2(\rho,\eta)$ is the variance of the output $\hat{z}_1$ of the quasilinear system. The following theorem establishes performance limitations on $\gamma^2(\rho,\eta)$.

Theorem 5.6. *Under Assumption 1,*

(i) $\gamma^2(\rho,\eta)$ *is an increasing function of* ρ *and*

$$\lim_{\rho\to 0^+} \gamma^2(\rho,\eta) = \mathrm{tr}\left\{C_1 \bar{R}_\eta C_1^T\right\}, \tag{5.27}$$

where $(\bar{R}_\eta \geq 0, \bar{Q}_\eta \geq 0)$ *is the unique solution of*

$$\left(A - \frac{2}{\pi\eta} B_2 B_2^T \bar{Q}_\eta\right)\bar{R}_\eta + \bar{R}_\eta \left(A - \frac{2}{\pi\eta} B_2 B_2^T \bar{Q}_\eta\right)^T + B_1 B_1^T = 0, \tag{5.28}$$

$$A^T\bar{Q}_\eta + \bar{Q}_\eta A - \frac{2}{\pi\eta}\bar{Q}_\eta B_2 B_2^T \bar{Q}_\eta + C_1^T C_1 = 0; \tag{5.29}$$

(ii) $\gamma^2(\rho,\eta)$ *is an increasing function of* η *and*

$$\lim_{\eta\to 0^+} \gamma^2(\rho,\eta) = \gamma_{\rho 0}^2, \tag{5.30}$$

where $\gamma_{\rho 0}^2$ *denotes the optimal output variance achievable by conventional LQR, i.e., with linear instrumentation;*

(iii) if A *is Hurwitz,*

$$\lim_{\rho\to\infty} \gamma^2(\rho,\eta) = \lim_{\eta\to\infty} \gamma^2(\rho,\eta) = \gamma_{OL}^2, \tag{5.31}$$

where γ_{OL}^2 *denotes the open-loop output variance of* z_1.

Proof. See Appendix. □

Thus, for any η, the output variance cannot be made smaller than $\mathrm{tr}\left\{C_1 \bar{R}_\eta C_1^T\right\}$; for a given ρ, the output variance cannot be made smaller than $\gamma_{\rho 0}^2$; as η and ρ tend to ∞, the optimal strategy is to operate the system open-loop.

5.3.3 ILQR stability verification

The problem of ILQR stability verification consists of investigating the stability properties of the closed-loop LPNI system (5.11), with ILQR controller (5.17) and instrumentation (5.18). To address this problem, consider the following undisturbed version of (5.11):

$$\begin{aligned} \dot{x}_G &= A x_G + B_2 sat_\alpha\left(K x_G\right) \\ z &= C_1 x_G + D_{12} u. \end{aligned} \tag{5.32}$$

Assume that the pair (K, α) is obtained from (5.17) and (5.18), and (Q, R, N, λ) is the corresponding solution of (5.19)-(5.22).

Theorem 5.7. *For the closed-loop system* (5.32) *with* (5.17), (5.18)*:*

(i) $x_G = 0$ *is the unique equilibrium;*

(ii) this equilibrium is exponentially stable;

(iii) a subset of its domain of attraction is given by

$$\mathcal{X} = \left\{ x_G \in R^{n_x} : x_G^T \left(Q B_2 B_2^T Q\right) x_G \leq \frac{4(\rho+\lambda)^2 \alpha^2}{N^4} \right\}. \tag{5.33}$$

Proof. See Appendix. □

Remark 5.8. The additive disturbance w may force the system to exit the domain of attraction. One may use tools from absolute stability theory [15], such as the Popov stability criterion [44], to verify that destabilization by such a disturbance is impossible.

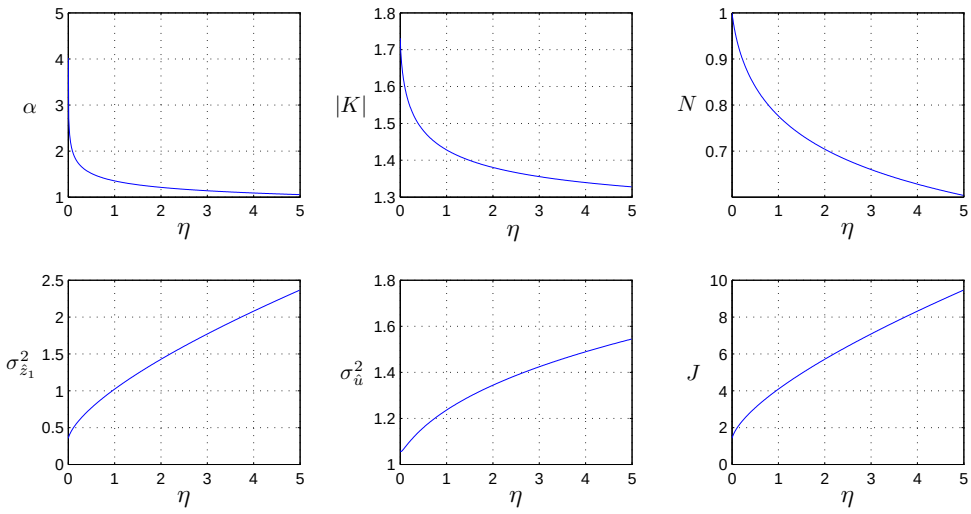

Figure 5.3: ILQR solution for a double integrator as a function of actuator penalty η

5.3.4 Illustrative example

The following example illustrates the behavior of the ILQR solution as the instrumentation penalty η is increased. Consider the standard double-integrator plant in the form (5.9), with system matrices

$$A = \begin{bmatrix} 0 & 0 \\ 1 & 0 \end{bmatrix}, B_1 = B_2 = \begin{bmatrix} 1 \\ 0 \end{bmatrix}$$
$$C_1 = \begin{bmatrix} 0 & 1 \\ 0 & 0 \end{bmatrix}, D_{12} = \begin{bmatrix} 0 \\ \sqrt{\rho} \end{bmatrix}, \tag{5.34}$$

and assume that $\rho = 1$.

Figure 5.3 shows the behavior of the ILQR solution for a range of η. Clearly, as η approaches 0^+, α and $|K|$ increase, the equivalent gain N tends to 1, and the ILQR solution coincides with the conventional LQR solution. As η increases, the output variances $\sigma^2_{\hat{z}_1}$ and $\sigma^2_{\hat{u}}$ increase, as does the optimal ILQR cost J. This is consistent with Theorem 5.6, noting that the double-integrator plant (5.34) does not have a finite open-loop steady state variance.

5.4 ILQG Theory

5.4.1 ILQG synthesis

Consider the open-loop LPNI system of Figure 5.2 represented as

$$\begin{aligned} \dot{x}_G &= Ax_G + B_1 w + B_2 sat_\alpha(u) \\ z &= C_1 x_G + D_{12} u \\ y &= C_2 x_G \\ y_m &= sat_\beta(y) + D_{21} w, \end{aligned} \tag{5.35}$$

with output feedback controller

$$\begin{aligned} \dot{x}_C &= Mx_C - Ly_m \\ u &= Kx_C, \end{aligned} \tag{5.36}$$

and assume the following:

Assumption 2. (a) (A, B_2) is stabilizable and (C_2, A) is detectable; (b) (A, B_1) is stabilizable and (C_1, A) is detectable; (c) $D_{12} = [0 \ \sqrt{\rho}]^T$, $\rho > 0$ and $D_{21} = [0 \ \sqrt{\mu}]$, $\mu > 0$; (d) $D_{12}^T C_1 = 0$ and $B_1 D_{21}^T = 0$; (e) A has no eigenvalues in the open right-half plane.

Remark 5.9. Assumptions (a)-(d) are standard in conventional LQG theory, while (e) is used to ensure stability of the closed-loop system.

From (5.35) and (5.36), the closed-loop LPNI system is

$$\begin{aligned} \dot{x}_G &= Ax_G + B_1 w + B_2 sat_\alpha(Kx_C) \\ \dot{x}_C &= Mx_C - L\left(sat_\beta(C_2 x_G) + D_{21} w\right) \\ z &= C_1 x_G + D_{12} K x_C. \end{aligned} \tag{5.37}$$

Applying stochastic linearization to (5.37) results in

$$\begin{aligned}
\dot{\hat{x}}_G &= A\hat{x}_G + B_1 w + B_2 N_a K \hat{x}_C \\
\dot{\hat{x}}_C &= M\hat{x}_C - LN_s C_2 \hat{x}_G - LD_{21} w \\
\hat{z} &= C_1 \hat{x}_G + D_{12} K \hat{x}_C \\
\hat{u} &= K\hat{x}_C \\
\hat{y} &= C_2 \hat{x}_G \\
\hat{y}_m &= N_s C_2 \hat{x}_G + D_{21} w \\
N_a &= \operatorname{erf}\left(\frac{\alpha}{\sqrt{2}\sigma_{\hat{u}}}\right) \\
N_s &= \operatorname{erf}\left(\frac{\beta}{\sqrt{2}\sigma_{\hat{y}}}\right),
\end{aligned} \tag{5.38}$$

which can be rewritten as

$$\begin{aligned}
\dot{\hat{x}} &= \left(\tilde{A} + \tilde{B}_2 \tilde{N} \tilde{C}_2\right)\hat{x} + \tilde{B}_1 w \\
\hat{z} &= \tilde{C}_1 \hat{x}, \\
\hat{u} &= \tilde{K}\hat{x},
\end{aligned} \tag{5.39}$$

where

$$\begin{aligned}
\tilde{A} &= \begin{bmatrix} A & 0 \\ 0 & M \end{bmatrix}, \tilde{N} = \begin{bmatrix} N_a & 0 \\ 0 & N_s \end{bmatrix}, \\
\tilde{B}_1 &= \begin{bmatrix} B_1 \\ -LD_{21} \end{bmatrix}, \tilde{C}_1 = \begin{bmatrix} C_1 & D_{12}K \end{bmatrix}, \\
\tilde{B}_2 &= \begin{bmatrix} B_2 & 0 \\ 0 & -L \end{bmatrix}, \tilde{C}_2 = \begin{bmatrix} 0 & K \\ C_2 & 0 \end{bmatrix},
\end{aligned} \tag{5.40}$$

and $\hat{x} = [\hat{x}_G^T \;\; \hat{x}_C^T]^T$.

The *ILQG Problem* is stated as follows: Find the values of K, L, M, α and β, which ensure

$$\min_{K,L,M,\alpha,\beta} \left\{\sigma_{\hat{z}}^2 + \eta_a \alpha^2 + \eta_s \beta^2\right\}, \eta_a > 0, \eta_s > 0, \tag{5.41}$$

where the minimization is over all (K, L, M, α, β) such that $(\tilde{A} + \tilde{B}_2 \tilde{N} \tilde{C}_2)$ is Hurwitz.

Similar to the ILQR case, this problem can be rewritten as

$$\min_{K,L,M,\alpha,\beta} \left\{ \mathrm{tr}\left(\tilde{C}_1 \tilde{P} \tilde{C}_1^T\right) + \eta_a \alpha^2 + \eta_s \beta^2 \right\}, \tag{5.42}$$

where $\tilde{P}$ satisfies

$$\left(\tilde{A} + \tilde{B}_2 \tilde{N} \tilde{C}_2\right) \tilde{P} + \tilde{P} \left(\tilde{A} + \tilde{B}_2 \tilde{N} \tilde{C}_2\right)^T + \tilde{B}_1 \tilde{B}_1^T = 0 \tag{5.43}$$

with $\tilde{N}$ defined by

$$\mathrm{diag}\left\{\tilde{C}_2 \tilde{P} \tilde{C}_2^T\right\} - \frac{1}{2}\Theta \left[\mathrm{erf}^{-1}\left(\tilde{N}\right)\right]^{-2} = 0, \tag{5.44}$$

$$\Theta = \begin{bmatrix} \alpha^2 & 0 \\ 0 & \beta^2 \end{bmatrix}. \tag{5.45}$$

The Lagrange multiplier method is again used obtain a solution of this constrained optimization problem.

Theorem 5.10. *Under Assumption 2, the ILQG problem* (5.41) *is solved by*

$$K = -\frac{N_a}{\lambda_1 + \rho} B_2^T Q, \tag{5.46}$$

$$L = -P C_2^T \frac{N_s}{\mu}, \tag{5.47}$$

$$M = A + B_2 N_a K + L N_s C_2, \tag{5.48}$$

$$\alpha = \mathrm{erf}^{-1}(N_a)\sqrt{2}\sqrt{KRK^T}, \tag{5.49}$$

$$\beta = \mathrm{erf}^{-1}(N_s)\sqrt{2}\sqrt{C_2(P+R)C_2^T}, \tag{5.50}$$

where $(P, Q, R, S, N_a, N_s, \lambda_1, \lambda_2)$ *is a solution of*

$$AP + PA^T - \left(\frac{N_s^2}{\mu}\right) P C_2^T C_2 P + B_1 B_1^T = 0, \tag{5.51}$$

$$A^T Q + QA - \left(\frac{N_a^2}{\rho + \lambda_1}\right) Q B_2 B_2^T Q + C_1^T C_1 + \lambda_2 C_2^T C_2 = 0, \tag{5.52}$$

$$(A + B_2 N_a K) R + R (A + B_2 N_a K)^T + \mu L L^T = 0, \tag{5.53}$$

$$(A + L N_s C_2)^T S + S (A + L N_s C_2) + \rho K^T K = 0, \tag{5.54}$$

$$\lambda_1 - \frac{\rho}{\frac{N_a \sqrt{\pi}}{2\mathrm{erf}^{-1}(N_a)} \exp\left(\mathrm{erf}^{-1} (N_a)^2\right) - 1} = 0, \tag{5.55}$$

$$\left(C_2 P S P C_2^T\right) N_s^T \mu - \frac{\sqrt{\pi} \lambda_2 \beta^2}{4} \mathrm{erf}^{-1}(N_s)^{-3} \times \exp\left(\mathrm{erf}^{-1}(N_s)^2\right) = 0, \tag{5.56}$$

$$\eta_a - \frac{\lambda_1}{2\left(\mathrm{erf}^{-1}(N_a)\right)^2} = 0, \tag{5.57}$$

$$\eta_s - \frac{\lambda_2}{2\left(\mathrm{erf}^{-1}(N_s)\right)^2} = 0, \tag{5.58}$$

which minimizes the ILQG cost

$$\begin{aligned} &J_{ILQG} = \mathrm{tr}\left\{C_1 (P + R) C_1^T\right\} + \\ &\rho \tfrac{N^2}{(\rho+\lambda)^2} B_2^T Q R Q B_2 + 2\eta_a K R K^T \mathrm{erf}^{-1} (N_a)^2 + \\ &2\eta_s C_2 (P + R) C_2^T \mathrm{erf}^{-1} (N_s)^2 . \end{aligned} \tag{5.59}$$

Proof. See Appendix. □

The following technique can be used to obtain the ILQG solution:

For a given $\epsilon > 0$,

(a) With $h(\cdot)$ defined in (5.25), find an ϵ-precise solution N_a of the equation

$$h (N_a) - \frac{\rho}{\eta_a} = 0, \tag{5.60}$$

using bisection (with initial conditions $N_a^- = 0, N_a^+ = 1$);

(b) Find λ_1 from (5.55) or (5.57);

(c) For any N_s, the left hand side of (5.56) can now be determined by finding λ_2, P, Q, R, and S, by solving, in sequence, (5.58), (5.51), (5.52), (5.53) and (5.54). Hence, the left hand side of (5.56) can be expressed as function of N_s;

(d) Find all $N_s \in [0, 1]$ that satisfy (5.56) by using a root-finding technique such as numerical continuation [113], or generalized bisection [114];

(e) For each N_s found in the previous step, compute K, L, M, α, β from (5.46)-(5.50);

(f) Find the quintuple (K, L, M, α, β) that minimizes J_{ILQG} from (5.59).

Remark 5.11. The optimal ILQG solution may correspond to operating open-loop, i.e., $\alpha, \beta = 0$ and $K(sI - A)^{-1}L \equiv 0$.

Remark 5.12. In contrast to conventional LQG, due to the interdependence of (5.51)-(5.58) on both N_a and N_s, the seperation principle does not hold for ILQG.

5.4.2 ILQG controller structure

The ILQG controller (5.36) can be rewritten in the standard observer-based form as

$$\begin{aligned} \dot{x}_C &= Ax_C + B_2 N_a u - L\left(y_m - N_s C_2 x_C\right) \\ u &= Kx_C, \end{aligned} \tag{5.61}$$

which suggests the following nonlinear implementation:

$$\begin{aligned} \dot{x}_C &= Ax_C + B_2 sat_\alpha(u) - L\left(y_m - sat_\beta(C_2 x_C)\right) \\ u &= Kx_C. \end{aligned} \tag{5.62}$$

With (5.62), in the absence of the disturbance w, the estimation error $e = x_G - x_C$ satisfies

$$\dot{e} = Ae + L\left(sat_\beta\left(C_2 x_G\right) - sat_\beta(C_2 x_C)\right), \tag{5.63}$$

so that when $C_2 x_C$ and $C_2 x_G$ are sufficiently small,

$$\dot{e} = \left(A + LC_2\right) e, \tag{5.64}$$

and true estimation occurs. Note that (5.61) and (5.62) yield the same quasilinear closed-loop performance. The nonlinear ILQG controller (5.62) is used for stability verification in the next section.

5.4.3 ILQG stability verification

We now verify the stability of the LPNI system (5.35) controlled by the nonlinear ILQG controller (5.62) with ILQG instrumentation (5.49)-(5.50). Consider the undisturbed version of (5.35) and (5.62), i.e.,

$$\begin{aligned} \dot{x}_G &= Ax_G + B_2 sat_\alpha (Kx_C) \\ \dot{x}_C &= Ax_C + B_2 sat_\alpha(Kx_C) - L\left(y_m - sat_\beta(C_2 x_C)\right) \\ y_m &= sat_\beta(C_2 x_G) \\ z &= C_1 x_G + D_{12} u. \end{aligned} \tag{5.65}$$

Assume that (K, L, M, α, β) is the ILQG solution (5.46)-(5.50), and

$$(P, Q, R, S, N_a, N_s, \lambda_1, \lambda_2)$$

is the corresponding solution of (5.51)-(5.58). We have the following:

Theorem 5.13. *For the closed-loop system* (5.65) *with* (5.46)-(5.50)*:*

(i) $[x_G, x_C] = 0$ *is the unique equilibrium;*

(ii) this equilibrium is exponentially stable;

(iii) if $x_G(0) = x_C(0)$*, a subset of its domain of attraction is given by the set* $\mathcal{Y} \times \mathcal{Y}$*, where*

$$\mathcal{Y} = \left\{ x_G \in R^{n_x} : x_G^T \left(QB_2B_2^TQ\right) x_G \leq \frac{4(\rho + \lambda_1)^2 \alpha^2}{N_a^4} \right\} \cap$$
$$\left\{ x_G \in R^{n_x} : x_G^T C_2^T C_2 x_G \leq \beta^2 \right\}. \tag{5.66}$$

Proof. See Appendix. □

5.4.4 Illustrative example

Reconsider the double integrator example of Section 5.3.4, represented in the form (5.35), with A, B_2, C_1, D_{12} as defined in (5.34) and

$$B_1 = \begin{bmatrix} 0 & 0 \\ 1 & 0 \end{bmatrix}, D_{21} = \begin{bmatrix} 0 & \sqrt{\mu} \end{bmatrix}, C_2 = C_1. \tag{5.67}$$

Assume that $\rho = \mu = 1 \times 10^{-4}$ and consider the following two cases:

Case 1: Fix $\eta_s = 2 \times 10^{-3}$ and examine $\sigma^2_{\hat{z}_1}$, α, β as a function of η_a.

Case 2: Fix $\eta_a = 2 \times 10^{-3}$ and examine $\sigma^2_{\hat{z}_1}$, α, β as a function of η_s.

Figure 5.4 illustrates the ILQG solution for Case 1, where the η_a axis is displayed on a logarithmic scale. Clearly, as η_a increases, α decreases and $\sigma^2_{\hat{z}_1}$ increases. Note that β also decreases, showing that the synthesis of actuator and sensor are not decoupled.

Figure 5.5 shows the behavior for Case 2. As expected, when η_s increases, β decreases and $\sigma^2_{\hat{z}_1}$ increases. In addition, observe that α increases, again demonstrating the lack of seperation in ILQG.

5.5 Generalizations

5.5.1 Arbitrary nonlinearities

The ILQR and ILQG methodologies of Sections 5.3 and 5.4 are easily extended to nonlinearities other than saturation. For such nonlinearities, the Lagrange multiplier

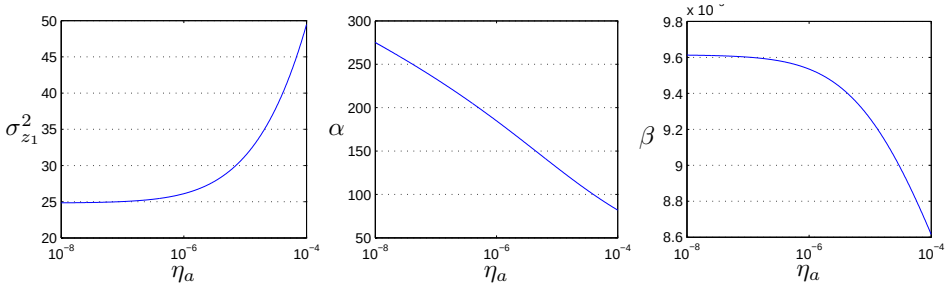

Figure 5.4: ILQG solution for a double integrator as a function of actuator penalty η_a

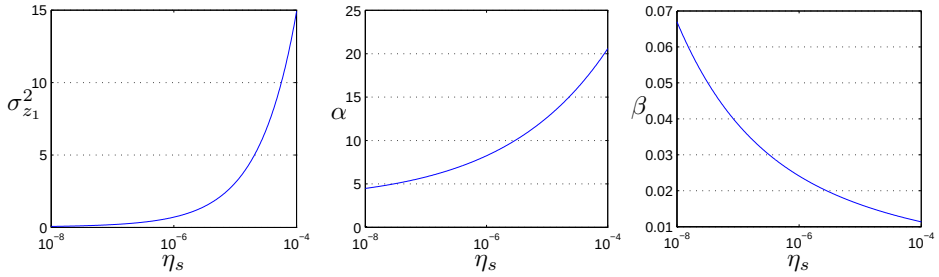

Figure 5.5: ILQG solution for a double integrator as a function of sensor penalty η_s

technique is applied as before, but using different expressions for the quasilinear gains. If $f_\alpha(u)$ and $g_\beta(y)$ are the actuator and sensor nonlinearities, the general expressions for the quasilinear gains are

$$N_a = \mathcal{F}\left(\sigma_{\hat{u}}\right) = \int_{-\infty}^{\infty} f'_\alpha(x) \frac{1}{\sigma_{\hat{u}}\sqrt{2\pi}} \exp\left(-\frac{x}{2\sigma^2_{\hat{u}}}\right) dx, \tag{5.68}$$

$$N_s = \mathcal{G}\left(\sigma_{\hat{v}}\right) = \int_{-\infty}^{\infty} g'_\beta(x) \frac{1}{\sigma_{\hat{y}}\sqrt{2\pi}} \exp\left(-\frac{x}{2\sigma^2_{\hat{y}}}\right) dx. \tag{5.69}$$

For example, if $g_\beta(y)$ is the symmetric deadzone defined in (4.34),

$$\mathcal{G}(\sigma_{\hat{y}}) = 1 - erf\left(\frac{\beta/2}{\sqrt{2}\sigma_{\hat{y}}}\right). \tag{5.70}$$

Similarly, if $g_\beta(y)$ is the mid-tread quantizer

$$\begin{aligned} g_\beta\left(y\right) = \frac{\beta}{2} \sum_{k=1}^{m} \left[\operatorname{sgn}\left(2y + \beta\left(2k-1\right)\right) \times \right. \\ \left. \operatorname{sgn}\left(2y - \beta\left(2k-1\right)\right)\right], \end{aligned} \tag{5.71}$$

then

$$\mathcal{G}(\sigma_{\hat{y}}) = Q_m\left(\frac{\beta}{\sqrt{2}\sigma_{\hat{y}}}\right), \tag{5.72}$$

where

$$Q_m\left(z\right) := \frac{2z}{\sqrt{\pi}} \left[\sum_{k=1}^{m} e^{-\frac{1}{4}(2k-1)^2(z)^2}\right]. \tag{5.73}$$

For the ILQR problem (5.14), the constraint (5.16) now becomes

$$KRK^T - \left[\mathcal{F}^{-1}\left(N\right)\right]^{-2} = 0. \tag{5.74}$$

Similarly, for ILQG, (5.44) becomes

$$\text{diag}\left\{\tilde{C}_2\tilde{P}\tilde{C}_2^T\right\} - \text{diag}\left(\left[\mathcal{F}^{-1}\left(N_a\right)\right]^{-2}, \left[\mathcal{G}^{-1}\left(N_s\right)\right]^{-2}\right) = 0, \tag{5.75}$$

where $\mathcal{F}$ and $\mathcal{G}$ are assumed to be invertible. Existence and uniqueness of the ILQR/ILQG solution will, of course, depend on the specific form of these functions.

5.5.2 Multivariable systems

The methods presented in Sections 5.3 and 5.4 can be extended to the multivariable case. Specifically, consider the MIMO version of (5.37), where $u \in \mathbf{R}^p$ and $y, y_m \in \mathbf{R}^q$, $p, q > 1$, where α, β are understood as

$$\alpha \equiv [\alpha_1 \ ... \ \alpha_p]^T, \ \beta \equiv [\beta_1 \ ... \ \beta_q]^T, \tag{5.76}$$

and

$$sat_\alpha(u) \equiv [sat_{\alpha_1}(u_1) \ ... \ sat_{\alpha_p}(u_p)]^T, \tag{5.77}$$

$$sat_\beta(y) \equiv [sat_{\beta_1}(y_1) \ ... \ sat_{\beta_p}(y_q)]^T. \tag{5.78}$$

As before, the quasilinearization of this system is given by (5.38)-(5.40) with the equivalent gains of (5.77) and (5.78) specified by

$$N_a = \text{diag}\left(N_{a_1}, N_{a_2}, ..., N_{a_p}\right), \tag{5.79}$$

and

$$N_s = \text{diag}\left(N_{s_1}, N_{s_2}, ..., N_{a_q}\right), \tag{5.80}$$

respectively, where

$$N_{a_k} = \text{erf}\left(\frac{\alpha_k}{\sqrt{2}\sigma_{\hat{u}_k}}\right), \ N_{s_l} = \text{erf}\left(\frac{\beta_l}{\sqrt{2}\sigma_{\hat{y}_l}}\right), \tag{5.81}$$

for $k = 1, ..., p$ and $l = 1, ..., q$.

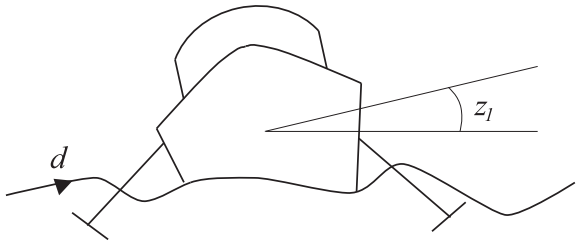

Figure 5.6: Ship-roll example

The ILQG problem (5.41) now becomes

$$\min_{K,L,M,\alpha,\beta} \left\{ \sigma_{\tilde{z}}^2 + \alpha^T W_a \alpha + \beta^T W_s \beta \right\}, \tag{5.82}$$

where W_a, W_s are diagonal and positive definite. Clearly, this can be rewritten as

$$\min_{K,L,M,\alpha,\beta} \left\{ \mathrm{tr}\left(\tilde{C}_1 \tilde{P} \tilde{C}_1^T \right) + \alpha^T W_a \alpha + \beta^T W_s \beta \right\}, \tag{5.83}$$

subject to the constraints (5.43) and (5.44), with Θ in (5.44) becoming

$$\Theta = \begin{bmatrix} \mathrm{diag}(\alpha\alpha^T) & 0 \\ 0 & \mathrm{diag}(\beta\beta^T) \end{bmatrix}. \tag{5.84}$$

The optimization is carried out in a manner analagous to the proof of Theorem 5.10, and the necessary conditions for minimality are obtained in terms of the Lagrange multiplier $\Lambda = [\lambda_1, ..., \lambda_{(p+q)}]$.

5.6 Example: Ship Roll Damping

This section considers the ship-roll damping problem originally described in [115] and studied in [5] in the context of SLQR/SLQG. The merits of ILQR and ILQG will be demonstrated in comparison with these other techniques.

5.6.1 Model and problem

Ship roll oscillations caused by sea waves lead to passenger discomfort. To minimize this discomfort, the roll angle of the ship should be maintained at less than 3

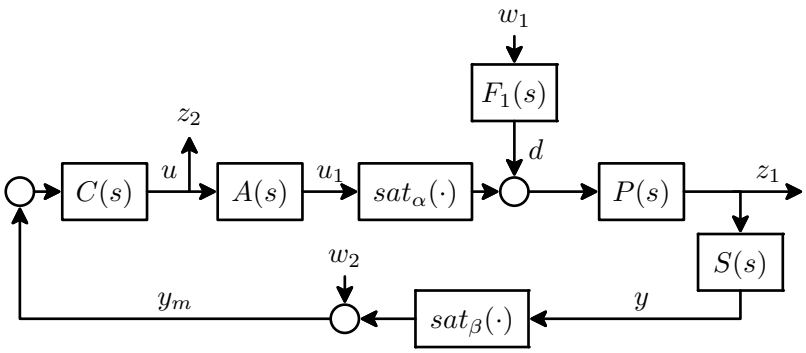

Figure 5.7: Block diagram for ship-roll example

degrees. One approach to reducing ship-oscillations involves the use of two actively controlled stabilizing wings attached to the stern, as illustrated in Figure 5.6. Clearly, the angular travel of these wings is constrained, leading to actuator saturation.

This system is represented by the block diagram of Figure 5.7, which is interpereted as follows:

i) $P(s)$: The ship transfer function from torque (in Nm) to roll angle z_1 (in radians);

ii) $F_1(s)$: The coloring filter that generates the random wave torque signal d from standard white noise w_1;

iii) $A(s)$: The transfer function from the voltage u (in V) to the actuator that drives the wings to the dipping angle u_1 (in rad);

iv) $sat_\alpha(u_1)$: Actuator saturation nonlinearity;

v) $S(s)$: The transfer function of the sensor (gyroscope) with output y (in V);

vi) $sat_\beta(y)$: Sensor saturation nonlinearity;

vii) $C(s)$: The controller that generates u.

As demonstrated in [5], using data from [115, 116], the above system can be represented in state-space form as:

$$\dot{x}_G = \begin{bmatrix} -1.125 & -1.563 & 0.985 & 0 \\ 1 & 0 & 0 & 0 \\ 0 & 0 & -0.286 & -0.311 \\ 0 & 0 & 1 & 0 \end{bmatrix} x_G + \begin{bmatrix} 0 \\ 0 \\ 1 \\ 0 \end{bmatrix} w_1 + \begin{bmatrix} 1 \\ 0 \\ 0 \\ 0 \end{bmatrix} sat_\alpha(u) \tag{5.85}$$

$$z_1 = \begin{bmatrix} 0 & 0.109 & 0 & 0 \end{bmatrix} x_G \tag{5.86}$$

$$y = \begin{bmatrix} 0 & 1.248 & 0 & 0 \end{bmatrix} x_G \tag{5.87}$$

$$y_m = sat_\beta(y) + \sqrt{\mu} w_2 \tag{5.88}$$

Note that the system is normalized so that $\alpha = 1$ corresponds to an angular travel of 18 degrees, which is the saturation authority given in [115].

In [5], this problem was studied in the context of SLQR and SLQG. In particular, when the instrumentation is fixed at $\alpha = 1$ and $y_m = y$ (i.e., the sensor is linear), SLQR and SLQG are used to synthesize a controller that achieves the performance specification $\sigma_{z_1} < 3$ degrees, where σ_{z_1} is the standard deviation of the roll angle. The subsequent sections demonstrate the ILQR and ILQG approach to this problem.

5.6.2 ILQR solution

Based on the previous subsection, the following design objectives are specified:

(1) $\sigma_{\hat{z}_1} < 3$ rad

(2) $\alpha \leq 1$.

Using the ILQR solution method with the tuned penalties $\eta = 3.5 \times 10^{-3}$ and $\rho = 1 \times 10^{-6}$, we obtain

$$K = \begin{bmatrix} -5.641 & -7.565 & -3.672 & 0.2058 \end{bmatrix}, \tag{5.89}$$

$$\alpha = 0.78 \Rightarrow 14 \text{ deg}, \tag{5.90}$$

resulting in

$$\sigma_{\hat{z}_1} = 2.72. \tag{5.91}$$

Numerical simultation of the nonlinear system with this controller and actuator reveals that

$$\sigma_{z_1} = 2.79, \tag{5.92}$$

which verifies the accuracy of the quasilinearization. Clearly, the design objectives are met. Note that by simultaneously synthesizing the controller and instrumentation, we find a solution that uses a saturation authority of less than 18 degrees.

5.6.3 ILQG solution

Using the tuned parameters $\eta_a = 2.55 \times 10^{-3}$, $\eta_s = 1 \times 10^{-10}$, $\rho = 1 \times 10^{-5}$ and $\mu = 1 \times 10^{-5}$, the ILQG solution method results in

$$K = \begin{bmatrix} -2.029 & -2.798 & -1.264 & 0.0709 \end{bmatrix}, \tag{5.93}$$

$$L = \begin{bmatrix} -80.77 & -16.09 & -281.41 & -100.38 \end{bmatrix}^T, \tag{5.94}$$

$$\alpha = 0.91, \ \beta = 0.35, \tag{5.95}$$

leading to

$$\sigma_{\hat{z}_1} = 2.56, \tag{5.96}$$

Simulation of the nonlinear system yields

$$\sigma_{z_1} = 2.77, \tag{5.97}$$

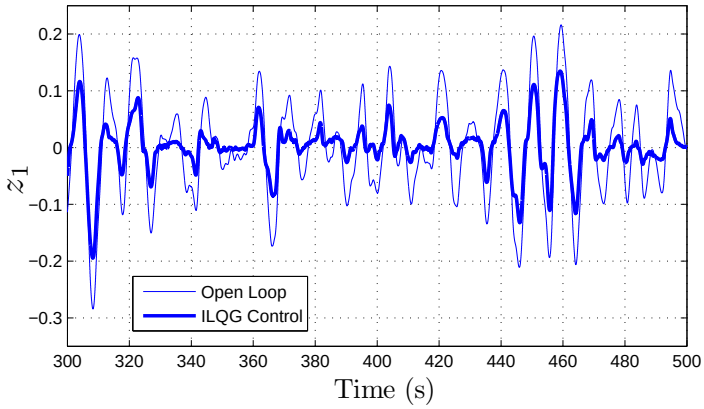

Figure 5.8: Time trace of z_1 for ship-roll example

which meets the performance specification. As anticipated, the performance of the actual nonlinear system (5.97) is within 8% of its quasilinear approximation (5.96). Figure 5.8 shows a time trace of z_1 for both the open- and closed-loop systems. Note that in open loop $\sigma_{z_1} = 5.5$, so that control results in a 50% performance improvement.

5.7 Summary

The instrumentation, i.e., sensors and actuators, in feedback control systems often contain nonlinearities, such as saturation, deadzone, quantization, etc. Standard synthesis techniques, however, do not take these nonlinearities into account. The main contribution of this chapter is the modification of the LQR/LQG methodology into the so-called Instrumented LQR/LQG (referred to as ILQR/ILQG), which allows for the synthesis of not only a controller but also the instrumentation in an optimal manner. This is accomplished by

(i) modifying the standard LQR/LQG performance index to include a parameterized instrumentation cost;

(ii) quasi-linearizing the linear plant/nonlinear instrumentation (LPNI) system us-

ing the method of stochastic linearization;

(iii) based on the Lagrange multiplier technique, deriving necessary conditions of optimality, which turn out to be closely related to the usual LQR/LQG necessary conditions but containing additional transcendental equations to account for the Lagrange multipliers related to the instrumentation cost;

(iv) providing a bisection-based algorithm for solving these equations with any desired accuracy;

(v) proving that the controller and the instrumentation, thus derived, ensure the asymptotic stability of the nonlinear closed loop system and providing an estimate of the resulting domain of attraction.

An application of ILQR/ILQG to a problem of ship roll disturbance rejection is also reported.

CHAPTER VI

CONCLUSIONS & FUTURE WORK

6.1 Conclusions

This dissertation has addressed the problem of control design for Linear Plant/ Nonlinear Instrumentation systems. Traditionally, design methods for this class of systems have been difficult to obtain, due to analytical difficulties posed by the nonlinearities. It has been shown herein that, by using the stochastic linearization approximation technique, such difficulties are overcome, leading to three design methodologies: the S-root locus, Boosting, and Instrumented LQR/LQG. These three results, along with a few others from the existing literature, form a new paradigm in control theory, referred to as *quasilinear control theory*.

Quasilinear control theory has the potential to be broadly applicable because saturation, quantization and other instrumentation nonlinearities are a ubiquitous limitation in control systems. Moreover, as suggested by the examples presented in this dissertation, these results have the ability to yield control strategies that are effective in real-world applications. Being based on widely known linear techniques such as Root Locus and LQR/LQG, quasilinear theory is a promising alternative for practicing control engineers. Indeed, each of the quasilinear methods of this dissertation can be carried out with a computational effort that is commensurate

with its conventional counterpart. Clearly, however, only extensive use of these new methodologies will confirm their potential.

6.2 Future Work

A number of extensions of this dissertation are possible as future research problems. A few possibilities are outlined below:

6.2.1 Analytical characterization of Gaussianization

It was shown in Chapter II that stochastic linearization is justified by a phenomenon called Gaussianization, i.e., the property that the statistical characteristics of the output of a low-pass filtering plant are closer to Gaussian than those at the input. As described, this phenomenon has been verified for certain classes of systems. A complete theory of Gaussianization in LPNI systems would analytically validate the accuracy of stochastic linearization. The method of *cumulants*, in particular, appears to be a promising tool for establishing such a theory [102].

6.2.2 Linear Matrix Inequality method

Many optimization problems in control theory can be formulated in terms of linear matrix inequalities. Numerical techniques for solving these LMIs have led to new methods for controller design [117]. Using stochastic linearization, it is possible to investigate how LMI-based methods can be used for LPNI systems.

6.2.3 Rate nonlinearities

This dissertation has focused on static magnitude nonlinearities - saturation, deadzone, quantization, etc. Of course, many types of instrumentation also exhibit *rate* nonlinearities. These can often be modeled as a linear system in combination with a magnitude nonlinearity. For example, a typical rate-saturated actuator is shown

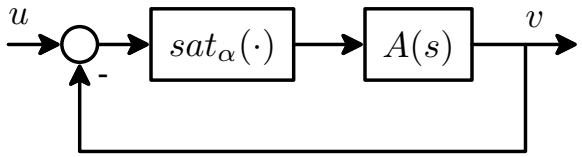

Figure 6.1: Typical rate-saturated actuator consisting of LTI system $A(s)$ and saturation nonlinearity

in Figure 6.1. The theory developed in this dissertation can be extended for such systems.

6.2.4 Experimental verification

Most of the verification in this dissertation is in the form of simulation studies. It would, of course, be interesting to perform a comprehensive experimental validation of these results in an industrial setting.

APPENDICES

APPENDIX A

Proofs for Chapter III

Proof of Lemma 3.6. Part (i): To prove continuity, note that (3.4) can be rewritten as

$$F(K, K_e(K)) = 0, \tag{A.1}$$

where

$$F(x, y) = y - x\text{erf}\left(\frac{\alpha}{\sqrt{2}x\left\|\frac{F_\Omega(s)C(s)}{1+yP(s)C(s)}\right\|_2}\right) \tag{A.2}$$

is an analytic function. Hence, $K_e(K)$ is a root of an analytic equation that depends on a parameter K. As it is well known, the roots of such an equation are continuous with respect to the parameter, and the result follows.

The proof of strict monotonicity is by contradiction. Indeed, let us assume that there exists K_1, K_2 such that $K_2 > K_1$ and $K_e(K_1) = K_e(K_2) = K_e^*$. This implies that

$$K_2\text{erf}\left(\frac{\alpha}{\sqrt{2}K_2\sigma^*}\right) = K_1\text{erf}\left(\frac{\alpha}{\sqrt{2}K_1\sigma^*}\right), \tag{A.3}$$

where

$$\sigma^* = \left\|\frac{F_\Omega(s)\,C(s)}{1 + K_e^* C(s)\,P(s)}\right\|_2. \tag{A.4}$$

However, it is straightforward to verify that the function

$$f(x) = x\text{erf}\left(\frac{c}{x}\right) \tag{A.5}$$

is strictly monotonic for all $c > 0$. Hence (A.3) implies $K_1 = K_2$, which contradicts the assumption that $K_2 > K_1$. Therefore, $K_e(K)$ must be a strictly monotonic function.

Part (ii):

Note that (3.4) can be expressed equivalently as

$$K_e(K) = K\text{erf}\left(\frac{\alpha}{\sqrt{2}K\phi(K)}\right), \tag{A.6}$$

where

$$\phi(K) = \left\| \frac{F_\Omega(s) C(s)}{1 + K_e(K) P(s) C(s)} \right\|_2. \tag{A.7}$$

By expanding erf$(\cdot)$ in (A.6), in Taylor series, one obtains

$$K_e(K) = \frac{\sqrt{2}K}{\sqrt{\pi}}\left(\frac{\alpha}{K\phi(K)} - \frac{1}{3}\left(\frac{\alpha}{K\phi(K)}\right)^3 ...\right). \tag{A.8}$$

It follows from continuity and strict monotonicity that the limit of $K_e(K)$ as $K \to \infty$ either exists or is infinity. The remainder of the proof is by contradiction. Namely, assume that β_1 and β_2 are any two distinct positive solutions of (3.36), while $K_e(K)$ is unique for all K. Taking the limit of (A.7) and (A.8) results in

$$\lim_{K\to\infty} K_e(K) = \lim_{K\to\infty}\left(\frac{\alpha\sqrt{2/\pi}}{\phi(K)} - \frac{\sqrt{2/\pi}}{3}\left(\frac{\alpha^3}{K^2\phi^3(K)}\right)\cdots\right) \tag{A.9}$$

and

$$\lim_{K\to\infty} \phi(K) = \left\| \frac{F_\Omega(s) C(s)}{1 + \left(\lim_{K\to\infty} K_e(K)\right) P(s) C(s)} \right\|_2. \tag{A.10}$$

These constitute equations for the limits of $K_e(K)$ and $\phi(K)$ when K tends to infinity. Two possible solutions of (A.9) and (A.10) exist, given by:

$$\lim_{K\to\infty} K_e(K) = \frac{\alpha\sqrt{2/\pi}}{\beta_i}.$$

$$\lim_{K\to\infty} \phi(K) = \beta_i, i = 1, 2.$$

Clearly, this contradicts the assumption of uniqueness of solution of $K_e(K)$ and hence, (3.36) cannot admit multiple positive solutions. □

Proof of Theorem 3.7. Proof of Part (i):

Necessity: Assume (3.37). Take the limit of (A.7) as $K \to \infty$, using the assumption that $T_\gamma(s)$ is stable for all $\gamma > 0$, to obtain

$$\lim_{K\to\infty} \phi(K) = \left\| \frac{F_\Omega(s) C(s)}{1 + \left(\frac{\alpha\sqrt{2/\pi}}{\beta}\right) P(s) C(s)} \right\|_2 \triangleq \phi, \tag{A.11}$$

where $\phi > 0$. By taking the limit of (A.8) it follows from (A.11) that

$$\lim_{K\to\infty} K_e(K) = \frac{\alpha\sqrt{2/\pi}}{\phi}. \tag{A.12}$$

Hence, from (3.37) we obtain

$$\phi = \beta. \tag{A.13}$$

Substituting (A.13) into (A.11) yields (3.36). The uniqueness of solution of (3.36) is guaranteed by Lemma 3.6.

Sufficiency: Assume (3.36) admits a unique solution $\beta > 0$. Recall that (A.9) and (A.10) are equations for the limits of $K_e(K)$ and $\phi(K)$ when K tends to infinity, and are satisfied by

$$\lim_{K\to\infty} K_e(K) = \frac{\alpha\sqrt{2/\pi}}{\beta}, \tag{A.14}$$

$$\lim_{K\to\infty} \phi(K) = \beta. \tag{A.15}$$

The right hand sides of (A.14) and (A.15) are the unique solutions of (A.9) and (A.10). Indeed, suppose that

$$\lim_{K\to\infty} K_e(K) = \frac{\alpha\sqrt{2/\pi}}{\beta_l},$$

$$\lim_{K\to\infty} \phi(K) = \phi_l.$$

also satisfy (A.9) and (A.10). It follows from necessity that β_l must be a solution of (3.36), and thus by Lemma 3.6, $\beta_l = \beta$. Then, (A.11) implies $\phi_l = \beta$. Hence, (A.14) and (A.15) are the only solutions of (A.9) and (A.10). The proof concludes by noting that (A.14) yields (3.37).

Proof of Part (ii):

Sufficiency: Recall that the limit of $K_e(K)$ either exists or is infinite. Hence, by part (i), if $\beta = 0$ is the only real solution of (3.36), then the limit of $K_e(K)$ must be infinity.

Necessity: Assume (3.38). Then it follows from part (i) that (3.36) cannot admit a unique positive solution. By Lemma 3.6, (3.36) cannot admit multiple positive solutions, and hence it follows that $\beta = 0$ must be the only real solution of (3.36). □

To prove Theorem 3.8 we need the following lemma.

Lemma 1.1. *Let $T_\gamma(s)$ be stable only for $\gamma \in [0, \Gamma)$, $\Gamma < \infty$, such that* (3.35) *holds, and* (3.4) *admit a unique solution for all $K > 0$, i.e., Case 2. Then*

$$K_e(K) < \Gamma \quad \forall K > 0. \tag{A.16}$$

Proof. The proof is by contradiction. Namely, assume that there exists $K^* > 0$ such that $\Gamma = K_e(K^*)$. Then it follows from (3.4) that

$$K_e(K^*) = K^* \mathrm{erf}\left(\frac{\alpha}{\sqrt{2}K^* \left\| \frac{F_\Omega(s)C(s)}{1+K_e(K^*)P(s)C(s)} \right\|_2} \right). \tag{A.17}$$

This, however, is a contradiction because the left hand side of (A.17) is equal to the positive number Γ, while the right hand side is 0. This contradiction completes the proof. □

Proof of Theorem 3.8. By Lemma 1.1, the limit of $K_e(K)$ as K tends to infinity must

exist and satisfy

$$\lim_{K\to\infty} K_e\left(K\right) \leq \Gamma.$$

The remainder of the proof follows is analagous to that of Theorem 3.7. □

Proof of Theorem 3.12. Part (i): We will prove that for any $K_e^d > 0$, there exists K^d such that $K_e(K^d) = K_e^d$. Consider $F(K^d, K_e^d)$, where $F(\cdot,\cdot)$ was defined in (A.2). Clearly,

$$F\left(0, K_e^d\right) = K_e^d > 0. \tag{A.18}$$

Moreover, Taylor series expansion of $\mathrm{erf}(\cdot)$ in (A.2) yields,

$$\lim_{K^d\to\infty} F\left(K^d, K_e^d\right) = K_e^d - \frac{\alpha\sqrt{2/\pi}}{\left\|\frac{F_\Omega(s)C(s)}{1+K_e^d P(s)C(s)}\right\|_2}. \tag{A.19}$$

Note that every positive solution β of (3.36) is related to a finite root K_e^d of the right hand side of (A.19) through

$$K_e^d = \frac{\alpha\sqrt{2/\pi}}{\beta},$$

and vice versa. It follows from (A.19) that

$$\lim_{K^d\to\infty} F\left(K^d, 0\right) = -\frac{\alpha\sqrt{2/\pi}}{\left\|F_\Omega\left(s\right)C\left(s\right)\right\|_2} < 0. \tag{A.20}$$

Since (3.36) admits no solution $\beta > 0$, the right hand side of (A.19) has no finite roots. Moreover, the right hand side of (A.19) is a continuous function of K_e^d. Hence, (A.20) implies that

$$\lim_{K^d\to\infty} F\left(K^d, K_e^d\right) < 0. \tag{A.21}$$

Recall that $F(K^d, K_e^d)$ is continuous and monotonically decreasing in K^d. It thus follows from (A.18) and (A.21) that for any $K_e^d > 0$, $F(K^d, K_e^d)$ changes sign exactly once as K^d goes from 0 to ∞. Hence, there exists a unique K^d such that $F(K^d, K_e^d) = 0$. Thus, $K_e(K^d) = K_e^d$, and the result follows immediately.

Part (ii): Note that for $K = 0$, (3.4) admits a unique solution $K_e(0) = 0$. Hence, by continuity, (3.4) defines a unique $K_e(K)$ when K is small enough. The S-origination point occurs when (3.4) starts admitting multiple solutions. □

Proof of Theorem 3.13. Part (i): By the continuity of roots of (A.2), all solutions $K_e(K)$ of (3.4) must be continuous in K. The remainder of the proof is analagous to that of sufficiency in Theorem 3.7. Namely, it follows that for each β_i,

$$\lim_{K\to\infty} K_e(K) = \frac{\alpha\sqrt{2/\pi}}{\beta_i} \tag{A.22}$$

and

$$\lim_{K\to\infty} \phi(K) = \beta_i \tag{A.23}$$

are valid solutions for the limiting values of $K_e(K)$ and $\phi(K)$ (i.e., (A.9) and (A.10)). Clearly, (A.22) yields (3.48).

Part (ii): It follows from (3.4) (and has been studied in [14]) that for any K, stochastic linearization must yield an odd number of solutions. Hence, if (3.36) yields an even number of (finite) solutions for the limit of $K_e(K)$, an additional solution must exist, corresponding to the solution $\beta_0 = 0$.

Part (iii): Let κ_1 denote the limiting gain (given by Part (i)) corresponding to the largest simple root of (3.36), and define K_e^t such that

$$\kappa_1 < K_e^t < \kappa_2,$$

where κ_2 denotes the next largest (if any) limiting gain. Clearly, from (A.18),

$$F\left(0, K_e^t\right) > 0, \tag{A.24}$$

and since $K_e^d = \kappa_1$ is the smallest simple root of the right hand side of (A.19), it follows from continuity and (A.20) that

$$\lim_{K^d\to\infty} F\left(K^d, K_e^t\right) > 0. \tag{A.25}$$

Recalling that $F(K^d, K_e^t)$ is continuous and monotonically decreasing in K^d, it follows from (A.24) and (A.25) that

$$F\left(K^d, K_e^t\right) \neq 0 \quad \forall K^d > 0. \tag{A.26}$$

Thus, $K_e(K^d) = K^t$ cannot be satisfied for any $K^d > 0$, and hence $K_e(K)$ cannot lie in the interval (κ_1, κ_2). The result follows directly.

□

Proof of Theorem 3.14. The proof is by construction. Namely, let $C(s)$ be given by the inverse of the plant, such that

$$C(s) = \frac{1}{P(s)}.$$

Then (3.4) reduces to

$$K_e = K\text{erf}\left(\frac{\alpha}{\sqrt{2}K\left\|F_\Omega(s)/P(s)\right\|_2}(1 + K_e)\right). \tag{A.27}$$

For any fixed $K > 0$, the right hand side of (A.27) is a strictly concave function of K_e, starting from a positive value

$$K\text{erf}\left(\frac{\alpha}{\sqrt{2}\left\|F_\Omega(s)/P(s)\right\|_2}\right) > 0$$

at $K_e = 0$ and bounded by K for all $K_e > 0$. Moreover, the left hand side of (A.27) is K_e. Hence, there exists a unique $K_e > 0$ that satisfies (A.27).

□

APPENDIX B

Proofs for Chapter IV

Proof of Theorem 4.2. Sufficiency: From (4.19) and (4.20),

$$K_a \mathcal{F}\left(K_a \left\| \frac{P(s)\,C(s)}{1+P(s)\,C(s)} \right\|_2\right) = 1. \tag{B.1}$$

It follows from (B.1) that (4.12) is a solution of (4.18). Thus, a-boosting is possible with the boosting gain K_a.

Necessity: a-Boosting is possible with the boosting gain K_a. Thus, (4.12) and (4.18) hold. Clearly, substituting the former into the latter yields (4.19) and (4.20).

□

Proof of Theorem 4.3. It is straightforward to show that the function

$$h(x) = x\mathrm{erf}\left(\frac{c}{x}\right) \tag{B.2}$$

is continuous and monotonically increasing $\forall c > 0$, with the property that

$$h(0) = 0 \tag{B.3}$$

and

$$\lim_{x\to\infty} h(x) = \frac{2}{\sqrt{\pi}}c. \tag{B.4}$$

Hence, (4.24) admits a positive solution if and only if

$$\frac{2}{\sqrt{\pi}}c > 1, \tag{B.5}$$

which is equivalent to (4.26). Moreover, any positive solution of (4.24) must be unique because $h(x)$ defined in (B.2) is monotonically increasing. □

Proof of Theorem 4.5. Observe from Figure 4.3 that

$$K_a N_a = K_a \mathcal{F}\left(\left\| \frac{P(s)\, C(s) N_s K_s K_a}{1 + P(s)\, N_s K_s N_a K_a C(s)} \right\|_2\right) \tag{B.6}$$

and

$$K_s N_s = K_s \mathcal{G}\left(\left\| \frac{P(s)}{1 + P(s)\, N_s K_s N_a K_a C(s)} \right\|_2\right). \tag{B.7}$$

Subtituting

$$K_a N_a = K_s N_s = 1 \tag{B.8}$$

into (B.6) and (B.7) yields (4.18) and (4.31), which establishes the separation principle. □

APPENDIX C

Proofs for Chapter V

Proof of Theorem 5.3. We use the Lagrange multiplier method to find the necessary conditions for optimality. First, the regularity of the constraints is verified. Let (K, N, R, α) satisfy (5.15) and (5.16), and for an arbitrary symmetric matrix Q and real number λ, define

$$\Phi(K, N, R, \alpha) = \operatorname{tr}\left(\left[(A + B_2NK)R + R(A + B_2NK)^T + B_1B_1^T\right]Q\right) + \lambda\left(KRK^T - \frac{\alpha^2}{2\left(\operatorname{erf}^{-1}(N)\right)^2}\right). \tag{C.1}$$

Differentiating Φ with respect to K, N, R, α and equating to zero, we obtain:

$$NB_2^TQR + \lambda KR = 0, \tag{C.2}$$

$$KRQB_2 + \lambda\frac{\sqrt{\pi}}{4}\alpha^2\frac{\exp\left(erf^{-1}(N)^2\right)}{erf^{-1}(N)^3} = 0, \tag{C.3}$$

$$(A + B_2NK)^TQ + Q(A + B_2NK) + \lambda K^TK = 0, \tag{C.4}$$

$$\frac{-2\lambda\alpha}{2\operatorname{erf}^{-1}(N)^2} = 0. \tag{C.5}$$

Since $N \in (0, 1)$ and $\alpha > 0$, it follows from (C.5) that $\lambda = 0$, which, through (C.4) implies that $Q = 0$. Consequently, (C.2) and (C.3) are satisfied and the constraints are regular.

Next, form the Lagrangian:

$$\begin{aligned}\Psi(K,N,R,Q,\lambda,\alpha) &= \operatorname{tr}\left(C_1 R C_1^T\right) + \rho K R K^T + \eta\alpha^2 \\ &+ \operatorname{tr}\left(\left[\left(A+B_2NK\right)R + R\left(A+B_2NK\right)^T + B_1B_1^T\right]Q\right) \\ &+ \lambda\left(KRK^T - \frac{\alpha^2}{2\left(\operatorname{erf}^{-1}(N)\right)^2}\right). \end{aligned} \tag{C.6}$$

Differentiating Ψ with respect to $K, N, R, Q, \lambda, \alpha$ results in

$$\left((\rho+\lambda)K + NB_2^TQ\right)R = 0, \tag{C.7}$$

$$KRQB_2 + \lambda\alpha^2\frac{\sqrt{\pi}}{4}\frac{\exp\left(\operatorname{erf}^{-1}(N)^2\right)}{\left(\operatorname{erf}^{-1}(N)\right)^3} = 0, \tag{C.8}$$

$$\begin{aligned}&\left(A+B_2NK\right)^TQ + Q\left(A+B_2NK\right) + C_1^TC_1 \\ &+ (\rho+\lambda)K^TK = 0,\end{aligned} \tag{C.9}$$

$$\left(A+B_2NK\right)R + R\left(A+B_2NK\right)^T + B_1B_1^T = 0, \tag{C.10}$$

$$KRK^T - \frac{\alpha^2}{2\operatorname{erf}^{-1}(N)^2} = 0, \tag{C.11}$$

$$2\eta\alpha - \frac{2\lambda\alpha}{2\operatorname{erf}^{-1}(N)^2} = 0. \tag{C.12}$$

The equations (5.17) and (5.18) for the parameters K and α follow immediately from (C.7) and (C.11), respectively. Substituting (5.17) into (C.9)-(C.10) yields (5.19)-(5.20). Multiplying (C.7) from the right by K^T and using (C.8) and (C.11) yields (5.21). Finally, (5.22) follows immediately from (C.12).

We now argue that the ILQR problem (5.13) has a solution, i.e., the minimum exists and is attained. For that purpose, note that (5.13) can be reformulated as

$$\min_{\alpha}\left\{\eta\alpha^2 + \min_{K}\sigma_{\hat{z}}^2\right\}. \tag{C.13}$$

It is known from [5] that, under Assumption 1, for every $\alpha > 0$, the gain K that solves the minimization problem

$$\min_K \sigma_{\hat{z}}^2 \tag{C.14}$$

exists. Moreover, the achieved minimum is continuous with respect to α. Thus, the function

$$q(\alpha) = \eta\alpha^2 + \min_K \sigma_{\hat{z}}^2 \tag{C.15}$$

is continuous for $\alpha \geq 0$ and tends to ∞ as $\alpha \to \infty$. Hence, $q(\alpha)$ achieves a minimum at some $a^* \geq 0$. Let K^* be the minimizer of (C.14) when $\alpha = \alpha^*$. Then the pair (K^*, α^*) solves (5.13).

Finally, we prove that (5.19)-(5.22) admits a unique solution. Since (A, B_2) is stabilizable and (C_1, A) is detectable, for any $N \in (0, 1), \lambda > 0$, the Ricatti equation (5.19) has a unique positive semidefinite solution Q such that $(A+B_2NK)$ is Hurwitz, where K satisfies (5.17). With this Q, since $(A + B_2NK)$ is Hurwitz, the Lyapunov equation (5.20) has a unique positive semidefinite solution for R. Hence, to show that (5.19)-(5.22) admits a unique solution, it is sufficient to show that (5.21), (5.22) yields a unique solution for (N, λ).

Recall that (5.21) can be substituted into (5.22) to yield (5.24). Furthermore, note that (5.25) can be rewritten as

$$h(N) = h_1(N)h_2(N), \tag{C.16}$$

where

$$h_1(N) = \text{erf}^{-1}(N), \tag{C.17}$$

$$h_2(N) = \left(N\sqrt{\pi}\text{exp}\left(\text{erf}^{-1}\left(N\right)^2\right) - 2\text{erf}^{-1}(N)\right). \tag{C.18}$$

Taking the derivatives of these functions with respect to N, one can show

$$h_1'(N), h_1''(N), h_2'(N), h_2''(N) > 0.$$

Moreover, $h_1(0) = h_2(0) = 0$ and thus,

$$h'(N) > 0,\ h''(N) > 0. \tag{C.19}$$

Clearly, $h(0) = 0$ and, furthermore, note that $h(N)$ has a vertical asymptote at $N = 1$. Thus, since $\rho, \eta > 0$, the left hand side of (5.24) changes sign exactly once in the interval $N \in (0, 1)$. Hence, (5.24) yields a unique solution N. Using this N, the value of λ is uniquely determined by either (5.21) or (5.22).

Since the optimization has an achievable solution, and the necessary conditions are uniquely satisfied, (5.17) and (5.18) constitute the globally minimizing solution. The cost (5.23) follows directly. □

Proof of Theorem 5.6. We begin by showing that the partial derivatives of $\gamma^2(\rho, \eta)$ are nonnegative. Define $\tau(\rho, \eta)$ as

$$\tau(\rho, \eta) = \frac{\rho + \lambda(\rho, \eta)}{N^2(\rho, \eta)}. \tag{C.20}$$

It is clear from (5.20) that $\gamma^2(\rho, \eta)$ depends on (ρ, η) through $\tau(\rho, \eta)$. Thus,

$$\begin{aligned} \frac{\partial}{\partial \rho}\gamma^2(\rho, \eta) &= \frac{\partial}{\partial \rho}\mathrm{tr}\left\{C_1 R(\tau(\rho, \eta)) C_1^T\right\} \\ &= \frac{d}{d\tau}\mathrm{tr}\left\{C_1 R(\tau) C_1^T\right\} \frac{\partial}{\partial \rho}\tau(\rho, \eta) \end{aligned} \tag{C.21}$$

and, similarly,

$$\frac{\partial}{\partial \eta}\gamma^2(\rho, \eta) = \frac{d}{d\tau}\mathrm{tr}\left\{C_1 R(\tau) C_1^T\right\} \frac{\partial}{\partial \eta}\tau(\rho, \eta). \tag{C.22}$$

We begin by obtaining $\mathrm{tr}\left\{C_1 R'(\tau) C_1^T\right\}$. Substituting (C.20) into (5.19) and (5.20) yields

$$\begin{aligned} &\left[A - \frac{1}{\tau}B_2 B_2^T Q(\tau)\right]^T Q(\tau) + Q(\tau)\left[A - \frac{1}{\tau}B_2 B_2^T Q(\tau)\right] \\ &\quad + \frac{1}{\tau}Q(\tau) B_2 B_2^T Q(\tau) + C_1^T C_1 = 0, \end{aligned} \tag{C.23}$$

$$\left[A-\frac{1}{\tau}B_2B_2^TQ\left(\tau\right)\right]R\left(\tau\right)+R\left(\tau\right)\left[A-\frac{1}{\tau}B_2B_2^TQ\left(\tau\right)\right]^T + B_1B_1^T=0. \tag{C.24}$$

Differentiating these equations with respect to τ results in

$$\left[A-\frac{1}{\tau}B_2B_2^TQ\left(\tau\right)\right]^TQ'\left(\tau\right)+Q'\left(\tau\right)\left[A-\frac{1}{\tau}B_2B_2^TQ\left(\tau\right)\right] + \frac{1}{\tau^2}Q\left(\tau\right)B_2B_2^TQ\left(\tau\right)=0, \tag{C.25}$$

$$\left[A-\frac{1}{\tau}B_2B_2^TQ\left(\tau\right)\right]R'\left(\tau\right)+R'\left(\tau\right)\left[A-\frac{1}{\tau}B_2B_2^TQ\left(\tau\right)\right]^T + \frac{1}{\tau}B_2B_2^T\left[\frac{1}{\tau}Q\left(\tau\right)-Q'\left(\tau\right)\right]R\left(\tau\right) + \frac{1}{\tau}R\left(\tau\right)\left[\frac{1}{\tau}Q\left(\tau\right)-Q'\left(\tau\right)\right]B_2B_2^T=0. \tag{C.26}$$

To simplify the notation, we omit below the arguments of Q and R. Premultiplying (C.24) by Q and subtracting from (C.23) results in

$$\frac{1}{\tau}B_2^TQRQB_2+\mathrm{tr}\left\{C_1RC_1^T\right\}-\mathrm{tr}\left\{B_1^TQB_1\right\}=0. \tag{C.27}$$

Taking the derivative of this equation with respect to τ gives

$$-\frac{1}{\tau^2}B_2^TQRQB_2+\frac{1}{\tau}B_2^T\left[Q'RQ+QR'Q+QRQ'\right]B_2 + \mathrm{tr}\left\{C_1R'C_1^T\right\}-\mathrm{tr}\left\{B_1^TQ'B_1\right\}=0. \tag{C.28}$$

Premultiply (C.26) by Q, postmultiply (C.23) by R', and subtract the latter from the former. Taking the trace of the result yields

$$\mathrm{tr}\left\{C_1R'C_1^T\right\}-\frac{2}{\tau^2}B_2^TQRQB_2 + \frac{1}{\tau}B_2^T\left[Q'RQ+QR'Q+QRQ'\right]B_2=0. \tag{C.29}$$

From (C.27), (C.28) and (C.29) we obtain

$$\mathrm{tr}\left\{C_1 R' C_1^T\right\} = -\tau \mathrm{tr}\left\{C_1 Q'' C_1^T\right\}. \tag{C.30}$$

Differentiating (C.25) with respect to τ results in

$$\begin{aligned}\left[A - \frac{1}{\tau} B_2 B_2^T Q\right]^T Q'' + Q'' \left[A - \frac{1}{\tau} B_2 B_2^T Q\right] \\ - \frac{2}{\tau}\left[\frac{1}{\tau} Q - Q'\right] B_2 B_2^T \left[\frac{1}{\tau} Q - Q'\right] = 0.\end{aligned} \tag{C.31}$$

Since the matrix $(A - \frac{1}{\tau} B_2 B_2^T Q)$ is Hurwitz, and the pair (A, B_2) is stabilizable, (C.29) implies that $Q''(\tau) \leq 0$ and thus, from (C.30)

$$\mathrm{tr}\left\{C_1 R'(\tau) C_1^T\right\} \geq 0. \tag{C.32}$$

Now, using (5.21), (5.22) we can differentiate τ with respect to η and ρ to obtain

$$\frac{\partial}{\partial \eta}\tau(\rho, \eta) = \frac{2\mathrm{erf}^{-1}(N)^2}{N^2} > 0, \tag{C.33}$$

$$\frac{\partial}{\partial \rho}\tau(\rho, \eta) = \frac{1}{N^2} > 0. \tag{C.34}$$

From (C.32)-(C.34), the partial derivatives in (C.21), (C.22) are nonnegative. Now, we prove each of the three statements of the theorem.

(i) Note that $\gamma^2(\rho, \eta)$ is bounded from below, and hence, its limit as ρ tends to 0^+ exists. Similarly, $\tau(\rho, \eta) > 0$, and thus, from (C.34), its limit as ρ tends to 0^+ also exists. Using (5.21) and (5.22) and a few algebraic manipulations, it is possible to show that

$$\lim_{\rho \to 0^+} \tau(\rho, \eta) = \lim_{N \to 0^+} \frac{\eta\sqrt{\pi}\mathrm{erf}^{-1}(N) \exp\left(\mathrm{erf}^{-1}(N)^2\right)}{N} = \frac{\pi\eta}{2}, \tag{C.35}$$

and thus, with $R(\tau)$ and $Q(\tau)$ from (C.23) and (C.24),

$$\lim_{\rho \to 0^+} \gamma^2(\rho, \eta) = \mathrm{tr}\left\{C_1 R\left(\frac{\pi\eta}{2}\right) C_1^T\right\}. \tag{C.36}$$

Then (5.27), (5.28) and (5.29) follow immediately from (C.36), (C.23) and (C.24), respectively, using the notation

$$\bar{R}_\eta := R\left(\frac{\pi\eta}{2}\right),\ \bar{Q}_\eta := Q\left(\frac{\pi\eta}{2}\right). \tag{C.37}$$

It follows from Theorem 5.3 that the solution of (5.28)-(5.29) exists and is unique, with the property that $\bar{R}_\eta \geq 0$, $\bar{Q}_\eta \geq 0$.

(ii) In a similar fashion to part (i), note that the limits of $\gamma^2(\rho,\eta)$ and $\tau^2(\rho,\eta)$ as η tends to 0^+ exist. From (5.24), as η tends to 0^+, N tends to 1. From (5.21), as N tends to 1, λ tends to 0. Thus,

$$\lim_{\eta\to 0^+} \tau\left(\rho,\eta\right) = \rho, \tag{C.38}$$

and hence,

$$\lim_{\eta\to 0^+} \gamma^2(\rho,\eta) = \mathrm{tr}\left\{C_1 R\left(\rho\right) C_1^T\right\}, \tag{C.39}$$

which yields (5.30), using the notation $\gamma_{\rho 0}^2 := \mathrm{tr}\left\{C_1 R\left(\rho\right) C_1^T\right\}$. Note from (5.19)-(5.20) that finding $R(\rho)$ is equivalent to solving the conventional LQR problem.

(iii) Note from (C.33) and (C.34) that $1/\tau(\rho,\eta)$ is monotonically decreasing in ρ and η, and bounded from below by 0. Using (5.21) and (5.22), it is possible to show that

$$\lim_{\eta\to\infty} \frac{1}{\tau\left(\rho,\eta\right)} = \lim_{\rho\to\infty} \frac{1}{\tau\left(\rho,\eta\right)} = 0. \tag{C.40}$$

Since A is Hurwitz, it follows from (5.19) and (5.20) that

$$\lim_{\eta\to\infty} \gamma^2(\rho,\eta) = \lim_{\rho\to\infty} \gamma^2(\rho,\eta) = \mathrm{tr}\left\{C_1 R_{OL} C_1^T\right\}, \tag{C.41}$$

where $R_{OL} \geq 0$ is the solution of the Lyapunov equation

$$AR_{OL} + R_{OL}A + B_1 B_1^T = 0. \tag{C.42}$$

Thus, (5.31) follows immediately from (C.41) using the notation

$$\gamma_{OL}^2 := \mathrm{tr}\left\{C_1 R_{OL} C_1^T\right\}.$$

From (C.42), R_{OL} is the open-loop covariance matrix, and hence, γ_{OL}^2 is the open-loop output variance.

□

Proof of Theorem 5.7. Let (N, Q, R, λ) be the unique solution of (5.19)-(5.22), and let K be obtained from (5.17). We begin by establishing that the matrix $(A + B_2 K)$ is Hurwitz. Note that Q satisfies the Ricatti equation (5.19). Using straightforward algebraic manipulations, we obtain

$$\left|1 - K\left(j\omega I - A\right)^{-1} B_2 N\right|^2 = 1 + \frac{1}{\tau}\left|C_1\left(j\omega I - A\right)^{-1} B_2\right|^2, \tag{C.43}$$

where $\tau = (\rho + \lambda)/N^2$. From (C.43), the Nyquist plot of $-K\left(j\omega I - A\right)^{-1} B_2 N$ never enters the unit disk centered at the point $(-1, 0)$ in the complex plane. Thus, $A + B_2 N \kappa K$ is Hurwitz for all $\kappa > 1/2$. The result follows by setting $\kappa = 1/N$. Then, the statements of the theorem are proved as follows.

(i) Note that x_G is an equilibrium point of (5.32) if

$$Ax_G + B_2 sat_\alpha(Kx_G) = 0. \tag{C.44}$$

Since $(A + B_2 K)$ is nonsingular, this equation implies that

$$x_G + (A + B_2 K)^{-1} B_2 [sat_\alpha(Kx_G) - Kx_G] = 0. \tag{C.45}$$

Premultiplying (C.45) by K yields

$$[1-\Gamma]Kx_G + \Gamma sat_\alpha(Kx_G) = 0, \tag{C.46}$$

where

$$\Gamma = K(A+B_2K)^{-1}B_2. \tag{C.47}$$

Using the Schur complement [118], we have

$$\begin{aligned} 1-\Gamma &= \det[I-(A+B_2K)^{-1}B_2K] \\ &= \det[(A+B_2K)]\det(A) \geq 0. \end{aligned} \tag{C.48}$$

It follows that $\Gamma \leq 1$, and hence, (C.46) is satisfied only if $Kx_G = 0$. Thus, from (C.45), $x_G = 0$ is the unique equilibrium.

(ii) The Jacobian linearization of (5.32) about $x_G = 0$ is given by

$$\Delta\dot{x}_G = (A+B_2K)\Delta x_G. \tag{C.49}$$

Since $(A+B_2K)$ is Hurwitz, the result follows from Lyapunov's indirect method [44].

(iii) To prove (iii), we establish asymptotic stability of the origin via Lyapunov function. Recall that (A, B_2) is stabilizable and (C_1, A) is detectable. Also, note that the origin of (5.32) is asymptotically stable if and only if it is asymptotically stable for the controllable and observable portion of its Kalman canonical decomposition. Thus, assume without loss of generality that (A, B_2) is controllable and (C_1, A) is observable. Then it follows from (5.19) that $Q > 0$. Consider the candidate Lyapunov function

$$V(x_G) = x_G^T(\varepsilon Q)x_G, \tag{C.50}$$

where

$$\varepsilon = \frac{N^2}{\rho + \lambda}. \tag{C.51}$$

It is straightforward to show that

$$\dot{V}(x_G) = -x_G^T(\varepsilon C_1^T C_1)x_G - \varepsilon(\rho + \lambda)[\frac{2u}{N}sat_\alpha(u) - u^2], \tag{C.52}$$

and thus,

$$\dot{V}(x_G) \leq 0 \tag{C.53}$$

if

$$|u| \leq 2\alpha/N. \tag{C.54}$$

Clearly, this is equivalent to

$$|B_2^T(\varepsilon Q)x_G| \leq 2\alpha, \tag{C.55}$$

and hence, $\dot{V}(x_G) \leq 0$ for all $x_G \in \mathcal{X}$, where

$$\mathcal{X} = \left\{ x_G \in R^{n_x} : x_G^T \left(QB_2B_2^TQ \right) x_G \leq \frac{4\alpha^2}{\varepsilon^2} \right\}. \tag{C.56}$$

Now, define the set $\mathcal{S}$ such that

$$\mathcal{S} = \left\{ x_G \in \mathcal{X} : \dot{V}\left(x_G\right) = 0 \right\}, \tag{C.57}$$

and assume that the trajectory $x_G(t)$ belongs to $\mathcal{S}$ for all t. Then, from (C.52), $C_1x_G = 0$ and since (C_1, A) is observable, $x_G = 0$. Thus, by LaSalle's Theorem, the equilibrium point $x_G = 0$ is asymptotically stable and $\mathcal{X}$ is a subset of its domain of attraction.

□

Proof of Theorem 5.10. The proof is similar to that of Theorem 5.3. First, we use the method of Lagrange multipliers to find the necessary conditions for optimality.

To verify the regularity of the contraints, let $(K, L, M, N_a, N_s, \tilde{P}, \alpha, \beta)$ satisfy (5.43) and (5.44), and for arbitrary symmetric matrices $\tilde{Q}$ and $\Lambda = \mathrm{diag}(\lambda_1, \lambda_2)$, define

$$\begin{aligned}\Phi\left(K, L, M, N_a, N_s, \tilde{P}, \alpha, \beta\right) &= \mathrm{tr}\left\{\left[\left(\tilde{A} + \tilde{B}_2\tilde{N}\tilde{C}_2\right)\tilde{P}\right.\right. \\ &\left.\left. + \tilde{P}\left(\tilde{A} + \tilde{B}_2\tilde{N}\tilde{C}_2\right)^T + \tilde{B}_1\tilde{B}_1^T\right]\tilde{Q}\right\} \\ &+ \mathrm{tr}\left\{\Lambda\left[\mathrm{diag}\left\{\tilde{C}_2\tilde{P}\tilde{C}_2^T\right\} - \frac{1}{2}\Theta\left[\mathrm{erf}^{-1}\left(\tilde{N}\right)\right]^{-2}\right]\right\}. \end{aligned} \tag{C.58}$$

Differentiating Φ with respect to α, β and $\tilde{P}$, and the setting the result to zero yields

$$\frac{-2\lambda_1\alpha}{2\mathrm{erf}^{-1}\left(N_a\right)^2} = 0, \tag{C.59}$$

$$\frac{-2\lambda_2\beta}{2\mathrm{erf}^{-1}\left(N_s\right)^2} = 0, \tag{C.60}$$

$$\left(\tilde{A} + \tilde{B}_2\tilde{N}\tilde{C}_2\right)^T\tilde{Q} + \tilde{Q}\left(\tilde{A} + \tilde{B}_2\tilde{N}\tilde{C}_2\right) + \Lambda\tilde{C}_2^T\tilde{C}_2 = 0. \tag{C.61}$$

Since $N_a \in (0, 1)$, $N_s \in (0, 1)$, and $\alpha, \beta > 0$, it follows from (C.59) and (C.60) that $\lambda_1 = \lambda_2 = 0$, which, from (C.61), implies that $\tilde{Q} = 0$. It is straightforward to show that, consequently,

$$\frac{\partial\Phi}{\partial K} = \frac{\partial\Phi}{\partial L} = \frac{\partial\Phi}{\partial M} = \frac{\partial\Phi}{\partial N_a} = \frac{\partial\Phi}{\partial N_s} = 0, \tag{C.62}$$

and, thus, the constraints are regular.

Consider the Lagrangian

$$\begin{aligned}\Psi\left(K, L, M, N_a, N_s, \tilde{P}, \tilde{Q}, \alpha, \beta, \lambda_1, \lambda_2\right) &= \mathrm{tr}\left\{\tilde{C}_1\tilde{P}\tilde{C}_1^T\right\} \\ &+ \mathrm{tr}\left\{\left[\left(\tilde{A} + \tilde{B}_2\tilde{N}\tilde{C}_2\right)\tilde{P} + \tilde{P}\left(\tilde{A} + \tilde{B}_2\tilde{N}\tilde{C}_2\right)^T + \tilde{B}_1\tilde{B}_1^T\right]\tilde{Q}\right\} \\ &+ \mathrm{tr}\left\{\Lambda\left[\mathrm{diag}\left\{\tilde{C}_2\tilde{P}\tilde{C}_2^T\right\} - \frac{1}{2}\Theta\left[\mathrm{erf}^{-1}\left(\tilde{N}\right)\right]^{-2}\right]\right\}. \end{aligned} \tag{C.63}$$

and the partition

$$\tilde{P} = \begin{bmatrix} P_{11} & P_{12}^T \\ P_{12} & P_{11} \end{bmatrix}, \tilde{Q} = \begin{bmatrix} Q_{11} & Q_{12} \\ Q_{12}^T & Q_{22} \end{bmatrix}.$$

Differentiating Ψ with respect to K, L, M, N_a, N_s,$\tilde{P}$, $\tilde{Q}$, λ_1, λ_2, α, β, and equating the results to zero yields the necessary conditions for optimality

$$KP_{22} + \frac{N_a}{\rho + \lambda_1}\left(Q_{11}P_{12}^T + Q_{12}P_{22}\right) = 0, \tag{C.64}$$

$$Q_{22}L - \left(Q_{12}^T P_{11} + Q_{22}P_{12}\right) C_2^T \frac{N_s}{\mu} = 0, \tag{C.65}$$

$$Q_{12}^T P_{12}^T + Q_{22}P_{22} = 0, \tag{C.66}$$

$$K\left(P_{12}Q_{11} + P_{22}Q_{12}^T\right) B_2 + \frac{\sqrt{\pi}}{4}\lambda_1 \exp\left(\mathrm{erf}^{-1}(N_a)^2\right) \times \left(\mathrm{erf}^{-1}(N_a)^{-3}\right), \tag{C.67}$$

$$C_2\left(P_{11}Q_{12} + P_{12}^T Q_{22}\right) L + \frac{\sqrt{\pi}}{4}\lambda_2 \exp\left(\mathrm{erf}^{-1}(N_s)^2\right) \times \left(\mathrm{erf}^{-1}(N_s)^{-3}\right) = 0, \tag{C.68}$$

$$\left(\tilde{A} + \tilde{B}_2\tilde{N}\tilde{C}_2\right)^T \tilde{Q} + \tilde{Q}\left(\tilde{A} + \tilde{B}_2\tilde{N}\tilde{C}_2\right) + \tilde{C}_1^T\tilde{C}_1 + \tilde{C}_2^T\Lambda\tilde{C}_2 = 0, \tag{C.69}$$

$$\left(\tilde{A} + \tilde{B}_2\tilde{N}\tilde{C}_2\right)\tilde{P} + \tilde{P}\left(\tilde{A} + \tilde{B}_2\tilde{N}\tilde{C}_2\right)^T + \tilde{B}_1\tilde{B}_1^T = 0, \tag{C.70}$$

$$KP_{22}K^T - \frac{\alpha^2}{2\mathrm{erf}^{-1}\left(N_a\right)^2} = 0, \tag{C.71}$$

$$C_2P_{11}C_2^T - \frac{\beta^2}{2\mathrm{erf}^{-1}\left(N_s\right)^2} = 0, \tag{C.72}$$

$$2\eta_a\alpha - \frac{2\lambda_1\alpha}{2\mathrm{erf}^{-1}\left(N_a\right)^2} = 0, \tag{C.73}$$

$$2\eta_s\alpha - \frac{2\lambda_2\beta}{2\mathrm{erf}^{-1}\left(N_s\right)^2} = 0. \tag{C.74}$$

In the subsequent analysis we assume that P_{22} and Q_{22} are invertible, although similar results can be obtained by using pseudoinverses. From (C.64) and (C.65), we

obtain

$$K = -\frac{N_a}{\rho + \lambda_1} B_2^T \left(Q_{11} P_{12}^T + Q_{12} P_{22} \right) P_{22}^T, \tag{C.75}$$

$$L = Q_{22}^{-1} \left(Q_{12}^T P_{11} + Q_{22} P_{12} \right) C_2^T \frac{N_s}{\mu}. \tag{C.76}$$

Defining $T := P_{12}^T P_{22}^{-1}$, it follows from (C.75) that

$$K = -\frac{N_a}{\rho + \lambda_1} B_2^T \left(Q_{11} - Q_{12} Q_{22}^T Q_{12}^T \right) T. \tag{C.77}$$

Note from (C.66) that $T^{-1} = -Q_{22}^{-1} Q_{12}^T$, and, thus, from (C.76)

$$L = -T^{-1} \left(P_{11} + P_{12}^T P_{22}^{-1} P_{12} \right) C_2^T \frac{N_s}{\mu}. \tag{C.78}$$

Then, with

$$Q = Q_{11} - Q_{12} Q_{22}^T Q_{12}^T, \;\; P = P_{11} + P_{12}^T P_{22}^{-1} P_{12}, \tag{C.79}$$

(C.77) and (C.78) become

$$K = -\frac{N_a}{\rho + \lambda_1} B_2^T Q T, \tag{C.80}$$

and

$$L = -\frac{N_a}{\mu} T^{-1} P C_2^T. \tag{C.81}$$

By substituting (C.80) and (C.81) into (C.69) and (C.70), it is straightforward to show that

$$M = T^{-1} \left(A + B_2 N_a K T^{-1} + T L N_s C_2 \right) T. \tag{C.82}$$

The equations (5.46)-(5.48) for the parameters K, L, M follow immediately from (C.80)-(C.82), noting that T is a similarity transformation and does not affect the the controller transfer function $K(sI - M)^{-1}L$. The equations (5.49) and (5.50) for α and β follow directly from (C.71) and (C.72), respectively.

We now verify (5.51)-(5.58). Equations (5.51)-(5.54) follow by substituting (C.80)-(C.82) into (C.69) and (C.70), where

$$R = P_{12}^T P_{22}^{-1} P_{12}, \;\; S = Q_{12} Q_{22}^{-1} Q_{12}^T. \tag{C.83}$$

Multiplying (C.64) from the right by K^T, substituting into (C.67), and then using (C.71), yields (5.55). Multiplying (C.65) from the left by L^T and substituting into (C.68) yields (5.56). Finally, (5.57) and (5.58) follow immediately from (C.73) and (C.74).

We now argue that the ILQG problem (5.41) has a solution, i.e., the minimum exists and is attained. Note that (5.41) can be reformulated as

$$\min_{\alpha,\beta} \left\{ \eta_a \alpha^2 + \eta_s \beta^2 + \min_{K,L,M} \sigma_{\hat{z}}^2 \right\}. \tag{C.84}$$

It is known from [83] that, under Assumption 2, for every $\alpha, \beta > 0$, the triple (K, L, M) that solves

$$\min_{K,L,M} \sigma_{\hat{z}}^2, \tag{C.85}$$

exists. Moreover, the achieved minimum is continuous in α and β. Thus, the function

$$q_G(\alpha, \beta) = \eta_a \alpha^2 + \eta_s \beta^2 + \min_{K,L,M} \sigma_{\hat{z}}^2 \tag{C.86}$$

is continuous for $\alpha, \beta > 0$ and tends to ∞ as $\alpha \to \infty$ and $\beta \to \infty$. Hence, $q_G(\alpha, \beta)$ achieves a minimum at some $\alpha^* \geq 0$, $\beta^* \geq 0$. Let (K^*, L^*, M^*) be the minimizer of (C.85) when $\alpha = \alpha^*$ and $\beta = \beta^*$. Then the quintuple $(K^*, L^*, M^*, \alpha^*, \beta^*)$ solves (5.41).

The ILQG cost (5.59) follows immediately from (5.46)-(5.50). Since the optimization has an achievable solution, any solution of (5.51)-(5.58) that minimizes (5.59) solves the ILQG problem. □

Proof of Theorem 5.13. Let $(N_a, N_s, \lambda_1, \lambda_2, P, Q, R, S)$ be the minimizing solution of (5.51)-(5.58) and let K and L be obtained from (5.46) and (5.47). Similar to the proof of Theorem 5.7, we first establish that $(A + B_2 K)$ and $(A + LC_2)$ are Hurwitz.

Since P and Q satisfy (5.51) and (5.52), it is readily shown that

$$\left|1 - K\left(j\omega I - A\right)^{-1} B_2 N_a\right|^2 = 1 + \frac{1}{\tau_1}\left|C_1\left(j\omega I - A\right)^{-1} B_2\right|^2 + \frac{\lambda_2}{\tau_1}\left|C_2\left(j\omega I - A\right)^{-1} B_2\right|^2, \tag{C.87}$$

and

$$\left|1 - C_2\left(j\omega I - A\right)^{-1} N_s L\right|^2 = 1 + \frac{1}{\tau_2}\left|C_2\left(j\omega I - A\right)^{-1} B_1\right|^2, \tag{C.88}$$

where $\tau_1 = (\rho + \lambda_1)/N_a^2$ and $\tau_2 = \mu/N_s^2$. Thus, $(A + B_2 N_a \kappa_a K)$ and $(A + L N_s \kappa_s C_2)$ are Hurwitz for all $\kappa_a > 1/2$, $\kappa_s > 1/2$, and the result follows by setting $\kappa_a = 1/N_a$ and $\kappa_s = 1/N_s$.

(i) The point $[x_G, x_C]$ is an equilibrium of the system if

$$Ax_G + B_2 sat_\alpha\left(Kx_C\right) = 0, \tag{C.89}$$

$$Ax_C + B_2 sat_\alpha(Kx_C) - L\left(y - sat_\beta(C_2 x_C)\right) = 0, \tag{C.90}$$

or, equivalently,

$$Ax_G + B_2 sat_\alpha\left(Kx_C\right) = 0, \tag{C.91}$$

$$Ae + L\left(sat_\beta(C_2 x_G) - sat_\beta(C_2 x_C)\right) = 0, \tag{C.92}$$

where $e = x_G - x_C$. Since $(A + B_2 K)$ and $(A + LC_2)$ are nonsingular we can write

$$x_G + (A + B_2 K)^{-1} B_2 sat_\alpha\left(Kx_C\right) - (A + B_2 K)^{-1} B_2 K x_G = 0, \tag{C.93}$$

$$e + (A + LC_2)^{-1} L\left(sat_\beta(C_2 x_G) - sat_\beta(C_2 x_C)\right) - (A + LC_2)^{-1} LC_2 e = 0. \tag{C.94}$$

Premultiplying (C.94) by C_2 results in

$$\left(1 - \Gamma_C\right) C_2 x_G + \Gamma_C sat_\beta\left(C_2 x_G\right) = \left(1 - \Gamma_C\right) C_2 x_C + \Gamma_C sat_\beta\left(C_2 x_C\right), \tag{C.95}$$

where $\Gamma_C = C_2(A + LC_2)^{-1}L$. Since

$$1 - \Gamma_C = \det(A + LC_2)^{-1} \det(A) \geq 0, \tag{C.96}$$

it follows that $\Gamma_C \leq 1$. If $\Gamma_C \neq 1$, then (C.95) implies that $C_2 x_G = C_2 x_C$, which, from (C.94), implies $e = 0$, i.e., $x_G = x_C$. Then, it follows from (C.89), (C.93) and the proof of Theorem 5.7 that $x_G = 0$, and, necessarily, $x_C = 0$. If $\Gamma_C = 1$, then from (C.95)

$$sat_\beta(C_2 x_G) = sat_\beta(C_2 x_C), \tag{C.97}$$

which, from (C.92) implies that $Ae = 0$. Then, from (C.89)

$$Ax_C + B_2 sat_\alpha(Kx_C) = 0, \tag{C.98}$$

which, through the proof of Theorem 5.7 implies that $x_C = 0$. Thus, from (C.97), $C_2 x_G = 0$, and it follows from (C.94) that $e = 0$. Thus, $x_G = 0$ and the result is established.

(ii) The Jacobian linearization of the system about the equilibrium $[x_G, x_C] = 0$ is given by

$$\Delta \dot{x}_G = (A + B_2 K)\Delta x_G, \tag{C.99}$$

$$\Delta \dot{e} = (A + LC_2)\Delta e, \tag{C.100}$$

Since $(A + B_2 K)$ and $(A + LC_2)$ are Hurwitz, the result follows from Lyapunov's indirect method.

(iii) As in the proof of Theorem 5.7, assume without loss of generality that (A, B_2) is controllable and (C_1, A) is observable. Consider the candidate Lyapunov function

$$V(x_G, e) = V_1(x_G) + V_2(e), \tag{C.101}$$

where

$$V_1(x_G) = x_G^T(\varepsilon_1 Q)x_G, \tag{C.102}$$

$$V_2(e) = e^T M e, \tag{C.103}$$

where $\varepsilon_1 = N_a^2/(\rho + \lambda_1)$, and where, since $(A + LC_2)$ is Hurwitz, M is the positive definite solution of

$$(A + LC_2)^T M + M(A + LC_2) + I = 0. \tag{C.104}$$

It follows that

$$\dot{V}_1(x_G) = -x_G^T(\varepsilon_1 C_1^T C_1 + \varepsilon_1 \lambda_2 C_2^T C_2)x_G - \varepsilon_1(\rho + \lambda_1)[\frac{2u}{N} sat_\alpha(u) - u^2], \tag{C.105}$$

$$\begin{aligned}\dot{V}_2(e) = &\left(e^T A^T + \left(sat_\beta(C_2 x_G) - sat_\beta(C_2 x_C)\right)^T L^T\right) Me \\ &+ e^T M \left(Ae + L\left(sat_\beta(C_2 x_G) - sat_\beta(C_2 x_C)\right)\right).\end{aligned} \tag{C.106}$$

Thus, $\dot{V}_1(x_G) \leq 0$ if

$$|u| \leq \frac{2\alpha}{N}, \tag{C.107}$$

and by the proof of Theorem 5.7, $\dot{V}_1(x_G) \leq 0$ for all $x_G \in \mathcal{X}_1$, where

$$\mathcal{X}_1 = \left\{x_G \in R^{n_x} | x_G^T \left(QB_2B_2^TQ\right) x_G \leq \frac{4\alpha^2}{\varepsilon_1^2}\right\} \tag{C.108}$$

Now, assume that $x_G = x_C$. It follows from (C.106) and (C.104) that

$$\dot{V}_2(e) = -e^T e, \tag{C.109}$$

if

$$|C_2 x_G| \leq \beta, \tag{C.110}$$

and thus, $\dot{V}_2(e) \leq 0$ for all $x_G \in \mathcal{X}_2$, where

$$\mathcal{X}_2 = \left\{x_G \in R^{n_x} | x_G^T C_2^T C_2 x_G \leq \beta^2\right\}. \tag{C.111}$$

Then, from (C.108) and (C.111), $\dot{V}(x_G, x_C) \leq 0$ for all $(x_G, x_C) \in \mathcal{Y} \times \mathcal{Y}$, where

$$\mathcal{Y} = \mathcal{X}_1 \cap \mathcal{X}_2. \tag{C.112}$$

Now, define the set $\mathcal{S}$ such that

$$\mathcal{S} = \left\{ (x_G, x_C) \in \mathcal{Y} \times \mathcal{Y} | \dot{V}(x_G, x_C) = 0 \right\}, \tag{C.113}$$

and assume that the trajectory $(x_G(t), x_C(t))$ belongs to $\mathcal{S}$ for all t. Then it follows from (C.105)-(C.109) that $C_1 x_G = 0$ and $e = 0$. Thus, since (C_1, A) is observable, $x_G = x_C = 0$, and by LaSalle's theorem, $[x_G, x_C] = 0$ is asymptotically stable and $\mathcal{Y} \times \mathcal{Y}$ is a subset of its domain of attraction.

□

BIBLIOGRAPHY

BIBLIOGRAPHY

[1] J. Roberts and P. Spanos. *Random Vibration and Statistical Linearization*. Wiley, 1990.

[2] T. B. Goh, Z. Li, and B. M. Chen. Design and implementation of a hard disk servo system using robust and perfect tracking approach. *IEEE Trans. on Control Systems Technology*, 9:221–233, 2001.

[3] E. J. Ohlmeyer. Root-mean-square miss distance of proportional navigation missile against sinusoidal target. *Journal of Guidance, Control and Dynamics*, 19(3):563–568, 1996.

[4] K. J. Astrom and L. Rundqwist. Integrator windup and how to avoid it. *Control Conference, American*, 26, 1982.

[5] C. Gökçek, P. T. Kabamba, and S. M. Meerkov. An LQR/LQG theory for systems with saturating actuators. *IEEE Transactions on Automatic Control*, 46(10):1529–1542, 2001.

[6] R. C. Boonton. Nonlinear control systems with random inputs. *IRE Trans. on Circuit Theory*, CT-1:9–18, 1954.

[7] I. E. Kazakov. Approximate method for the statistical analysis of nonlinear systems. Technical Report VVIA 394, Trudy, 1954.

[8] A. Gelb and W. E. V. Velde. *Multiple Input Describing Function and Nonlinear Design*. New York: McGraw-Hill, 1968.

[9] G. Q. Cai and Y. Suzuki. On statistical quasi-linearization. *Internation Journal of Non-Linear Mechanics*, 40:1139–1147, 2005.

[10] S. H. Crandall. On using non-gaussian distributions to perform statistical linearization. *International Journal of Non-Linear Mechanics*, 39:1395–1406, 2004.

[11] J. Skrzypczyk. Accuracy analysis of statistical linearization methods applied to nonlinear dynamical systems. *Reports on Mathematical Physics*, 36:1–20, 1995.

[12] I. Elishakoff. Stochastic linearization technique: A new interpretation and a selective review. *The Shock and Vibration Digest*, 32:179–188, 2000.

[13] W. M. Wonham and W. F. Cashman. A computational approach to optimal control of stochastic saturating systems. *Int. Journal of Control*, 10:77–98, 1969.

[14] C. Gökçek, P. T. Kabamba, and S. M. Meerkov. Disturbance rejection in control systems with saturating actuators. *Nonlinear Analysis*, 40:213–226, 2000.

[15] M. A. Aizermann and F. R. Gantmacher. *Absolute stability of regulator systems*. Holden-Day, 1964.

[16] S. Lefschetz. *Stability of Nonlinear Control Systems*. New York: Academic, 1965.

[17] V. M. Popov. On the absolute stability of nonlinear control systems. *Automation and Remote Control*, 22:961979, 1961.

[18] A. T. Fuller. In the large stability of replay and saturating control systems with linear controllers. *Int. Journal of Control*, 10-4:457–480, 1969.

[19] E. D. Sontag H. J. Sussmann and Y. Yang. A general result on the stabilization of linear systems using bounded controls. *IEEE Transactions on Automatic Control*, 39:2411–2425, 1994.

[20] A. R. Teel. Semi-global stabilization on linear controllable systems with input nonlinearities. *IEEE Trans. on Automatic Control*, 40:96–100, 1995.

[21] A. Saberi, Z. Lin, and A. Teel. Control of linear systems with saturating actuators. *IEEE Trans. on Automatic Control*, 41:368–378, 1996.

[22] E. G. Gilbert and K. T. Tan. Linear systems with state and control constraints: The theory and application of maximal output admissible sets. *IEEE Trans. of Automatic Control*, 36:1008–1020, 1991.

[23] V. Kapila. *Actuator Saturation Control*. Marcel Dekker, 2001.

[24] T. Hu and Z. Lin. *Control Systems with Actuator Saturation: Analysis and Design*. Birkhauser, Boston, 2001.

[25] D. S. Bernstein and A. N. Michel. A chronological bibliography on saturating actuators. *International Journal of Robust and Nonlinear Control*, 5:375–380, 1995.

[26] I-K. Fong and C-C. Hsu. State feedback stabilization of single input systems through actuators with saturation and deadzone characteristics. In *Proceedings of the 39th IEEE Conference on Decision and Control (Cat. No.00CH37187)*, volume vol.4, pages 3266–71, Sydney, NSW, Australia, 2000. IEEE. Copyright 2001, IEE.

[27] K. Hui and C.W Chan. Stabilization of systems with deadzone nonlinearity. In *Proceedings of the 1998 IEEE International Conference on Control Applications (Cat. No.98CH36104)*, volume vol.2, pages 1036–40, Trieste, Italy, 1998. IEEE. Copyright 1999, IEE.

[28] G. Tao and P. V. Kokotovic. Adaptive control of system with unknown output backlash. *Automatic Control, IEEE Transactions on*, 40:326–330, 1995.

[29] T. Pare, A. Hassibi, and J. How. Asymptotic stability for systems with multiple hysteresis nonlinearities. In *Proceedings of the 1999 American Control Conference (Cat. No. 99CH36251)*, volume 5, pages 3038–43, San Diego, CA, USA, 1999. IEEE. Copyright 1999, IEE.

[30] T. Ninomiya, I. Yamaguchi, and T. Kida. Feedback control of plants driven by nonlinear actuators via input-state linearization. *Journal of Guidance, Control, and Dynamics*, 29:20–4, 2006. Copyright 2006, The Institution of Engineering and Technology.

[31] G. Tao and P. V. Kokotovic. *Adaptive Control of Systems with Actuator and Sensor Nonlinearities*. Adaptive and learning systems for signal processing, communications, and control. Wiley, New York, 1996.

[32] G. Kreisselmeier. Stabilization of linear systems in the presence of output measurement saturation. *Systems & Control Letters*, 29:27–30, September 1996. Copyright 1996, IEE.

[33] Z.1 Lin and T.1 Hu. Semi-global stabilization of linear systems subject to output saturation. *Systems & Control Letters*, 43:211–17, July 2001. Copyright 2001, IEE.

[34] Y-Y. Cao, Zongli Lin, and B.M. Chen. An output feedback H_∞ controller design for linear systems subject to sensor nonlinearities. *IEEE Trans. on Circuits and Systems*, 50(7):914–921, 2003.

[35] G. N. Nair and R. J. Evans. Stabilizability of stochastic linear systems with finite feedback data rates. *SIAM Journal on Control and Optimization*, 43:413–436, 2005.

[36] F. Fagnani and S. Zampieri. Stabilizing quantized feedback with minimal information flow: the scalar case. In *Proceedings Fifteenth International Symposium on Mathematical Theory of Networks and Systems*, pages 1–15, Notre Dame, IN, USA, 2002. Univ. Notre Dame. Copyright 2003, IEE.

[37] N. Elia and S.K. Mitter. Stabilization of linear systems with limited information. *IEEE Transactions on Automatic Control*, 46:1384–400, September 2001. Copyright 2001, IEE.

[38] D. F. Delchamps. Stabilizing a linear system with quantized state feedback. *IEEE Transactions on Automatic Control*, 35:916–924, 1990.

[39] F. Fagnani and S. Zampieri. Quantized stabilization of linear systems: complexity versus performance. *IEEE Transactions on Automatic Control*, 49:1534–48, September 2004. Copyright 2004, IEE.

[40] D. Liberzon and D. Nesic. Input-to-state stabilization of linear systems with quantized state measurements. *IEEE Transactions on Automatic Control*, 52:767–781, 2007.

[41] R. W. Brockett and D. Liberzon. Quantized feedback stabilization of linear systems. *IEEE Transactions on Automatic Control*, 45:1279–1289, 2000.

[42] W-W. Che and G-H. Yang. H_∞ controller design for linear systems with quantized feedback. In *16th IEEE International Conference on Control Applications. Part of IEEE Multiconference on Systems and Control*, pages 1318–23, Singapore, 2007. IEEE. Copyright 2008, The Institution of Engineering and Technology.

[43] A. Isidori. *Nonlinear Control Systems*. Springer, 3rd edition, August 1995.

[44] H. K. Khalil. *Nonlinear Systems*. Prentice Hall, 3 edition, December 2001.

[45] X. Ma and G. Tao. Adaptive actuator compensation control with feedback linearization. *Automatic Control, IEEE Transactions on*, 45:1705–1710, 2000.

[46] G. Vossoughi and M. Donath. Dynamic feedback linearization for electrohydraulically actuated control systems. *Journal of Dynamic Systems, Measurement, and Control*, 117:468, 1995.

[47] T. Kimura, S. Hara, T. Fujita, and T. Kagawa. Feedback linearization for pneumatic actuator systems with static friction. *Control Engineering Practice*, 5:1385–1394, 1997.

[48] H. Risken. *The Fokker-Planck Equation: Methods of Solution and Applications*. Springer-Verlag, 1989.

[49] D. Liberzon and R. W. Brockett. Nonlinear feedback systems perturbed by noise: Steady-state probability distributions and optimal control. *IEEE Transactions on Automatic Control*, 45:1116–1130, 2000.

[50] V. A. Yakubovich, S. Nakaura, and K. Furuta. Tracking domains for unstable plants with saturating-like actuators. In *Decision and Control, 1999. Proceedings of the 38th IEEE Conference on*, volume 3, 1999.

[51] Y. Eun, P. T. Kabamba, and S. M. Meerkov. System types in feedback control with saturating actuators. *Automatic Control, IEEE Transactions on*, 49:287–291, 2004.

[52] M. Goldfarb and T. Sirithanapipat. The effect of actuator saturation on the performance of pd-controlled servo systems. *Mechatronics*, 9:497–511, 1999.

[53] Y. Eun, P. T. Kabamba, and S. M. Meerkov. Tracking of random references: Random sensitivity function and tracking quality indicators. *IEEE Transactions on Automatic Control*, 48(9):1666–1671, 2003.

[54] Y. Eun, P. T. Kabamba, and S. M. Meerkov. Analysis of random reference tracking in systems with saturating actuators. *IEEE Transactions on Automatic Control*, 50(11):1861–1866, 2005.

[55] J. E. Gibson and F. B. Tuteur. *Control System Components*. McGraw-Hill, 1958.

[56] R. B. Northrop. *Introduction to Instrumentation and Measurements*. CRC-Press, 1 edition, June 1997.

[57] Y. Hurmuzlu. *The Mechanical Systems Design Handbook: Modeling, Measurement, and Control*. CRC Press LLC, 1 edition, December 2001.

[58] J. W. Dally, W. F. Riley, and K. G. McConnell. *Instrumentation for Engineering Measurements*. Wiley, 1984.

[59] C. W. de Silva. *Sensors and Actuators: Control System Instrumentation*. CRC, 1 edition, 2007.

[60] J. E. Huber, N. A. Fleck, and M. F. Ashby. The selection of mechanical actuators based on performance indices. *Proceedings: Mathematical, Physical and Engineering Sciences*, 453:2185–2205, 1997.

[61] Y. Eun, C. Gökçek, P. T. Kabamba, and S. M. Meerkov. Selecting the level of actuator saturation for small performance degradation of linear designs. *Proceedings of the 40th IEEE Conference on Decision and Control*, pages 1769–1774, 2001.

[62] R. E. Skelton and M. DeLorenzo. Space structure control design by variance assignment. *Journal of Guidance, Control, and Dynamics*, 8:454–462, 1985.

[63] R. E. Skelton. Some open problems in structural control. *American Control Conference, 1995. Proceedings of the*, 3, 1995.

[64] R. E. Skelton and F. Li. Economic sensor/actuator selection and its application to flexible structure control. *Smart Structures and Materials 2004: Modeling, Signal Processing, and Control. Edited by Smith, Ralph C. Proceedings of the SPIE,*, 5383:194–201, 2004.

[65] M. V. Kothare, P. J. Campo, M. Morari, and C. N. Nett. A unified framework for the study of anti-windup designs. *Automatica (Journal of IFAC)*, 30:1869–1883, 1994.

[66] S. Crawshaw and G. Vinnicombe. Anti-windup synthesis for guaranteed L_2 performance. *Proceedings of the Conference on Decision and Control*, pages 1063–1068, 2002.

[67] K. Ohishi and T. Mashimo. A design method of digital robust speed servo system considering output saturation. *Electrical Engineering in Japan*, 132:68–78, 2000.

[68] F. Suzuki, Y. Chun, and Y. Hori. Anti-windup control using saturated state observer. *Advanced Motion Control, 1998. AMC'98-Coimbra., 1998 5th International Workshop on*, pages 64–69, 1998.

[69] T. Chen and B. A. Francis. *Optimal Sampled-data Control Systems*. Springer, 1995.

[70] A. Ichikawa and H. Katayama. *Linear Time Varying Systems and Sampled-Data Systems*. Springer-Verlag New York, Inc., 2001.

[71] G. Herrmann, S. K. Spurgeon, and C. Edwards. Stability and performance recovery within discretized non-linear control systems. In *Decision and Control, 2003. Proceedings. 42nd IEEE Conference on*, volume 6, 2003.

[72] W.M. Haddad and V. Kapila. Actuator amplitude saturation control for systems with exogenous disturbances. *International Journal of Systems Science*, 33:939–47, September 2002. Copyright 2003, IEE.

[73] V.-S. Chellaboina, W.M. Haddad, and J-H. Oh. Fixed-structure controller design for discrete-time systems with actuator amplitude and rate saturation constraints. In *Proceedings of the 1999 American Control Conference (Cat. No. 99CH36251)*, volume vol.3, pages 1992–6, San Diego, CA, USA, 1999. IEEE. Copyright 1999, IEE.

[74] M.A. Dahleh and J.B. Pearson. L_1-optimal compensators for continuous-time systems. *IEEE Transactions on Automatic Control*, AC-32:889–95, October 1987. Copyright 1988, IEE.

[75] G.F. Wredenhagen and P.R. Belanger. Piecewise-linear LQ control for systems with input constraints. *Automatica*, 30:403–416, 1994.

[76] A. R. Teel. Linear systems with input nonlinearities: global stabilization by scheduling a family of h-type controllers. *International Journal of Robust and Nonlinear Control*, 5:399–411, 1995. Copyright 1995, IEE.

[77] F. Wu and K.M. Grigoriadis. LPV-based control of systems with amplitude and rate actuator saturation constraints. In *American Control Conference, 1999. Proceedings of the 1999*, volume 5, pages 3191–3195 vol.5, 1999.

[78] I.E. Kose and F. Jabbari. Control of systems with actuator amplitude and rate constraints. In *American Control Conference, 2001. Proceedings of the 2001*, volume 6, pages 4914–4919 vol.6, 2001.

[79] F. Allgower and A. Zheng. *Nonlinear Model Predictive Control*. Birkhauser Basel, 2000.

[80] C. E. Garcia, D. M. Prett, and M. Morari. Model predictive control: theory and practice-a survey. *Automatica*, 25:335–348, 1989.

[81] V. Kapila and S. Valluri. Model predictive control of systems with actuator amplitude and rate saturation. In *Proceedings of the 37th IEEE Conference on Decision and Control (Cat. No.98CH36171)*, volume vol.2, pages 1396–401, Tampa, FL, USA, 1998. IEEE. Copyright 1999, IEE.

[82] J.J. Beaman. Nonlinear quadratic gaussian control. *International Journal of Control*, 39:343–61, February 1984. Copyright 1984, IEE.

[83] C. Gokcek. Quasilinear quadratic gaussian control for systems with saturating actuators and sensors. In *Proc. American Control Conference*, pages 6 pp.–, 2006.

[84] A. Koivo. Quantization error and design of digital control systems. *Automatic Control, IEEE Transactions on*, 14:55–58, 1969.

[85] J.Y. Hung. A dynamic output feedback controller with compensation for sensor quantization. In *Industrial Electronics, 2004 IEEE International Symposium on*, volume 1, pages 395–399 vol. 1, 2004.

[86] A. S. Hodel and J. Y. Hung. A state estimator with reduced sensitivity to sensor quantization. *Industrial Electronics Society, 2003. IECON'03. The 29th Annual Conference of the IEEE*, 1, 2003.

[87] Y. Yang, N. P. Rees, and T. Chuter. Application of a kalman filter at ukirt. *Astronomical Data Analysis Software and Systems IX*, 2000.

[88] J. Raisch. *Control of continuous plants by symbolic output feedback*, pages 370–390. Springer-Verlag, 1995.

[89] H. Ishii and B. A. Francis. Stabilizing a linear system by switching control with dwell time. *Automatic Control, IEEE Transactions on*, 47:1962–1973, 2002.

[90] A. V. Savkin and R. J. Evans. *Hybrid Dynamical Systems: Controller and Sensor Switching Problems*. Birkhauser, 2002.

[91] S. Suranthiran and S. Jayasuriya. Use of non-convex optimization to recover signals distorted by memoryless non-invertible sensor nonlinearities. *American Control Conference, 2005. Proceedings of the 2005*, pages 2634–2639, 2005.

[92] S. Suranthiran and S. Jayasuriya. A filtering methodology to recover signals distorted by sensor nonlinearity. *Proceedings of the Japan-USA Symposium on Flexible Automation*, pages 1027–1034, 2002.

[93] J.C. Patra, G. Panda, and R. Baliarsingh. Artificial neural network-based nonlinearity estimation of pressure sensors. *Instrumentation and Measurement, IEEE Transactions on*, 43:874–881, 1994.

[94] G. L. Dempsey, J. S. Alig, N. L. Alt, B. A. Olson, and D. E. Redfield. Control sensor linearization using artificial neural networks. *Analog Integrated Circuits and Signal Processing*, 13:321–332, July 1997.

[95] M. C. De Oliveira and J. C. Geromei. Linear output feedback controller design with joint selection ofsensors and actuators. *Automatic Control, IEEE Transactions on*, 45:2412–2419, 2000.

[96] R. E. Skelton. Integrated structure and controller design. *American Control Conference, 1995. Proceedings of the*, 1, 1995.

[97] F. Li, M. de Oliveira, and R.E. Skelton. Integrating control design and sensor/actuator selection. In *Decision and Control, 2006 45th IEEE Conference on*, pages 6612–6617, 2006.

[98] H. Kwakernaak and R. Sivan. *Linear Optimal Control Systems*. Wiley-Interscience, 1 edition, October 1972.

[99] R. L Burden and J. D. Faires. *Numerical Analysis*. Brooks/Cole, 7th edition, 2000.

[100] W. M. Wonham and A. T. Fuller. Probability densities of the smoothed random telegraph signal. *International Journal of Electronics*, 4:567–576, 1958.

[101] Z. Kotulski and K. Sobczyk. Linear systems and normality. *Journal of Statistical Physics*, 24:359–373, 1981.

[102] L. D. Lutes. Cumulants of stochastic response for linear systems. *Journal of Engineering Mechanics*, 112:1062–1075, 1986.

[103] A. DasGupta. *Asymptotic Theory of Statistics and Probability*. Springer, 2008.

[104] H. S. Bae and J. C. Gerdes. Command modification using input shaping for automated highway systems with heavy trucks. *California PATH Research Report*, 1(UCB-ITS-PRR-2004-48), 2004.

[105] T. Hu and Z. Lin. *Control Systems with Actuator Saturation*. Birkauser, 2001.

[106] A. Saberi, A. A. Stoorvogel, and P. Sannuti. *Control of Linear Systems with Regulation and Input Constraints*. Springer-Verlag, 2001.

[107] G. F. Franklin, J. D. Powell, and M. L. Workman. *Digital Control of Dynamic Systems*. Addison-Wesley, 2nd edition, 1998.

[108] B. Kuo and F. Golnaraghi. *Automatic Control Systems*. Wiley & Sons, 8th edition, 2003.

[109] G. F. Franklin, J. D. Powell, and A. Emami-Naeini. *Feedback Control of Dynamic Systems*. Prentice Hall, 4th edition, 2002.

[110] S. Ching, P. T. Kabamba, and S. M. Meerkov. A root locus approach to designing tracking controllers in systems with saturating actuators. In *Proceedings of the 2007 American Control Conference*, New York, NY, 2007.

[111] M. I. Freidlin and A. D. Wentzell. *Random perturbations of dynamical systems*. Springer, 1998.

[112] K. M. Grigoriadis and R. E. Skelton. Minimum-energy covariance controllers. *Automatica*, 33-4:569–578, 1997.

[113] E. L. Allgower and K. Georg. *Introduction to Numerical Continuation Methods*. Society for Industrial Mathematics, 2003.

[114] R. Baker Kearfott. Abstract generalized bisection and a cost bound. *Mathematics of Computation*, 49:187–202, 1987.

[115] L. Fortuna and G. Muscato. A roll stabilization system for a monohull ship: modeling, identification, and adaptive control. *Control Systems Technology, IEEE Transactions on*, 4:18–28, 1996.

[116] T. Fossen. *Guidance and Control of Ocean Vehicles*. Wiley, 1994.

[117] S. P. Boyd. *Linear Matrix Inequalities in System and Control Theory*. Society for Industrial and Applied Mathematics, Philadelphia, 1994.

[118] F. Zhang. *The Schur Complement and Its Applications*. Springer, 2005.